Norwegian University
of Life Sciences

Master's Thesis 2022 60 ECTS
Faculty of chemistry, biotechnology, and food sciences

Development of non-animal derived scaffolds for cell-based meat production

Oskar Nordberg
Food Science

Preface

This thesis concluded my master studies majoring in Food Science and Technology at the Norwegian University of Science and Technology. The thesis was conducted for and at Nofima AS in Ås and was a part of the strategic research programs "Precision – Precision technology: Biotechnology, smart sensors, and advanced data analysis" and "SusHealth – Norwegian agricultural products and ingredients for a healthy and sustainable future", funded by the Norwegian Fund for Research Fees for Agricultural products (FFL).

I would like to thank my supervisors at Nofima Senior Scientist Sissel Beate Rønning and Senior Scientist Mona Elisabeth Pedersen for taking on the task of guiding me through this process and passing on their knowledge along the way, as well as helping out with proofreading and corrections in the finalizing stages of the thesis. I would also want to give a big thanks to Principal Engineer Nina Solberg at Nofima for being my sparring partner in laboratory related and general questions about the different aspects of my thesis, teaching me proper laboratory techniques, and cheering for me on good days and giving motivational support on tougher days. I would like to thank Head of Laboratory Vibeke Høst for teaching me different staining techniques used in my thesis, Dimitrios Tzimorotas for the production of bacterial nanocellulose scaffolds, and Senior Scientists Svein Halvor Knutsen and Stefan Sahlstrøm, and Postdoc Sara Gaber for producing soy and faba bean scaffolds as well as answering all questions between heaven and earth about legumes.

I also need to thank my family for supporting me throughout 22 years of school and studies. There have been a few different majors of study, and you have supported me in whatever I decided to do. I promise I am finally content and feel I have found my field of interest that I want to be working in for the rest of my life. Last, but not least I have to give a big thanks to my fiancée for being my rock this past year. Without you I would not have been able to complete my thesis in a matter I am satisfied with.

My final words are that working with and writing this thesis has been fun and exciting, but also demanding at the same time. It has been a very educational process where I have had to learn almost everything from scratch, in other words: It has been a very steep learning curve.

Ås, December 15, 2022

Oskar Nordberg

Abstract

The increasing global population, together with an increasing middle class, will lead to an increased demand for meat and meat products in the future. As the production of meat is a major burden on the climate, new sustainable ways of producing meat must be developed. After Mark J. Post made the first laboratory-made hamburger in 2013, additional companies have signed in the pursuit of developing cell-based meat products. In Indonesia, chicken nuggets made using cell-based technology are now sold, and UPSIDE Foods in the USA has received approval for their application for GRAS-status on their technology from the FDA. There is still a lot of research before being able to handle the scale-up from laboratory trials to mass production, but progress is being made in the right direction.

The main goal of this study was to develop edible scaffolds that are non-animal derived. We developed 2 types of scaffolds: I) protein-based scaffolds from textured soy and faba beans, II) bacterial nanocellulose from Kombucha bacteria. Bovine muscle cells were seeded onto these scaffolds. In addition, we compared whether modification with extracellular proteins (entactin, laminin, collagen) could improve cell growth on the various scaffolds. Adhesion, proliferation, and differentiation of the cells on BNC were analyzed by immunofluorescence microscopy and quantified by RT-qPCR analysis of mRNA expression in the myogenic factors Pax7, MyoD1, myogenin, the differentiation marker desmin, the cell adhesion markers ITGβ5 and SDC4, and the cytoskeleton/focal adhesion marker VCL. Cells seeded on BNC that did not proliferate further, were after 30 days incubation trypzinated off and seeded into ECL-coated wells to examine whether they still had proliferation and differentiation potential. Cell adhesion on scaffolds of soy and faba bean was analyzed by immunofluorescence microscopy.

The results showed that the cells were able to adhere to both types of scaffold, and to proliferate and differentiate on the BNC scaffold without ECL. On the faba bean scaffold the number of cells increased with ECL, while on the soy scaffold there was no difference. Cells seeded on ECL-coated BNC showed signs of increased proliferation and differentiation compared to the scaffold without ECL coating. It was concluded that both scaffolds show potential to be used in cell-based meat production, but porous scaffolds from textured soy and faba bean have some challenges with technical abilities and sterility that must be resolved before further trials can be carried out.

Sammendrag

Den stadig økende globale befolkningen vil, sammen med en økende middelklasse, føre til en økt etterspørsel av kjøtt og kjøttprodukter i framtiden. Det må utvikles nye bærekraftige måter å produsere kjøtt på siden dagens kjøttproduksjon har en stor, negative belastning på klima og miljøet. Etter Mark J. Post lagde den første laboratorie-lagde hamburgeren i 2013, har ytterlige aktører meldt seg på i feltet. I Indonesia selges det i dag kylling nuggets laget ved bruk av cellebasert teknologi, og UPSIDE Foods i USA har fått godkjenning på sin søknad om GRAS-status for sin teknologi fra FDA. Det gjenstår fremdeles en del forskning for å håndtere oppskaleringen fra laboratorieforsøk til masseproduksjon, men skritt tas i riktig retning.

Hovedmålet med denne studien var å utvikle spiselige scaffolds som ikke er laget av materialer fra dyr. Vi produserte 2 typer scaffolds: I) proteinbaserte scaffolds fra ekstrudert soya og faba bønner, II) bakteriell nanocellulose fra Kombucha bakterier. Bovine muskelceller ble sådd ut på disse scaffoldene. I tillegg sammenlignet vi om modifisering med ekstracellulære proteiner (entactin, laminin, collagen) kunne forbedre celleveksten på de ulike scaffoldene. Adhesjon, proliferasjon og differensiering av cellene på BNC ble analysert ved immunfluoriserende mikroskopi og kvantifisert ved RT-qPCR analyse av mRNA fra myogenfaktorene Pax7, MyoD1, myogenin, differensieringsmarkøren desmin, celleadhesjonsmarkørene ITGβ5 og SDC4, og cytoskjelett/ fokal adhesjonsmørkøren VCL. Celler sådd ut på BNC som ikke prolifererte videre, ble etter 30 dager inkubasjon ble trypsinert av og sådd ut i ECL-belagte brønner for å undersøke om de fortsatt hadde proliferasjon- og differensieringspotensiale. Celle adhesjon på scaffolds av soya og åkerbønne ble analysert ved immunfluoriserende mikroskopi.

Resultatene viste at cellene klarte å feste seg til begge typer scaffold, og proliferere og differensiere på BNC scaffold uten ECL. På scaffold av åkerbønne økte antallet celler med ECL, mens på scaffold av soya var det ingen forskjell. Celler sådd ut på ECL-belagt BNC viste tegn til økt proliferasjon og differensiering sammenlignet med scaffold uten ECL-belegg. Det ble konkludert med at begge scaffold viser potensiale for å brukes i cellebasert kjøtt produksjon, men porøse scaffold fra soya og åkerbønne har noen utfordringer med tekniske egenskaper og sterilitet som må løses før videre forsøk kan utføres.

Abbreviations

BNC	Bacterial nanocellulose
CBM	Cell-based meat
cDNA	Complementary DNA
CT	Cycle threshold
DM	Differentiation medium
DMEM	Dulbecco's modified eagle medium
DMSO	Dimethyl sulfoxide
DNA	Deoxyribonucleic acid
DPBS	Dulbecco's phosphate buffered saline
ECL	Entactin – Collagen IV – Laminin
ECM	Extracellular matrix
EPF	Extruded protein fractions
FBS	Fetal bovine serum
Fungizone (FZ)	Amphotericin B
MALDI-TOF	Matrix assisted laser desorption ionization
MRF	Myogenic regulatory factors
mRNA	Messenger ribonucleic acid
OCT	Optimal cutting temperature compound
PBS	Phosphate buffered saline
PBS-T	Phosphate buffered saline - tween
PCA	Plate count agar
PCR	Polymerase chain reaction
Pen-Strep (PS)	Penicillin – streptomycin
PFA	Paraformaldehyde
PM	Proliferation medium
RNA	Ribonucleic acid
RT	Room temperature
RT-qPCR	Reverse transcription quantitative real-time polymerase chain reaction
SD	Standard deviation
TPA	Texture profile analysis
TSA	Tryptic soy agar
WHC	Water holding capacity

1. Introduction

It is estimated that the global population will surpass 9 billion people by 2050 and will continue to increase rapidly until it surpasses 11 billion people by the end of the century (FAO, 2017a). According to van Dijk et al. (2021) the food demand will increase by 35-56% from year 2010 to 2050. The global meat protein demand is projected to increase by 14% from 2021 to 2030 (OECD/FAO, 2021), and is expected to increase further towards the midst of the century. This is a result of the steadily increasing middleclass and elderly population and its demand for high-quality animal proteins and meat products (Delgado, 2003).

The livestock sector is responsible for 14.5% of anthropogenic greenhouse gas (GHG) emissions, and cattle is responsible for 41% of the sectors emissions alone (Gerber, et al., 2013). In addition to GHG emissions, the livestock sector uses 8% of the worlds freshwater resources (Gerber, et al., 2013) and occupies 70% of arable land (FAO, 2017b). If one includes the whole agricultural sector, the freshwater usage increases to 70% according to FAO (2017b). With the increased global meat demand, more arable land is needed. Big portions of the arable land are a product of deforestation in favor of feed production in form of monoculture farming, which significantly increases GHG emissions and a loss of biodiversity (Tuomisto, 2019). Another negative effect of monoculture farming is that the soil loses its natural defense system and is to a greater extent exposed to erosion which contributes to water pollution due to excess nitrogen and phosphate from fertilizers and pesticides seep into the groundwater, in addition to veterinary medicines such as antibiotics, vaccines and growth hormones from animal husbandry (FAO, 2017b).

Cattle is the animal having the highest environmental footprint of all livestock, and it is therefore crucial to find solutions to how the increasing meat demand can be met while simultaneously ensuring the welfare of the globe (Tuomisto, 2019). A modern approach for reaching these goals is necessary, with cell-based meat being a promising solution. Winston Churchill said back in 1932: “We shall escape the absurdity of growing a whole chicken in order to eat the breast or wing, by growing these parts separately under a suitable medium” (Churchill, 1932). 40 years later muscle stem cells were discovered (Mauro, 1961), 80 years later the first lab grown hamburger was made in 2013 by Mark Post and his colleagues (O'Riordan, Fotopoulou, & Stephens, 2017), just recently (November 2022) FDA gave their GRAS-approval on UPSIDE Foods’ cultured chicken cell material (Fasano, 2022), and cell-based chicken nuggets are already being sold in Singapore (Waltz, 2021) giving hope for Churchill’s prophecy to come true.

2. Theory

2.1 Cell-Based Meat

Cell-based meat (CBM) goes by many names such as cultivated meat, cellular agriculture, and lab-grown meat amongst others. CBM is produced by growing animal cell cultures using a combination of tissue engineering, biotechnology, molecular biology, and synthetic processing techniques and processes. In doing so, it is possible to reproduce meat products as an alternative to traditional animal agriculture. By extracting adult stem cells (satellite cells) from a living animal or a steak, skeletal muscle cells can be cultured through a proliferating phase followed by a differentiating phase. The main goal in these phases is to obtain the maximum number of cells and formation of skeletal muscle cells, respectively (Post, 2012).

Muscle cells are harvested from either a live animal or a beef using a biopsy needle (Figure 2.1). Myosatellite cells are then isolated to ensure the growth of muscle cells instead of other types of cells. The satellite cells activate and enters the myogenic cell cycle, which is explained in greater detail below in chapter 2.3. To increase the cell count through proliferation, a serum-based medium is introduced to the cells. This medium consists of glucose, amino acids, minerals, vitamins, pH buffer and serum. The serum used is often fetal bovine serum (FBS), which is blood derived from calf fetuses. Due to the ethical concerns about the harvesting methods, alternatives to FBS are being researched (Chelladurai, et al., 2021). A combination of myoblast and muscle-derived fibroblast cells has been proven to increase the proliferation of myoblasts (Rønning, Pedersen, Andersen, & Hollung, 2013).

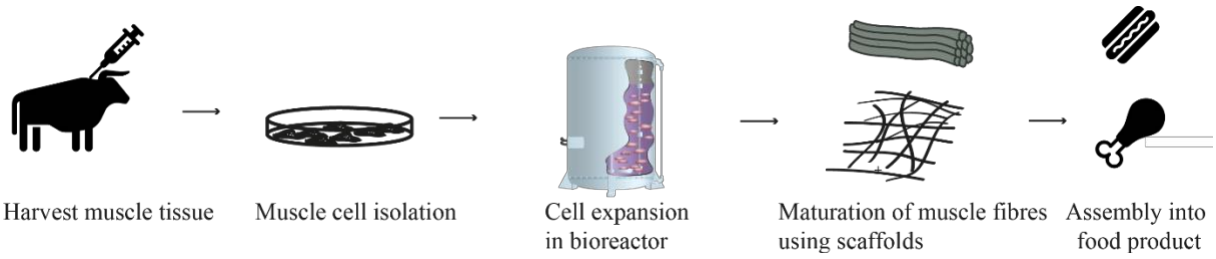

Figure 2.1: *A simplified schematic overview of cell-based meat production (Figure by Sissel Beate Rønning, Nofima).*

After initial cell expansion, the cells are ready to be further expanded in a bioreactor. In the bioreactor, the cells are introduced to the substrate they will adhere to and proliferate and differentiate from. Myoblasts are anchorage-dependent cells, meaning they need a solid substrate for proliferation (Bhat, Bhat, & Kumar, 2020). This substrate could be either scaffolds of various types and materials, or microcarriers made of different polymers. When

they have adhered to and further proliferated on the scaffold/microcarrier, the myoblasts go through the differentiation phase by either spontaneous or medium-induced differentiation. In the differentiation phase the myoblasts commit to becoming specialized muscle cells. In an edible scaffold-based approach, when the cells are committed to becoming muscle cells, maturation into muscle fibers take place in or on the scaffold, which becomes a part of the end product. If the scaffold/ microcarrier is non-edible, the cells would need to be detached and differentiated in a separate system before maturing into muscle fibers. After this last phase, processing and assembling into a desired food product is carried out.

2.2 The skeletal muscle

Meat as we know it is post-mortem skeletal muscle, which is made up of around 90% myofibers and 10% connective- and fat tissue (Listrat, et al., 2016). Myofibers are large syncytial cells with numerous post-mitotic myonuclei (Randolph & Pavlath, 2015). The endomysium surrounding muscle fiber, the perimysium, surrounding bundles of muscle fibers, and epimysium, surrounding the entire muscle, are the three types of connective tissue found in skeletal muscle (Listrat, et al., 2016). The satellite cells (Figure 2.2), which are crucial in muscle regeneration after muscle injury (Fu, Wang, & Hu, 2015), are located between the basal lamina and the myofiber cell membrane (Randolph & Pavlath, 2015).

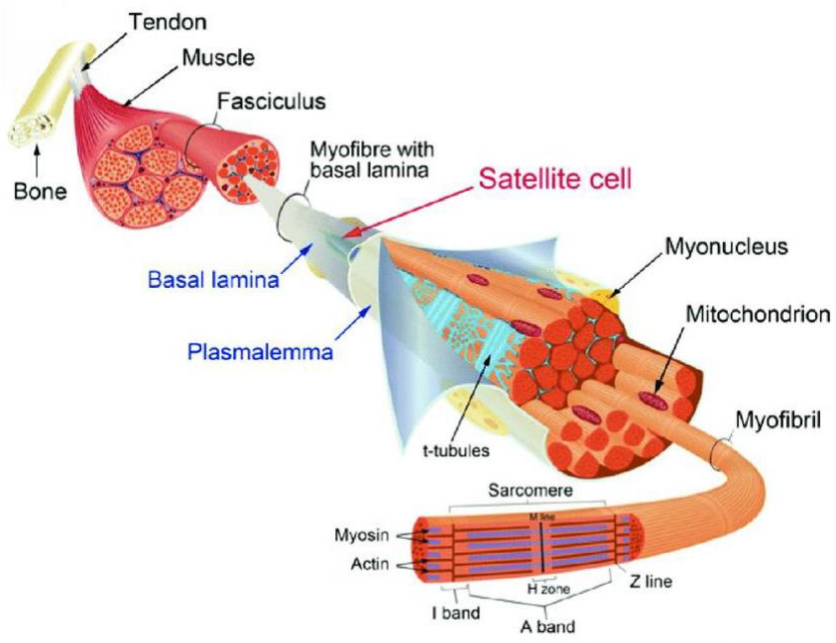

Figure 2.2: Structure of the skeletal muscle and satellite cell niche (Meiliana, Dewi, & Wijaya, 2015)**.**

2.3 Myogenic regulatory factors

Upon muscle regeneration growth factors, chemokines and cytokines are released to active satellite cells (Rodgers, et al., 2014). Prior to activation, the adult stem cells remain in a non-cycling, quiescent state (Cheung & Rando, 2013). After satellite cell activation the satellite cells enter the cell cycle as myoblasts where they are exposed to extrinsic signals (Figure 2.3), causing them to proliferate and fuse to terminally differentiate becoming post-mitotic myofibers (Abmayr & Pavlath, 2012). In order to maintain and replenish the pool of quiescent satellite cells for subsequent rounds of regeneration, a subset of myogenic cells repopulate the satellite cell niche (Collins, et al., 2005).

Pax3 and Pax7 impact the specification and differentiation of myogenic precursor cells (MyoG) by controlling the expression of the genes encoding the myogenic regulatory factors (MRFs) myogenic factor 5 (Myf5), myogenic differentiation 1 (MyoD1), muscle-specific regulatory factor 4 (Mrf4), and myogenin (Mayran, Pelletier, & Drouin, 2015). The MRFs are basic helix-loop-helix domain DNA-binding proteins which binds to promoters and enhancers of muscle-specific genes (Berkes & Tapscott, 2005). Embryonic myoblasts are produced from a population of myogenic precursor cells that express the early MRFs, including MyoD1 and Myf5 (Kassar-Duchossoy, et al., 2004) which are crucial commitment factors for myoblast formation (Rudnicki, et al., 1993), as well as other distinctive markers like Pax3 or isoform 3 of myosin heavy chains (Myh3) (Pin & Merrifield, 1998). Additionally, MyoD activates differentiation by influencing the cell cycle regulators, acting as a molecular switch (Jin, et al., 2007) as well as it may affect the replenishment of the quiescent satellite cell pool (Kanisicak, Mendez, Yamamoto, Yamamoto, & Goldhamer, 2009). The expression of up- and downregulation of Pax7 and MyoD can be used to determine the self-renewal, proliferation, and differentiation status of satellite cells, embodied as $Pax7^{+}/MyoD^{-}$, $Pax7^{+}/MyoD^{+}$, and $Pax7^{-}/MyoD^{+}$ respectively (Wang, et al., 2015).

Embryonic myoblasts then differentiate into primary myotubes. The late MRFs, Mrf4, MyoG, and myosin heavy chain isoforms 7 (Myh7), are expressed by slow-twitching myofibers produced by primary myotubes (Biressi, et al., 2007); (Pin & Merrifield, 1998). Mrf4 is the most abundantly expressed MRF in mature myofibers, but its exact role in myogenesis is still not mapped. It has been shown to serve a homeostatic role in repressing MEF2 activity thus controlling hypertrophy (Zammit, 2017). Studies have shown that MyoD and members of the MEF2 family work combinatorically to activate transcription and myogenesis. MEF2 factors

are crucial for muscle differentiation. The majority of skeletal muscle genes require members of the MyoD and MEF2 families to activate their transcription (Dodou, Xu, & Black, 2003). Myh7 is the only myosin heavy chain isoform expressed in type I slow myofibers, whereas Myh2, Myh1 and Myh4 are expressed in type IIA, IIX and IIB respectively and can be classified thereafter (Wang, et al., 2015). Previously it has been thought that Myh genes are only activated in differentiated cells, but Wang et al. (2015) has found Myh7 activated in a subset of myoblasts engaged in proliferation. Myogenin is an essential protein for postnatal muscle development including muscle cell differentiation, myocyte fusion, myofiber maturation, and muscle growth, as well as prenatal development (Meadows, Cho, Flynn, & Klein, 2008). Six1 and Six4 homeobox proteins are expressed to specifically activate fast-type muscle genes (Niro, et al., 2010). Two mechanisms govern how six homeobox proteins regulate hypaxial myogenesis: 1) The expression of Pax3 in the mouse embryo's ventrolateral lip of the dermomyotome, which regulates the genesis of hypaxial myogenic progenitors, requires six proteins and the Eya cofactors. 2) Six proteins are required for the somitic expression of Mrf4 and myogenin (Grifone, et al., 2005).

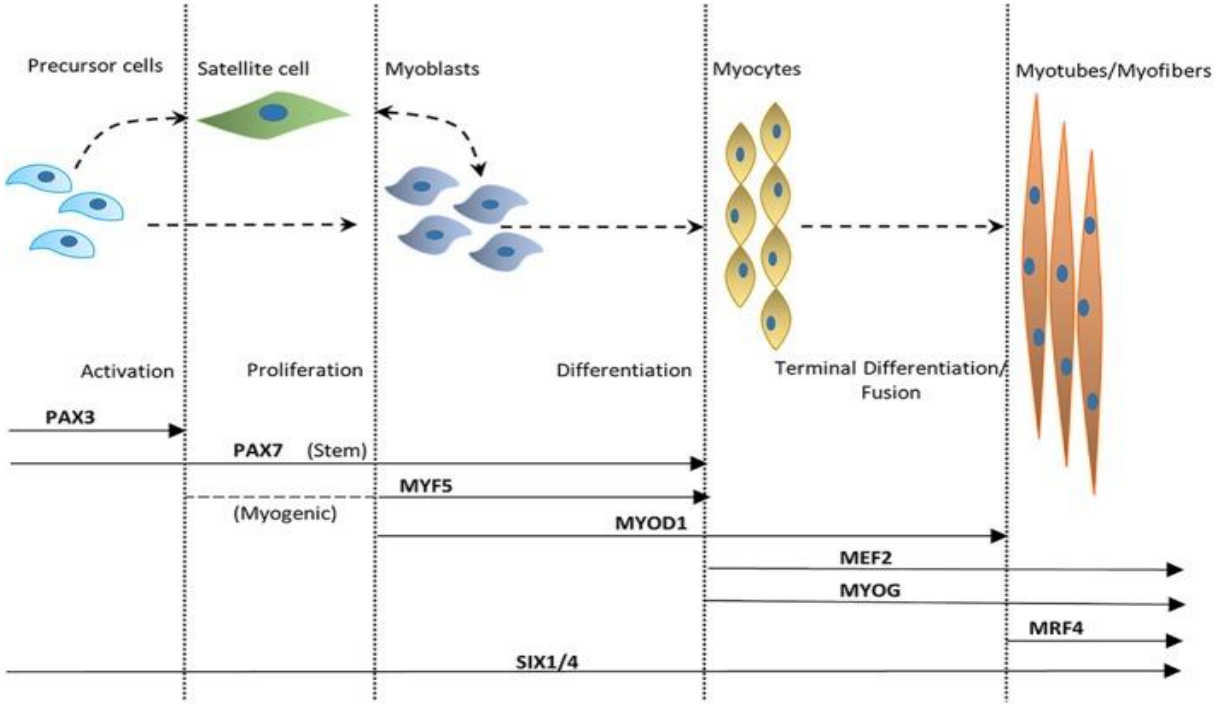

Figure 2.3: Formation of myofibers from quiescent cells*. A simplified overview of myogenesis and associated transcription factors.* (Mukund & Subramaniam, 2020).

2.4 Extracellular matrix

The extra cellular matrix (ECM) provides a framework, or scaffold, for cell adhesion, proliferation, and differentiation, and has a vital role in myoblast alignment (Bach, Beier, Stern-Staeter, & Horch, 2004). ECM is a network of secreted proteoglycans and fibrous proteins such as collagens, elastins, fibronectins, and laminins that filles in the intercellular spaces between cells (Ahmad, Shaikh, Ahmad, Lee, & Choi, 2020), with collagen being the most abundant accounting for 1-10% of skeletal muscle dry weight (Dransfield, 1977); (Gillies & Lieber, 2011). The ECM surround the cells and carries out a number of distinct functions that are essential for controlling the cell activity. (Teti, 1992). The area in direct contact with cells is named basal membrane and consist of a specific composition of ECM differing regarding collagen types and proteoglycans compared to the rest of the ECM (Frantz, Stewart, & Weaver, 2010). Interstitial matrices are connective tissue matrices comprised of the secreted proteoglycans, glycosaminoglycans, and fibrous proteins. Basal membranes interact with cells and are composed of a greater variety of molecules than the interstitial matrix (Ahmad, Shaikh, Ahmad, Lee, & Choi, 2020). Cell adhesion molecules like integrins and syndecans interact with ECM molecules and regulate biological communication between ECM and cell the cell (Huang & Ingber, 1999). Syndecans are membrane-intercalated proteoglycans that interacts with integrins by acting as integrin ligands (Morgan, Humphries, & Bass, 2007). Integrins function as links between the ECM and the cytoskeleton (Yue, 2014), and are heterodimeric receptors composed of α and β subunits (Barczyk, Carracedo, & Gullberg, 2010). Major matrix-binding integrins are the β1 integrins with affinity to fibronectin, collagens, and laminins (Yue, 2014).

2.5 Scaffolds

In CBM production, non-animal derived biocompatible, biodegradable, and edible scaffolds (Ahmad, et al., 2021) are replacing the native organ ECM (Valdoz, et al., 2021). It is therefore desirable to find a biomaterial with surface properties such as epitopes and structure similar to muscle in vivo promoting cell adherence, proliferation and differentiation (Seah, Singh, Tan, & Choudhury, 2021); (Bomkamp, et al., 2022). For cell growth and the transportation of oxygen, nutrients and metabolic waste, scaffolds should be three-dimensional, highly interconnected porous networks with the proper porosity, pore size, and pore structure (Hutmacher, 2000). In order to replicate the growth of cell/tissue in vitro or in vivo, scaffolds need to be biodegradable and have an appropriate degradation rate leaving nothing inedible in the end product (Ma, 2004). The scaffold needs to be sterilizable in order to prevent infection.

The chosen sterilization method must preserve the biodegradable scaffolds' structural and biochemical qualities when sterilizing them, ensuring that the scaffolds will function as intended post-sterilization (Dai, Ronholm, Tian, Sethi, & Cao, 2016). Similar to current methods for processing real meat products, properties of the finished product, such as texture or taste, could be processed downstream (King, 2019). There are multiple types of scaffolds that could serve for this purpose. Microcarriers, porous scaffolds, hydrogels, 3D-printed scaffolds, and fiber scaffolds are all tried and found promising in cultivating cells (Bomkamp, et al., 2022). Collagens are often recognized as the benchmark for ECM replicated scaffolds, but since it is derived from animals it would somewhat undermine the purpose of producing meat in this way (Aamodt & Grainger, 2016). If the scaffolds are to be a part of the final product, it should aid in organoleptic properties and be made of food-grade and nutritious materials (Seah, Singh, Tan, & Choudhury, 2021).

Textured soy protein is an inexpensive byproduct from soybean oil production which still retains its high protein content (>50%) (Day, 2013). Soy is often used as the preferred plant protein to replace meat due to it being a complete source of protein, meaning it contains all essential amino acids (Michelfelder, 2009). Due to this, soybeans are widely used in animal feed with 70-75% of the global soybean production (Brack, Glover, & Wellesley, 2016). However, the production of soy is not environmentally sustainable. Soy production is one of the biggest contributors of deforestation in agriculture, leading to less carbon capturing by the trees and loss of biodiversity due to monoculture farming (WWF, 2014). In addition, due to soy being an annual crop coupled with lack of wind cover from trees, depleting of nutrient-rich topsoil and a high water requisite for growth, resulting in more fertilizers needed and depletion of local water resources for humans, flora, and fauna (WWF, 2014). Faba beans are a great nitrogen fixator in agriculture positively impacting growth of grains and cereals (Klippenstein, Khazaei, & Schoenau, 2021), and has a high protein content in mature seeds (Dhull, Kidwai, Noor, Chawla, & Rose, 2021). Faba beans are suitable for growth in the Norwegian climate (Svanes, Waalen, & Uhlen, 2022) and can be used in crop rotation to improve soils physicochemical and biological state, thus reduce the need for synthetic fertilizers (Aschi, et al., 2017). The proteins ensure nutritional value for both consumers and cells, and functions as anchoring points for cell adherence (Ben-Arye, et al., 2020). When soy and faba bean are expanded in the extruder they make a porous scaffold (Kearns, Rokey, & Huber, 1988), which allows for cell migration and cell medium to be exchanged (Zeltinger,

Sherwood, Graham, Müeller, & Griffith, 2001) and transport of oxygen and waste products to and from the cells (Bomkamp, et al., 2022).

Nanocellulose produced from bacteria (BNC) is fibrous type scaffold, with much smaller pores than textured soy and faba bean scaffolds (Al-Hagar & Abol-Fotouh, 2022). The BNC is produced as a sheet of cellulose with the cells adhering to, and proliferating from, the surface. Due to the smaller pores in the scaffold the cells will be encouraged binding to the substrate, but differentiation to myotubes will be directed across the surface (Rybchyn, Biazik, Charlesworth, & le Coutre, 2021) and not throughout as in extruded scaffolds. BNC has also been proven as a fat replacer with satisfactory levels of organoleptic properties and flavor (Lin & Lin, 2006). Due to its unique nano-morphology, the surface area is greatly increased resulting in higher water holding capacity in addition to elasticity and high wet strength (Meftahi, et al., 2010). Cellulose in natural form is not digestible by humans due to the lack of cellulase enzyme, but BNC are made of biodegradable polymers (Zinge & Kandasubramanian, 2020) making it suitable for CBM production.

2.6 Aim of this study

Main objective:

- The main objective of this study was to develop edible non-animal derived scaffolds for cell-based meat production. Two different 3D structured scaffolds were tested, a sheet of bacterial nanocellulose and textured proteins from soy and faba bean.

Interim objectives:

- One subgoal of this study was to characterize the scaffolds in order to determine whether they were suitable for cell adhesion, proliferation, and differentiation.
- Another subgoal of this study was to sterilize the EPF scaffolds due to bacterial infections.
- The last subgoal of this study was to establish whether the scaffolds were eligible for the intended purpose through examining cell growth.

3. Materials

Table 3.1: Laboratory equipment

Equipment	Supplier
6-, 12-, 24- and 48 well cell culture plates	Falcon, VWR
Nunclon surface 175 cm^2 cell growth flasks	Nunc
Eppendorf tubes	Eppendorf
Falcon tubes 15 ml and 50 ml	Sarstedt
Filtered pipette tips	Sarstedt, Thermo Scientific
Pipettes	Thermo Scientific
Glass bottom 24-well culture plates	MatTek Corporation
Serological pipettes	VWR
Cell scraper	VWR
Optically clear sealing tape	Sarstedt
96 well PCR-Plate half skirt	Sarstedt
Flat 8 Cap Strip	Thermo Scientific
Multipette E3	Eppendorf
Combitips advanced 0.2 ml	Eppendorf
Superfrost Plus	Thermo Scientific
Coverslip 24x50 mm	VWR
MicroAmp 8-Tube Strip, 0.2 ml	Thermo Fisher Scientific
Via2-Cassette	Chemometec

Table 3.2: Instruments

Instrument	Supplier
Vacusafe (liquid disposal system)	Integra Biosciences
NucleoCounter NC-202	Chemometec
Centrifuge 5430	Eppendorf
Mars LAF-bench	ScanLaf
INCU-Line (incubator)	VWR
Galaxy 170 R (incubator)	New Brunswick
Accu-jet Pro (pipette)	Brand
QuantStudio 5	Thermo Fisher Scientific
Micro Star 17R (centrifuge)	VWR
MS1 Minishaker	IKA
XSR105 DualRange (weight)	Mettler Toledo
GeneAmp PCR System 9700	Thermo Fisher Scientific
Heraeus Megafuge 8 (centrifuge)	Thermo Scientific
NanoDrop ND-1000 Spectrophotometer	Thermo Scientific
CM3050 S (camera)	Leica
TA.XT. Plus 100C Texture Analyser	Stable Micro Systems
DMIL LED (inverted phase contrast microscope)	Leica

EOS 5500D (camera)	Canon
DM6000 B (microscope)	Leica
DMC4500 (camera)	Leica
ED 23 (heating chamber)	Binder
Axio Observer Z1 (microscope)	Zeiss
AxioCam MRc 5 (camera)	Zeiss

Table 3.3: Software for data analysis

Software	Supplier
NC-View	Chemometec
QuantStudio Design & Analysis Software	Thermo Fisher Scientific
ND-1000 V3.8.1	Thermo Fisher Scientific
Leica Application Suite V4.13	Leica
ZEN pro 2012	Zeiss
Prism9	GraphPad

Table 3.4: Chemicals

Chemicals	Supplier
VectaMount AQ Aqueous Mounting Medium	Vector Laboratories
10X Blocking Buffer (ab126587)	Abcam
Triton X-100	Sigma Life Science
Tween-20	Sigma Life Science
Lugol's Iodine Solution	BDH
Aniline Blue - Orange G Solution	Electron Microscopy Sciences
Formaldehyde solution (36.5 - 38% in H2O)	Sigma Life Science
O.C.T. Compound	Tissue-Tek
E-C-L Cell Attachement Matrix (Collagen IV-laminin) 1mg/ml	EMD Millipore
Ultroser G	Sartorius
Ultrapur Water	EMD Millipore
Fetal Bovine Serum (FBS)	Sigma-Aldrich
Phosphate Buffered Saline (PBS) tablets	Medicago
RLT Lysis Buffer	Qiagen
Dimethyl sulfoxide	Sigma Life Science
0.05% Trypsin-EDTA	Gibco
Dulbecco's Phosphate Buffered Saline (DPBS)	Gibco
Bouin's fixative	Polysciences, Inc.
TaqMan Gene Expression Master Mix	Thermo Fisher Scientific
Molecular Biology Reagent Water	Sigma Life Science

Table 3.5: Cell medium

Medium	Components	Supplier
Proliferation medium (PM)	500 ml DMEM with GlutaMAX-1 10 ml FBS 10 ml Ultroser G 2.5 ml Pen-Strep 2.5 ml Fungizone	Gibco Sigma-Aldrich Sartorius Life Technologies Sigma-Aldrich
Differentiation medium (DM)	500 ml DMEM with GlutaMAX-1 10 ml FBS 2.5 ml Pen-Strep 2.5 ml Fungizone 7.1 µl insulin	Gibco Sigma-Aldrich Life Technologies Sigma-Aldrich Sigma

Table 3.6: Antibiotics for EPF and cells

Antibiotics	Supplier
Sulfamethoxazole	Fluka Analytical
Trimethoprim	Sigma Life Science
Penicillin-Streptomycin (10,000 U/ml)	Life Technologies
Amphotericin B solution (Fungizone)	Sigma-Aldrich

Table 3.7: Antibodies for immunofluorescence

Antibodies for immunofluorescence	Supplier	Product nr.	Dilution:
NucBlue Live Cell Stain ReadyProbes reagent	Invitrogen	R37605	2 drops /ml
Desmin	Abcam	Ab8592	1:80
Alexa 546	Life Technologies	A11010	1:400
Phalloidin 488	Molecular Probes	A12379	1:400
Hoechst	Invitrogen	H1399	1:1000

Table 3.8: Kits for mRNA and cDNA

Kits	Supplier
Rnase-free Dnase Set (50)	Qiagen
TaqMan Reverse Transcription Reagents	Life Technologies
Rneasy Mini Kit (50)	Qiagen

Table 3.9: Probes for RT-qPCR

Probes	Product number	Supplier
EEF1A1	Bt03223794_g1	Thermo Fisher
Pax7	Hs00242962_m1	Thermo Fisher
MyoD1	Bt03244740_m1	Thermo Fisher
Myogenin	Bt03258928_m1	Thermo Fisher
Desmin	Bt03254509_g1	Thermo Fisher
SDC4	Commercially produced TaqMan probe for bovine syndecan4	Thermo Fisher
ITGβ5	Bt032223964_m1	Thermo Fisher
VCL	Bt004306073_m1	Thermo Fisher

4. Methods

4.1 Scaffold production

4.1.1 Extruded protein fractions of soy and faba

In the extrusion process fine fractions (proteins) of commercial texturized soy and faba protein concentrates are utilized to make extruded protein fractions (EPF). The extruder receives constant supplies of texturized flour. Twin-screws are used to accelerate the material in the barrel. The material is compressed, pulverized, kneaded, and heated by friction in the extruder. The machine's high pressure ensures that water remains liquid even at temperatures above 100 °C. Friction heats up the material quickly and uniformly. Protein and starch are transformed as a result of this brief contact to high temperatures and pressure, and anti-nutritional substances are decreased (Kearns, Rokey, & Huber, 1988).

Heated and compressed material continuously leaves the extruder, and the expansion is achieved at the outlet of the nozzle. Water immediately evaporates after the material exits the extruder through the outflow nozzle and enters the atmosphere. The material, including the water in the cells, expands. As a result, cellular structures are disrupted and protein and starch are transformed into the desired shape, as well as enhancing the nutritious value (Kearns, Rokey, & Huber, 1988).

Table 4.1: Raw-materials and composition used in the extrusion. F65X purchased from Vestkorn A/S. Soya aplha8 purchased from Solae, China.

Legume	Composition of ingredient	Moisture content %	Protein %
Faba bean	F65X	< 10	65
Soy	Soya alpha8	12.41	72.18

Table 4.2: Extruder barrel heating zones (HZ) temperature during processing.

Sample	HZ6 [°C]	HZ5 [°C]	HZ4 [°C]	HZ3 [°C]	HZ2 [°C]	HZ1 [°C]	Screw speed (rpm)	Feeding rate kg/h	Target Moisture %
Faba bean F65X	160	30	130	100	80	40	900	3	31±1
Soy (alpha8)	110	30	110	100	80	40	600	4	34±1

Production of EPF scaffolds was performed by Sara Gaber, Dejan Knezevic, Stefan Sahlstrøm, and Hanne Zobel at Nofima.

4.1.2 Bacterial Nanocellulose

BNC was produced by Dimitrios Tzimorotas at Nofima. *Kommagataeibacter xylinus* was isolated from a kombucha drink and was grown on HS-EtOH medium.

Method:

- 100 µl of overnight culture was grown on petri dishes with 20 ml medium.
- The petri dished were incubated at 25°C for 7 days in static conditions.
- The BNC (Figure 3.1) was then collected and washed with hot distilled water for 30 min, followed by 0.2N NaOH at 80°C for 30 min, and lastly rinsed with distilled water.
- The bacterial free nanocellulose was dried at 37°C until dry.

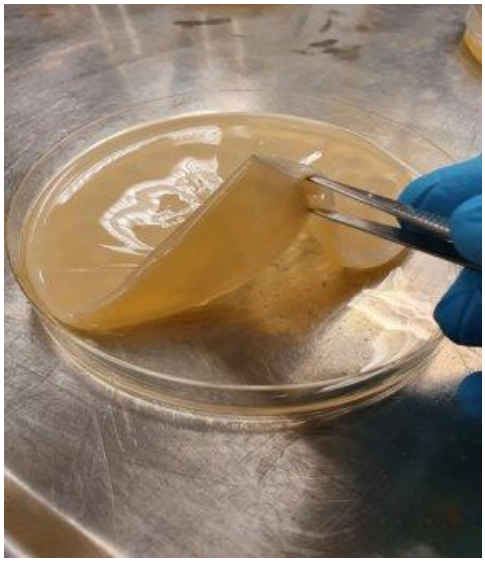

Figure 4.1: Bacterial nanocellulose. The BNC before removal of bacteria in saturated condition.

Tabel 4.3: HS-EtOH Medium used in production of BNC sheet.

HS-EtOH Medium compunds	Amount per 100 ml
Glucose	2 g
Yeast extract	0.5 g
Bacterial peptone	0.5 g
Sodium phosphate dibasic	0.27 g
Citric acid	0.115 g
Magnesium sulfate	0.05 g
Ethanol	1 ml
pH adjustment to 5.7 using 80% citric acid	

4.2 Characterization of the scaffolds

To get a better appreciation of the internal structure of the EPF scaffolds, the scaffolds were sectioned using a cryostat and further visualized for carbohydrate and protein epitopes by staining methods described below. The sections were cut at 10 μm thickness to ensure that the structure was visible in a light microscope, whilst still being thick enough to withstand the external forces of the sectioning.

Method:

- Pieces of EPF from soy and faba were soaked in PBS for 10 min before they were cut in lengths of 5 mm. The width varied naturally due to the curvy shape of the EPF.
- They were stored in 70% EtOH over night at 4°C.
- The next day they were washed 3 x 10 min in PBS and patted dry on a piece of paper before they were covered in OCT for 10 min.
- Then they were frozen in dry ice until they were frozen all the way through and fixed in the cryostat with OCT for sectioning at 10 μm thickness.
- The sections were collected on adhesion slides and stored at -20°C.

4.2.1 Lugol's iodine stain

The reddish color in the iodine staining comes from a slight affinity between amylopectin and iodine and the intensity of the stain can indicate the amylopectin content (Jackson, 2003). Normally a blue stain would be seen when amylose and iodine interact, but potassium iodide is added to Lugol's iodine solution to make it soluble in water (Halpern, 2022).

Method:

- The sections were taken out of the freezer and left for 10 min in a fume hood for drying.
- The 1:4 Iodine-Lugol solution was placed on the section for 1 min before they were rinsed in dH_2O and patted dry with a piece of paper.
- They were mounted with glycerol and a cover slip.

4.2.2 Aniline Blue – Orange G solution stain

The Aniline Blue stain was discovered to stain callose in higher plants back in 1890 by the French botanist Louis Mangin (Evans, Hoyne, & Stone, 1984). It stains the (1→3)-β-D glucans and its soluble derivatives. The intensity of the staining is due to factors as the degree of polymerization, and degree and nature of the (1→3)-β-D glucan chain (Evans, Hoyne, & Stone, 1984). An insoluble dye-protein combination is created when negatively charged sulfonic groups in azo dyes, such as Orange G, interact stoichiometrically with positively charged components in proteins. Protein components with high pKa values are known to be positively charged in an acidic environment and can bond with negatively charged azo dyes. This applies to proteins that contain basic amino acid residues and free terminal amino groups such as ε-amino group of lysine, imidazole of histidine, and guanidine of arginine (Moore, DeVries, Griffiths, & Abernethy, 2010).

Method:

- The sections were taken out of the freezer and left for 10 min in a fume hood for drying.
- The section slides were put in a glass jar of Bouin's fixative for 30 min before they were rinsed in dH_2O and excessive fluid around the sections were carefully removed with a piece of paper.
- They were then placed in the fume hood over night to dry.
- The next day they were placed in 1:10 Aniline Blue – Orange G solution for 4 min before quickly rinsed in dH_2O and fixated with glycerol and a cover slip.

4.2.3 Swelling, Texture Profile Analysis, and Water Holding Capacity

The EPF were further characterized for organoleptic properties to see whether they were suitable as a food grade material. They were measured on swelling, water holding capacity (WHC) and the textural characteristics hardness, resilience, cohesion, and springiness.

Method:

- The weighing vessels were marked and weighed, before the EPF of soy and faba were cut and placed in separate vessels for measuring the dry weight of the EPF.

- The EPF were put in 15 ml tubes and covered in a mixture of PBS, 1% Pen-Strep, 1% Fungizone and 2.5% Co-trimoxazole (1.25 µg/ml trimethoprim and 23.75 µg/ml sulfamethoxazole) and left for two days in RT.
- After sterilization the EPF were washed 3 x 10 min in PBS, weighed again and TPA were performed at 1h and 4h after being washed with compression at 70% strain.
- Excessive fluids were removed with a paper towel to ensure only the liquids inside the EPF would be measured.

Standard deviation was found using MS Excel function St.Dev. Standard error were found using this equation:

$$se(\bar{x_1} - \bar{x_2}) = s \times \sqrt{\frac{1}{n_1} + \frac{1}{n_2}}$$

Statistical significance was calculated using this formula:

$$t = \frac{\bar{x_1} - \bar{x_2}}{se(\bar{x_1} - \bar{x_2})}$$

4.2.4 Monosaccharide composition

The BNC scaffolds were analyzed for their monosaccharide composition by Svein Halvor Knutsen at Nofima to see if there were any monosaccharides other than glucose to account for when interpreting the results of cell expansion.

4.3 Sterilizing the EPF scaffolds

4.3.1 PBS and medium

To test the technical abilities of the EPF, the EPF scaffolds were placed in cell medium and PBS.

Method:

- Whole pieces of EPF were placed in 12 separate 50 ml tubes. Half of the samples were filled with 25 ml medium, the other half with 25 ml dH_2O.
- The tubes were then put in the incubator for visual analysis after 1d, 1w and 2w at 37°C.

4.3.2 Sterilization with 70% EtOH

Alcohols are used as a sterilizing agent due to their functionally active hydroxyl group(s). They are bactericidal and fungicidal, but not sporicidal meaning they cannot destroy bacterial spores (Prescott, Harley, & Klein, 2005). Ethanol is an alcohol that has immediate broad-spectrum antibacterial activity, damages cell membranes due to cell lysis from its dehydrating capabilities, and quickly denaturing of proteins while simultaneously interfering with metabolism (Rubin & Rottenberg, 1982). The reason it was tested is because it leaves no residue on the EPF after treatment (Zaman, Ferdouse, & Hossain, 2013).

Method:

- The EPF were soaked in PBS for 10 min before being cut into lengths of 5 mm pieces.
- Half the pieces were sterilized in 70% EtOH for 10 min and the other half for 60 min.
- They were then moved to separate 10 ml tubes with DMEM Glutamax and put in the incubator for 24h and 5d at 37°C.

4.3.3 Sterilization with Pen-Strep and Fungizone

Penicillin is a β-lactam antibiotic, which inhibits replication of $Gram^+$ bacteria by interfering with cell wall formation, whilst streptomycin is an aminoglycoside antibiotic, which kills $Gram^-$ bacteria through inhibition of protein synthesis (Zhu, et al., 2020). When used in combination they have shown definite synergism to kill bacteria (Moellering Jr, Medoff, Leech, Wennersten, & Kunz, 1972). Fungicidal drugs are split in two categories: fungicidal and fungistatic drugs. Antifungal drugs kill fungal pathogen, where fungistatic drugs inhibit growth (Graybill, Burgess, & Hardin, 1997). Amphotericin B (Fungizone) is classified as an antifungal drug, more specifically with concentration-depending fungicidal properties (Borman, et al., 2017).

Method:

- Whole pieces of EPF were put in 15 ml tubes and 10 ml PBS with 1% Pen-Strep and 1% Fungizone were added to be incubated for 1d, 1w and 2w at 37°C.

4.3.4 Identification of bacteria

Liquid samples from the 15 ml tubes containing 1% Pen-Strep and 1% Fungizone were analyzed by Anette Wold Åsli at Nofima, using MALDI-TOF for bacteria identification.

4.3.5 Heat sterilization of the EPF scaffolds

After the bacteria were identified as *Ralstonia Insidiosa* and *Burkholderia Cepacia*, different heat sterilizing techniques were tried to rid of these bacteria.

Heat sterilization can be divided in two categories: dry heat sterilization and wet heat sterilization. Dry heat sterilization is nontoxic, will not harm the environment and it penetrates the material, though over a longer period. This method has a slower rate of heat penetration and is considered a time-consuming method for killing bacteria. Dry heat kills microorganisms by oxidizing molecules through conduction of heat (Sastri, 2022). Due to this elongated heat treatment, materials that are susceptible for physicochemical changes are not suited for this sterilization method.

Wet heat sterilization utilizes the principles of heat, moisture, and pressure to break down the microorganism's protein structure and enzymes. The required time for bacteria to be killed is much lower than with dry heat. At 121°C the required time is only 15-20 min, where the with dry heat, depending on the operating temperature, the required time can vary from 30 min to >2hrs (Rashed, Hetta, Hashem, & El-Katatny, 2020).

4.3.5.1 Heat cabinet (dry heat sterilization)

Method:

- The EPF were split in two and put in separate sterile Falcon tubes with a metal cap.
- They were then placed in 180°C heat cabinet for 30 min.
- After they were cooled off, the tubes were added 5 ml DMEM Glutamax with 10% FBS, 1% Pen-Strep and 1% Fungizone and put in an incubator at 37°C for 1d and 7d.
- After incubation the fluids were spread out on TSA plates and incubated further for 48-72hrs at 37°C.
- Unheated samples were added as a control.

4.3.5.2 Autoclave (wet heat sterilization)

Method:

- The EPF were split in two and put in acid washed glass tubes with screw cap.
- They were then autoclaved at 121°C and 100 kPa for 20 min.

- After they were cooled off the tubes were added 5 ml DMEM Glutamax with 10% FBS, 1% Pen-Strep and 1% Fungizone and put in an incubator at 37°C for 1d and 7d.
- After incubation the fluids were spread out on TSA plates and incubated further for 48-72hrs.
- Unheated samples were added as a control.

4.3.6 Sterilization with PS + FZ and Co-trimoxazole

The antimicrobial effect of trimethoprim is to prevent susceptible organisms from producing tetrahydrofolate, the active form of folic acid. Folate from external sources cannot pass through bacterial cell walls. As a result, the proliferation and growth of these organisms depend on the endogenous synthesis of tetrahydrofolate from its precursor molecule, dihydrofolate. Dihydrofolate reductase, the enzyme that catalyzes the conversion of dihydrofolate to tetrahydrofolate, is competitively inhibited by trimethoprim. Tetrahydrofolate is an essential component of numerous biochemical processes and serves as a carrier of single carbon fragments. Protein and nucleic acid synthesis are disrupted when its production is halted. Thymine synthesis is the important metabolic pathway that trimethoprim inhibits (Gleckman, Blagg, & Joubert, 1981). Co-trimoxazole is the name of combined trimethoprim and sulfamethoxazole.

Contrary to humans, many microorganisms are capable of converting para-aminobenzoic acid (PABA) into dihydrofolate. The enzyme dihydrofolate reductase then converts dihydrofolate to tetrahydrofolate, which is the active form of the enzyme. Sulfonamides, such as sulfamethoxazole, compete with PABA, displace it, and prevent the biogenesis of dihydrofolate (Gleckman, Alvarez, & Joubert, 1979).

Method:

- A stock of 950 µg sulfamethoxazole and 50 µg trimethoprim per ml DMSO was prepared and mixed with DMEM Glutamax (83.5%), FBS (12%), Pen-Strep (1%) and Fungizone (1%), for a total of 25 µg/ml Co-trimoxazole (2.5%).
- The EPF were cut into smaller pieces and put in acid washed tubes with screw cap and autoclaved at 121°C and 100 kPa for 20 min.
- One additional empty tube was used as a negative control.

- Non-treated EPF were added to separate acid washed tubes, also here a negative control was added.
- The tubes were then added 5 ml of the medium and antibiotics mixture and incubated at 37°C for 1d and 12d.
- The tubes were vortexed and spread out on TSA plates for 72h incubation at 37°C.

4.3.7 Mass sterilization

Mass sterilization was attempted to save time and equipment by sterilizing multiple scaffolds at the same time.

Method:

- Two 500 ml glass bottles were autoclaved and Co-trimoxazole stock was made.
- In the bottles 2.5% Co-trimoxazole, 1% Pen-Strep, 1% Fungizone and 95.5% PBS was added, 75 ml in total.
- Then 10 pieces of soy and faba EPF were added to separate bottles, 7.5 ml antibiotic mixture per EPF in total.
- Liquid samples were collected from the bottles after 24, 48 and 72h in RT on TSA plates, and incubated for further 48h at 37°C.

4.3.8 New batches of EPF scaffolds

This time the EPF were freshly extruded and captured immediately in sterile plastic bags and autoclaved glass jars before touching anything else. They were then dried at 50°C for 2h to prevent spoilage during storage. A stock of Co-trimoxazole was made. The newly extruded EPF were placed in 15 ml tubes and incubated for 48h at 37°C in 5 ml of:

- PBS (100%)
- PBS (99%), Pen-Strep (0.5%) and Fungizone (0.5%)
- PBS (98%), Pen-Strep (1%) and Fungizone (1%)
- PBS (95.5%), Pen-Strep (1%), Fungizone (1%) and Co-trimoxazole (2.5%)

Method:

- After incubation liquid from the tubes were spread out on TSA plates and incubated for 72h on 37°C.

- Since the EPF were collected in different containers, it was also tested for differences in the collection methods.

4.3.9 Sterilization with different dilutions of Co-trimoxazole

A stock of Co-trimoxazole was made and mixed with PBS (93-97%), Pen-Strep (1%) and Fungizone (1%) in different dilutions: 1%, 2,5% and 5%.

- PBS (97%), Pen-Strep (1%), Fungizone (1%) and Co-trimoxazole (1%)
- PBS (95,5%), Pen-Strep (1%), Fungizone (1%) and Co-trimoxazole (2,5%)
- PBS (93%), Pen-Strep (1%), Fungizone (1%) and Co-trimoxazole (5%)

Method:

- 5 ml of each mixture were added to separate 15 ml tubes with EPF of soy and faba.
- After 48h incubation at 37°C they were spread out on TSA plates and incubated for another 48h at 37°C.

4.3.10 Origin of bacteria

The origin of bacteria was investigated to see whether the bacterial contamination was on the producers' side, or if it were a general problem in the water supply at Nofima.

Method:

- Samples of the water, soy powder that were used during the extrusion and a brand-new bag of faba powder were collected and incubated in a 50 ml tube with screw cap with 30 ml DMEM Glutamax at 37°C for 7d.
- After incubation the liquid were spread out on TSA and PCA plates and incubated at 37°C for 48h.

4.4 Bovine primary cell culture

Cells were stored in a mixture of DMSO and DMEM Glutamax in a liquid nitrogen tank and required some preparation before they could During preparation, the cells' ability to proliferate was NucleoCounter to estimate to growth rate of the cells. This was beneficial in terms of setting expectations for the cells' ability to further proliferate after cell adherence on the scaffolds. The flasks were coated with ECL. The proteins present in ECL is laminin, collagen type IV and entactin. Laminin and collagen type IV are proteins found in the basal lamina of skeletal muscle, and entactin supports cross-linking between laminin and collagen (Grzelkowska-Kowalczyk, 2016).

Table 4.4: Amount of ECL and PM used to coat flasks and wells. ECL in flasks were spread out using a cell scraper.

Plate/flask	ECL (µl)	Proliferation medium	Surface area (cm^2)
Big flask	175	Cell scraper	175
6 well plate	30	4	10
24 well plate	6	1	2

Method:

- 75 cm^2 flasks were coated with ECL and put in heat cabinet at 37°C for 1h.
- The cells were then taken out of the liquid nitrogen tank and thawed rapidly.
- The cells were then mixed with 10 ml proliferation medium (PM) and centrifuged at 2660 G for 5 min.
- The supernatant was removed, and the pellet was resuspended in 5 ml PM. This was done to remove toxic DMSO in which the cells were stored in.
- 25 ml PM and the cells were added to the flasks and put in the incubator at 37°C and 5% CO_2.
- When the flasks reached >70% confluency they were ready to be either split into new flasks to increase the cell count or to be used in the experiments.
- The medium was changed every 3-4 days.

When cells in the flasks are split, the medium was first removed with the Vacusafe before they were gently washed 1x with 10 ml DPBS and added 6 ml pre-heated trypsin (37°C) and placed in the incubator for 10 min or until the cells were detached from the surface. Trypsin is a proteolytic enzyme that cleaves peptides after lysine or arginine residues which are not

followed by proline and degrades cell surface proteins during incubation (Lai, et al., 2022). Depending on the confluency the cells were split in ≈equal parts into newly coated flasks. If they were being used directly in an experiment they went through the same procedure, but instead of being added to new flasks they were centrifuged and resuspended for removal of trypsin and were counted using the QuantStudio 5. When the cell count per ml were known, they were ready to be used in experiments or reinserted in the flasks to increase the cell count.

PM were prepared by thawing aliquoted FBS (10 ml), Ultroser G (10 ml), Pen-Strep (2.5 ml), and Fungizone (2.5 ml) and adding them to 500 ml DMEM Glutamax. In DM Ultroser G was substituted with 7.1 µl insulin for temporal control of differentiation (Bateman & McNeill, 2004). The insulin was prepared by diluting 1.74 mM 1:1000 in DMEM Glutamax.

4.4.1 Cell seeding on the EPF scaffolds

Method:

- Sterilized EPF were cut into smaller pieces and washed 3 x 10 min in DPBS.
- The EPF pieces were then added in separate wells of a 24-well cell culture plate and 2 ml of PM was added. Half of the EPF pieces were coated with ECL.
- The EPF pieces were then added ≈750k cells and put in the incubator at 37°C and 5% CO_2.
- After 2d the EPF pieces were moved to new wells to prevent the cells that had attached to the bottom of the wells to send chemical signals to the cells attached to the EPF pieces.
- PM medium was changed every 3-4 days.

4.4.2 Cell seeding on the BNC scaffolds

Method:

- The bacterial nanocellulose (BNC) pieces that were used in the experiment were punched out of a sheet of BNC and then placed in separate wells of a glass bottomed 24-well cell culture plate and 1 ml of PM was added. Half of the BNC pieces were coated with ECL.
- The BNC pieces were then added ≈300k cells and put in the incubator at 37°C and 5% CO_2.

- After 2d the BNC pieces were moved to new wells to prevent the cells that had attached to the bottom of the wells to send chemical signals to the cells attached to the BNC pieces.
- PM medium was changed every 3-4 days.
- The remainder of unused cells were stored at -80°C for further analysis.

4.4.3 Immunostaining

Nucleus staining of BNC

The NucBlue Live Cell Stain ReadyProbes reagent allows for nucleus staining of live cells without the need for fixation. This was conducted to see whether there were live cells attached to the BNC before completing the full protocol for immunostaining.

Method:

- 2 drops per ml medium of NucBlue Live Cell Stain ReadyProbes reagent were added to the wells containing BNC.
- They were put back in the incubator for 30 min and checked under the fluorescent microscope the assure there were live cells before the immunostaining protocol was initiated.

Fixation of cells

PFA alters the mechanical properties of the cell surface by creating covalent cross-links between cell membrane and cytoplasmic proteins. This is effectively gluing them together into an insoluble meshwork thus giving the cells the resistance required to be stained without losing its structure (Kim, Kim, Okajima, & Cho, 2017).

Method:

- The media was removed from the EPF/BNC and the pieces were washed 2 x 10 min with PBS.
- The cells were then fixated in 3.7% paraformaldehyde in PBS for 15 min in a fume hood.
- The samples were then washed 3 x 10 min with PBS.

Permeabilization

As a powerful non-ionic detergent, Triton X-100 is able to remove lipids from cell membranes, making the membrane more permeable to the fluorescent antibody. Due to its uncharged, hydrophilic head groups made of polyoxyethylene moieties, the permeabilization step removed more cellular membrane lipids to allow large molecules like antibodies to enter the cell (Cheng, et al., 2019).

Method:

- The cells were permeabilized in 0.1% Triton X-100 in PBS for 10 minutes.
- The samples were then washed 1 x 10 min with PBS-T (PBS with 0.1% Tween-20)

Blocking

To prevent antibodies from attaching to present non-target epitopes, tissue samples must first be blocked before application of antibodies (Im, Mareninov, Diaz, & Yong, 2019).

Method:

- The cells were blocked with 1x Blocking buffer in PBS for 30 min.

Direct (primary antibody) and indirect (secondary antibody) method

In the direct method, the primary antibody that will be reacting with the target epitope is directly conjugated with a fluorophore label. In the indirect method, there is a two-step incubation process: 1) a primary antibody binds to the target epitope, 2) the secondary antibody, which is fluorophore-tagged, recognizes and binds to the primary antibody. The primary antibody should be derived from a different species than the tissue sample in order to avoid the secondary antibody cross-reacting with endogenous immunoglobulins in the tissue sample. Due to this, the secondary antibody must be directed against the primary antibody host. Multiple secondary antibody modifications and conjugations are possible for the purpose of signal amplification and visualization. Secondary antibodies are frequently attached to fluorescent labels that emit upon photoexcitation (Im, Mareninov, Diaz, & Yong, 2019).

Primary antibody method:

- The desmin dilution was then added to the samples and left for 1h at RT.
- The samples were then washed 3 x 10 min with PBS-T.

Secondary antibody method:

- Dilutions of Hoechst (only for EPF), Alexa 546, and Phalloidin 488 were added to the samples and incubated in the dark for 1h at RT.
- The samples where then washed 3 x 10 min with PBS-T.

Table 4.5: Antibodies and dilution rates used for immunostaining of cells on EPF and BNC.

Antibody	Diluted with	Dilution
Desmin	0.1X Blocking buffer	1:80
Alexa 546	0.1X Blocking buffer	1:400
Phalloidin 488	0.1X Blocking buffer	1:400
Hoechst	0.1X Blocking buffer	1:1000

4.4.4 Quantification of mRNA expression of myogenic and adhesion markers during cell growth

4.4.4.1 Lysing Cells

In order to release intercellular materials like DNA, RNA, protein, or organelles from a cell, a process known as cell lysis or cellular disruption is used to break down or destroy the cell's outer membrane. For molecular diagnostics of mRNA transcriptome determination, and analysis of the composition of particular proteins, lipids, and nucleic acids individually or as complexes, cell lysis is a crucial unit operation (Islam, Aryasomayajula, & Selvaganapathy, 2017).

Materials:

- RNeasy Mini Kit (50)

Method:

- The medium was removed from the cell wells containing BNC with cells with Vacusafe and washed 2 x 10 min with DPBS.
- 350 µl RLT Lysis Buffer was added to each well and the cells were scraped off using a cell scraper.
- The samples were homogenized using a pipette.

4.4.4.2 Isolation of mRNA

Isolation of mRNA was performed to remove all other components than that of mRNA from the lysed cells. This was done by adding ethanol and centrifuging the samples over a specialized spin column with silica membrane that binds RNA (QIAGEN, 2022).

Materials:

- RNeasy Mini Kit (50)

Method:

- 350 µl 70% EtOH was added to the samples and mixed with a pipette.
- The samples were transferred to separate RNeasy spin column and placed in a 2 ml collection tube.
- The samples were centrifuged at 9.632 G for 15s and the eluate was discarded.
- 350 µl RW1 buffer was added to the column and centrifuged at 9.632 G for 15s. The eluate was discarded.
- 80 µl DNase solution mix was added directly to the membrane in the column and incubated at RT for 15 min.
- 350 µl RW1 buffer was added to the column and centrifuged at 9.632 G for 15s. The eluate was discarded.
- 500 µl RPE buffer was added to the column and centrifuged at 9.632 G for 15s. The eluate was discarded.
- 500 µl RPE buffer was added to the column and centrifuged at 9.632 G for 2 min. The eluate and collection tube were discarded.
- The column was placed in a new collection tube and centrifuged at 9.632 G for 1 min. The eluate and collection tube were discarded.
- The column was placed in an Eppendorf tube. 30 µl RNase-free water was added directly to the membrane in the column and centrifuged at 9.632 G for 1 min to eluate mRNA.
- The mRNA eluate was added directly to the membrane again and centrifuged at 9.632 G for 1 min.
- The mRNA yield was measured using NanoDrop ND-1000 Spectrophotometer. The blank sample was set with RNase-free water and the RNA sample size was 1.5 µl.

4.4.4.3 Making cDNA from mRNA

Reverse transcriptase is used to make double stranded cDNA helices from mRNA. In order to perform RT-qPCR, cDNA is made due to its higher stability compared to mRNA because it is not subject to RNases (Nikiforova & Nikiforov, 2011).

Materials:

- TaqMan Reverse Transcription Reagents.

Method:

- TaqMan mix was made by adding the reagents to an Eppendorf tube. 36.9 µl of the mix was pipetted to a cDNA reaction tube which was kept on ice. mRNA and RNase-free water was mixed for a total volume of 23.1 µl and added to the reaction tube.
- The amount of mRNA was calculated by setting the sample with the lowest mRNA yield as 100% and diluting the other mRNA samples so the amount of mRNA would be the same in each tube. The reaction tubes were sealed with flat cap strips.
- When the samples were readily mixed, they were put in the GeneAmp PCR System 9700 and heated with the following program:
    - 25°C for 10 min, 48°C for 30 min and 95°C for 5 min.

4.4.4.4 Reverse transcription quantitative real-time PCR

Reverse transcriptase quantitative real-time PCR allows for the quantification of the PCR product by amplification of DNA in real time while being measured by a fluorescent probe, most frequently an intercalating dye or a hydrolysis-based probe. Using this method, pathogens can be found and the number of copies of particular DNA sequences can be calculated. Additionally, it permits the measurement of RNA levels using cDNA in a qPCR reaction, allowing for the quick detection of changes in gene expression (Adams, 2020). In this study, for relative quantification eukaryotic translation elongation factor 1 alpha 1 (EEF1A1) was used as a reference sample.

Materials:

- TaqMan Universal PCR master mix
- TaqMan probes

Table 4.6: Probes used in RT-qPCR.

Probes	Product number	Supplier
EEF1A1	Bt03223794_g1	Thermo Fisher
Pax7	Hs00242962_m1	Thermo Fisher
MyoD1	Bt03244740_m1	Thermo Fisher
Myogenin	Bt03258928_m1	Thermo Fisher
Desmin	Bt03254509_g1	Thermo Fisher
SDC4	Commercially produced TaqMan probe for bovine syndecan4	Thermo Fisher
ITGβ5	Bt032223964_m1	Thermo Fisher
VCL	Bt004306073_m1	Thermo Fisher

Method:

- A mix of TaqMan Universal PCR master mix and dH_2O (2:1) was prepared in an Eppendorf tube and 97.5 µl were apportioned to each Eppendorf tube, eight in total. In each of the Eppendorf tubes 6.5 µl probe was added.
- 8 µl of this mix and 2 µl cDNA was then added to each well in a half skirt 96 well PCR-Plate using a Multipette E3 with 0.2 ml Combitips to ensure the same amount in each well.
- The plate was sealed off using and optically clear sealing tape. The plates were then centrifuged at 2576 G for 1 min, vortexed and then centrifuged at 2576 G for 1 min again to ensure that it was thoroughly mixed and sat in the bottom of the well.
- The plate was then inserted in the QuantStudio5 apparatus, and the following program was performed:

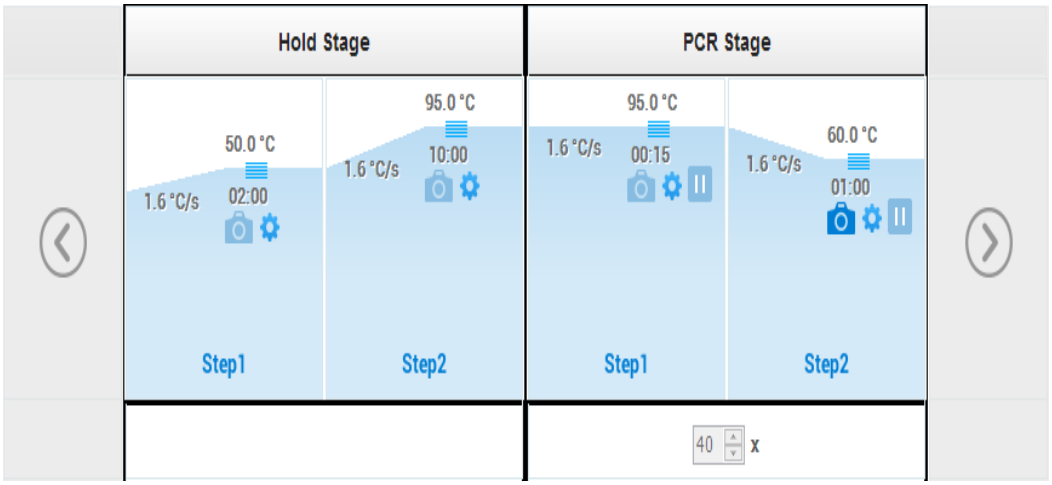

Figure 4.2: Thermal profile RT-qPCR. PCR Stage ran in 40 repeats.

Fold change was calculated following this:

- Average CT of EEF1A1 was calculated
- ΔCT is calculated by subtracting average EEF1A1 CT value from the average target gene CT value
- ΔΔCT = ΔCT target gene – ΔCT EEF1A1
- Relative quantification is found by calculating $2^{-\Delta\Delta CT}$
- Average relative quantification was calculated for target genes, and standard deviation was found by using St.Dev. function in excel.

For statistical analysis of initial cell batches before seeding on the scaffolds, BNC vol 3 was compared to BNC vol 2. BNC vol 2 was set as benchmark. For statistical analysis of cells grown on BNC for 2 and 15 days, BNC coated with ECL was compared to BNC with no coating. BNC with no coating was set as benchmark. Standard deviation was found using MS Excel function St.Dev. Standard error between the groups were found using this equation:

$$se(\bar{x_1} - \bar{x_2}) = s \times \sqrt{\frac{1}{n_1} + \frac{1}{n_2}}$$

Statistical significance was calculated using this formula:

$$t = \frac{\bar{x_1} - \bar{x_2}}{se(\bar{x_1} - \bar{x_2})}$$

4.4.5 Ability to proliferate and differentiate after cell expansion on BNC

This experiment was conducted to see whether the cells on the BNC scaffolds had gone into a senescent state.

Method:

- After pieces of BNC had been cultivated for 30d, the BNC were washed 1 x 10 min with DPBS.
- 2 ml pre-heated trypsin were added to the wells and placed in the incubator at 37°C and 5% CO_2 for 15-20 min. A pipette was used to detach the most steadfast cells.
- The mixture of cells and trypsin was added to a coated 6 well culture plate with 6 ml PM. PM media was changed after 2d and then every 3-4 days.
- After 14d the PM was removed, the cells were washed 1 x 10 min with DPBS, and DM was added.
- DM was changed every 3-4 days.

5. Results

5.1 Biomaterial properties of EPF and BNC scaffolds

Characterization of the EPF scaffolds was performed to establish if they were suitable as scaffolds for usage in CBM production in regard to cell adhesion, proliferation, differentiation, and pores big enough for cell migration and transport of oxygen, nutrients, and waste products.

Figure 5.1: *EPF scaffolds of faba (**left**) and soy (**right**) in dry state. Photographs taken with mobile phone camera.*

The EPF from faba bean or soy had similar structure and size (Figure **5.1**), but further in-depth characterization showed differences (Figure **5.2**). The EPF scaffolds were characterized by microscopy of cryosections to uncover the internal structure. This was done to determine if the pores were big enough for cell migration. The EPF scaffold structures were further characterized by different staining techniques to give an appreciation of some essential proteins and carbohydrates present in the EPF scaffolds.

EPF were cryosectioned to analyze the internal structure to see if cells could migrate towards the inside of the scaffolds and expand from there during the proliferating phase.

Figure 5.2: *Cryosection of EPF from faba(**left**) and soy (**right**). The figure shows randomly, but representatively selected images of the microstructure of faba and soy EPF. Scale bar 100* μm.

Visual inspection by microscopy of the cryosections (Figure **5.2**) showed that there were multiple porous structures and channels in EPF from both faba (**left**) and soy (**right**) big enough (>100 μm) with potential for cell migration. The EPF from faba had a more compact structure with many smaller pores, but a few big enough with potential for cells to attach and migrate through (**left**). The EPF from soy had a more open structure with fewer, but bigger pores (**right**). A quantification of pore sizes big enough for cell migration was not conducted, it was only established that EPF from both legumes had pores of adequate size.

The EPF scaffolds were stained with Lugol's Iodine to determine the starch content to assess the influence of liquid over time on the scaffolds.

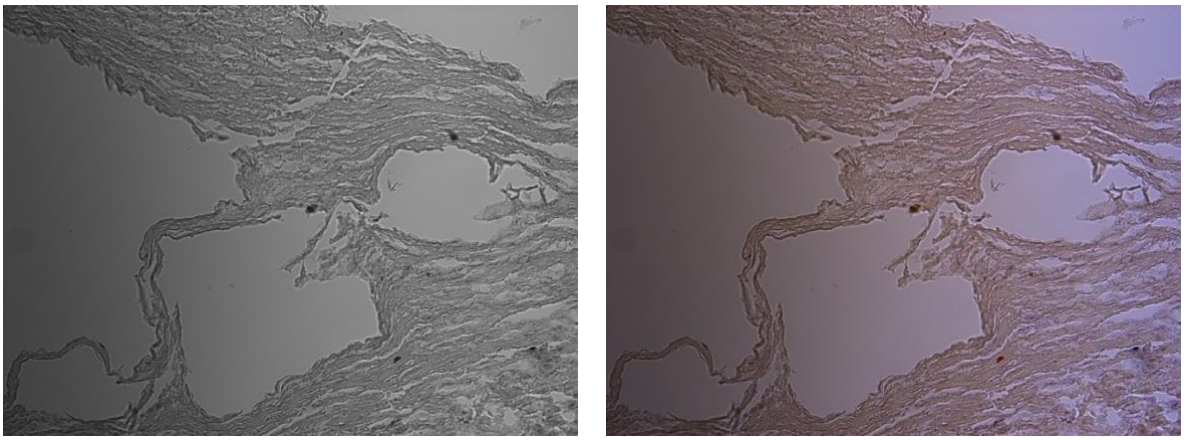

Figure 5.3: *EPF from faba stained with Lugol's Iodine. The black color (**left**) comes from interaction between amylose and iodine. The reddish-brownish color (**right**) comes from interaction between amylopectin and iodine.*

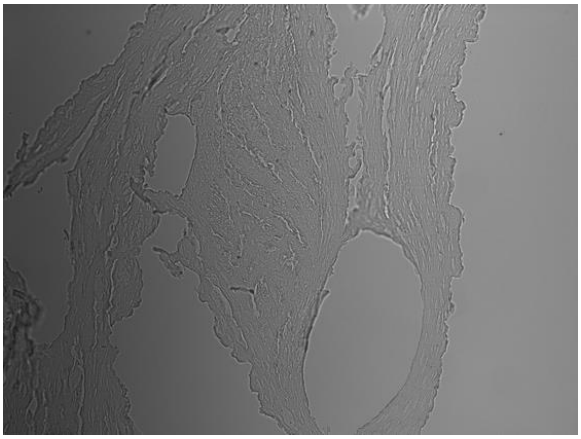

Figure 5.4: *EPF from soy stained with Lugol's Iodine. Little to no effect of iodine staining.*

The iodine staining showed that EPF scaffolds from faba (Figure **5.3**) contains starch in detectable concentration of both amylose and amylopectin to give signals with the staining method used. The starch content in EPF scaffolds from soy (Figure **5.4**) were not high enough to be detected by this staining method. The starch content was not quantified by other methods.

The EPF scaffolds were stained with Aniline Blue – Orange G to determine where polysaccharides and proteins could be found throughout the scaffolds.

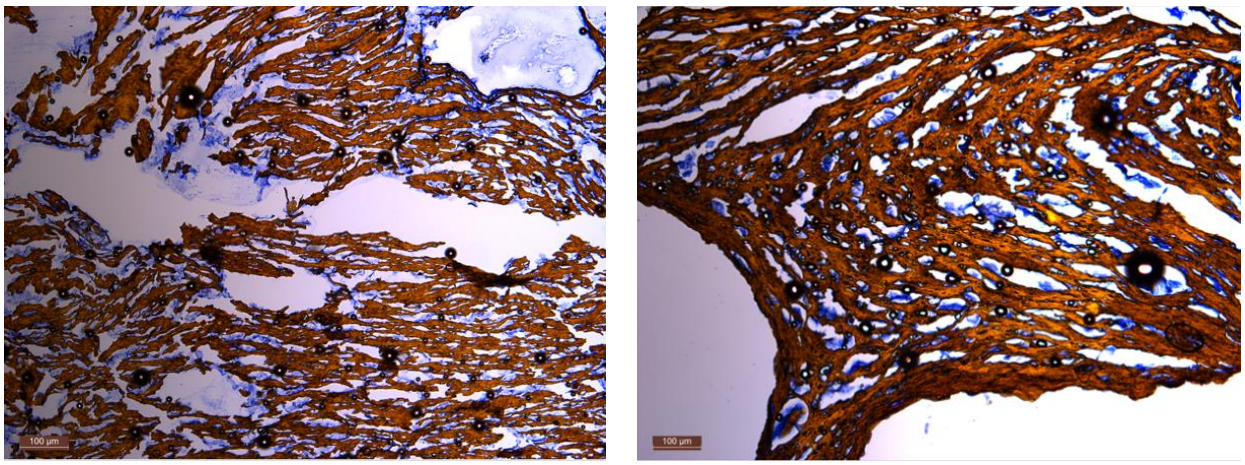

Figure 5.5: *EPF from faba (**left**) and soy (**right**) stained with Aniline Blue-Orange G. Aniline Blue stains for polysaccharides, Orange G for proteins. Scale bar 100* μm.

The Aniline Blue – Orange G staining (Figure **5.5**) showed the distribution of polysaccharides (blue) and proteins (orange) in the EPF scaffolds. The darker areas represent a higher concentration. The polysaccharide and protein content were not quantified but were used to visualize the distribution. It is also worth noting that the EPF scaffolds made from faba (**left**) seems like it is more solubilized in staining solution containing Aniline Blue – Orange G due

to its fragmentation during staining, whereas the EPF made from soy (**right**) seems like the structure is more intact.

The EPF scaffolds were analyzed for swelling, texture profile and water holding capabilities to determine how well they perform as a food grade scaffold for cell growth as well as the potential for being used for in vitro meat production.

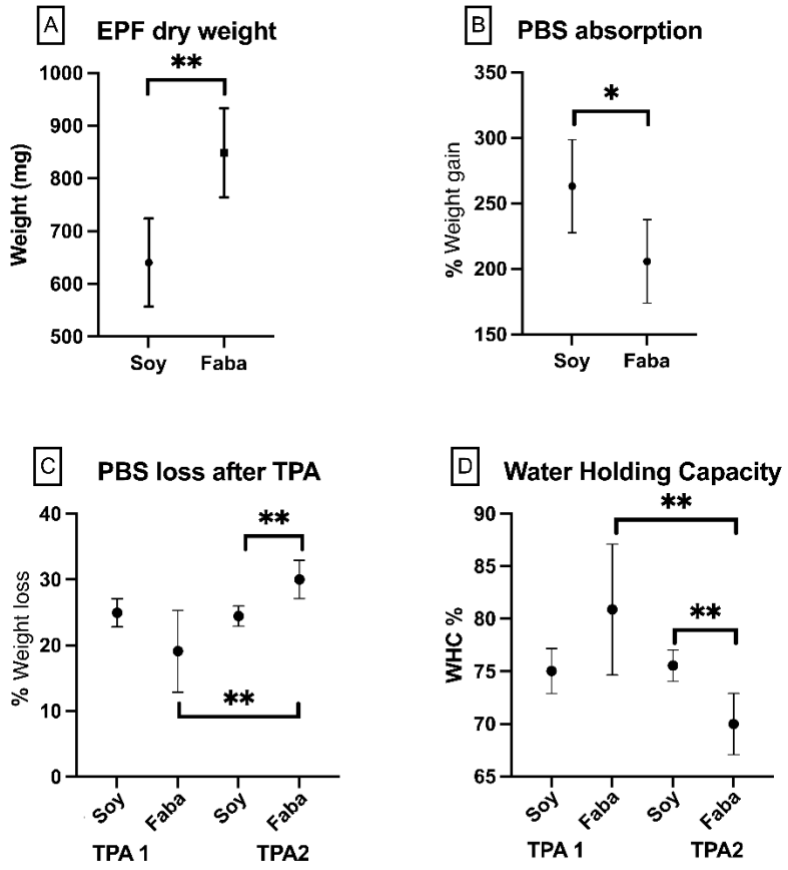

Figure 5.6: *Dry weight of the EPF and their water holding capacities.* ***A****: Dry weight of the scaffolds.* ***B****: Percentage of PBS absorbed per scaffolds own weight.* ***C****: Percentage of PBS lost during TPA per scaffolds absorption of PBS.* ***D****: The water holding capacity of the scaffold (PBS after TPA * 100/PBS before TPA). TPA1 and TPA2 indicates weighing of EPF after first and second run of TPA. Biological replications of 5 for each legume. Error bars (standard deviation) is representing how much the measurements in the group differ from the mean of the group. * = $p < 0.05$, ** = $p < 0.01$.*

The EPF scaffolds were cut in pieces in about the same length, but due to compactness and expansion of the different pieces the weight varied (Figure **5.6**) not only a lot between faba and soy, but also within EPF from the same legume (**A**). The PBS absorption were statistically significant between the two EPF scaffolds, with EPF scaffolds from soy being able to absorb more PBS of the two. It also showed a lot of variation within each legume type

due to its shape and structure (**B**). Measurements of PBS loss after both TPA were carried out. The PBS loss after both TPA for soy is consistent, where faba after TPA 2 has a statistically significant higher PBS loss compared to soy in TPA 2 and faba in TPA 1 (**C**). The water holding capacity of soy is consistent from TPA 1 to TPA 2, but for faba it is a statistically significant reduction from TPA 1 to TPA 2. There is also a statistically significance between soy and faba in TPA 2 where soy has a higher WHC (**D**).

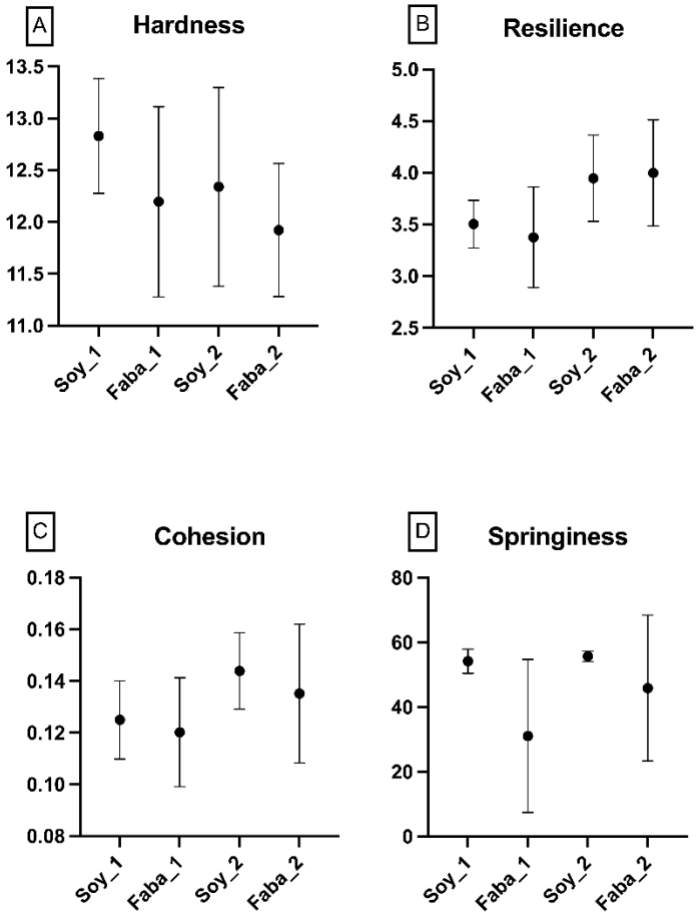

Figure 5.7: *Texture profile analysis of the EPF.* ***A****: How well the scaffolds resist deformation.* ***B****: How well the scaffold recovers from deformation.* ***C****: How well the scaffold withstands a second deformation relative to its resistance during the first compression.* ***D****: How well the scaffold physically springs back after the first deformation. _1 and _2 indicate first and second run of TPA. Biological replications of 5 for each legume. Error bars (standard deviation) is representing how much the measurements in the group differ from the mean of the group. No statistical significance within the time of TPA nor within scaffolds.*

There was no statistically significant difference within or between the EPF scaffolds after TPA 1 and TPA 2 (Figure **5.7**) regarding hardness (**A**), resilience (**B**), Cohesion (**C**) or springiness (**D**). It is worth mentioning that there were big variations within the scaffolds seen as big fluctuation in the standard deviations, except from the springiness in EPF from soy (**D**).

Images of the macro-(Figure **5.8**) and nanostructure (Figure **5.9**) was captured. This was done to get an appreciation of the topography of the scaffold.

Figure 5.8: *Sheet of dry BNC used for cell cultivation.*

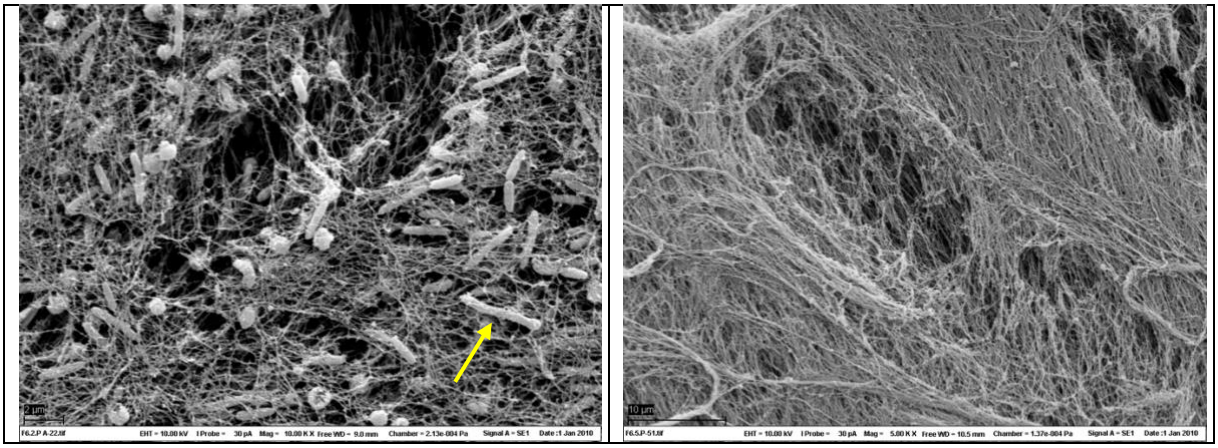

Figure 5.9: *SEM images of BNC taken by Vibeke Høst at Nofima. Pre-rinsing, still containing bacteria (**left**) and post-rinsing, bacteria-free (**right**). Images are taken at 10.000x (**left**) and 5.000x (**right**) magnification. **Yellow arrow** indicating bacteria. Scale bar: 10 µm (**left**) and 2 µm (**right**).*

The monosaccharide composition of the BNC was examined to see if there were compounds that would interact with cell adhesion, proliferation, and/or differentiation. The analysis was performed by Svein Halvor Knutsen at Nofima; this was the composition:

Table 5.1: *Monosaccharides present in BNC used in experiment. Data from technical duplicates.*

Sample	Rhamnose (mg)	Fucose (mg)	Arabinose (mg)	Xylose (mg)	Mannose (mg)	Galactose (mg)	Glucose (mg)	SUM (mg)
BNC	0.18	0.07	0.02	0.00	0.25	0.08	47.24	47.84

The analysis showed that the main monosaccharide present in the BNC was glucose with 98.7% of the total monosaccharide content while the rest of the monosaccharides only accounted for just over 1% altogether.

5.2 Production of EPF and BNC scaffolds

The EPF scaffolds contained bacteria that was needed to get rid of in order to conduct cell seeding experiments. Different sterilization methods and techniques was applied in order to remove the bacteria in the least invasive way. Whole pieces of EPF scaffolds were put in liquid (medium and dH_2O) to see how the contamination affected the samples.

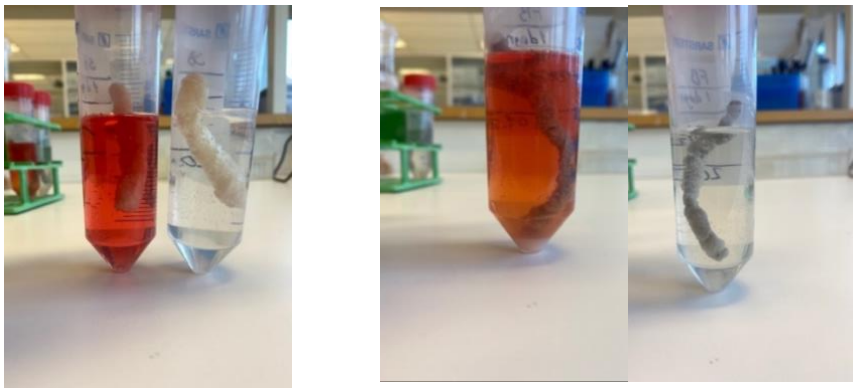

Figure 5.10: *Whole pieces of EPF from soy (**left**) and faba (**right**) in DMEM Glutamax and dH_2O after 1 day incubation at 37°C. Some sediment and change in pH (indicated by color change in medium) in faba incubated in medium.*

After 1 day incubation (Figure **5.10**) the EPF structure from soy (**left**) was intact. The EPF from faba (**right**) has produced some sediment as well as a more acidic environment in the medium and it looks like the outer layer of the scaffold is separating from the rest of the EPF in dH_2O.

Figure 5.11: *Sediment and bacterial growth in all samples after 6 days incubation. Tube **1** with soy in medium show sediment and slight color change. Tube **2** with soy in dH2O show sediment and cloudiness of the liquid. Tube **3** with faba in medium show sediment and a big color change. Tube **4** with faba in dH2O show sediment and some cloudiness of the liquid.*

After 6 days incubation (Figure **5.11**) there were excessive microbial growth, resulting in a more acidic environment in the medium, and cloudiness in the dH_2O. All samples had sediment. The experiment was discontinued due to this. To see if the bacteria could be killed with a simple sterilization technique consisting of pre-sterilizing them with 70% EtOH for 10 – 60 min before incubation with DMEM Glutamax.

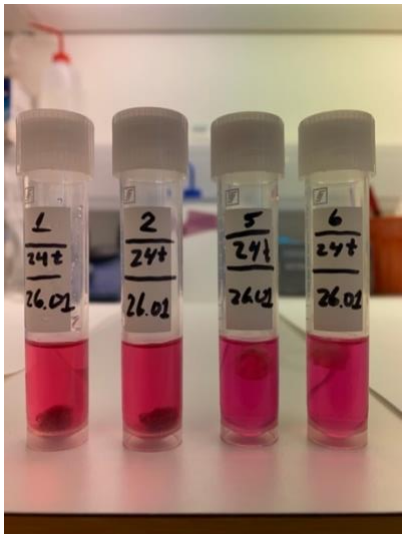

Figure 5.12: *Pre-sterilized EPF in 70% EtOH after 5 days incubation with DMEM Glutamax. 10 min faba (**1**), 60 min faba (**2**), 10 min soy (**5**), 60 min soy (**6**). Slight pH changes in all samples.*

There was a slight pH change (indicated by color change in medium) in all samples after 5 days (Figure **5.12**) incubation which could either be caused by bacteria or precipitation of available proteins in the EPF. The faba samples (**1, 2**) were slightly more acidic than the samples of soy(**5, 6**) with the color of phenol red turning pink. The sterilization technique showed an effect on inhibiting the bacterial growth, but not neutralize them. The internal microstructure showed little to no difference from before sterilization (Figure **5.2**), hence the structure was intact after 70% sterilization (Figure **5.13**).

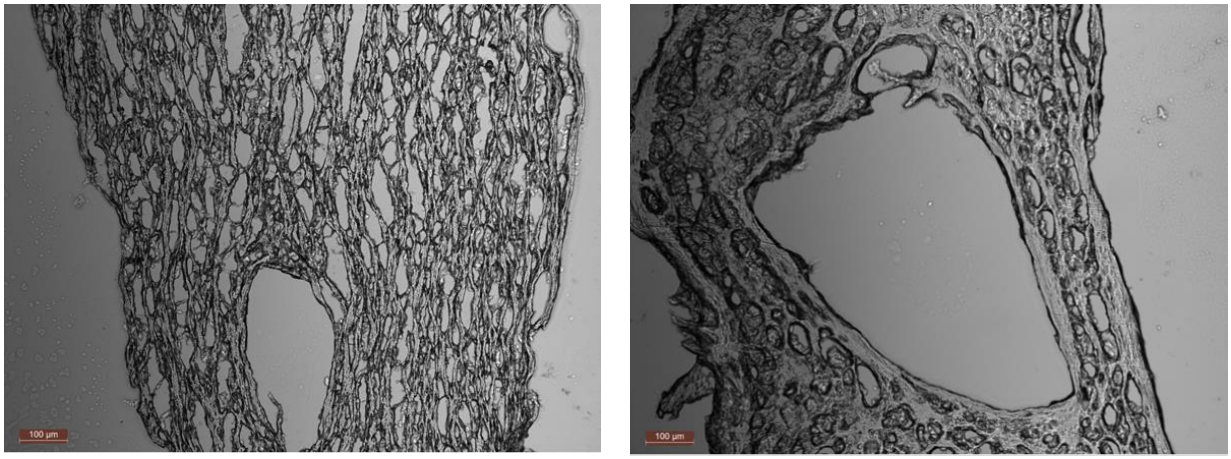

Figure 5.13: *Cryosection of EPF from faba (**left**) and soy (**right**) with 70% EtOH sterilization treatment. The figure shows randomly, but representatively selected images of the microstructure of soy EPF. Scale bare 100* μm.

The EPF scaffolds were tried sterilized with the same antibiotics used in the PM and DM for the cells, Pen-Strep and Fungizone. The antibiotic and the fungicidal drug were chosen because it has been showed that the cells are able to proliferate and differentiate with these treatment methods, and thus would not cause harm to the cells if they were to be used in cell experiments.

Figure 5.14: *Plates from liquid, later used in identification with Maldi-TOF. Soy on the left, faba on the right.*

Treatment with pen-strep and fungizone (Figure **5.14**) did not prevent bacterial growth, and the samples were sent to the microbiology department for analysis of the bacteria strains. The strains were then analyzed by Anette Wold Åsli using MALDI-TOF and were identified as *Burkholderia cepacia* and *Ralstonia insidiosa*.

After the bacteria were identified as *Burkholderia cepacia* and *Ralstonia insidiosa* and it was discovered that the bacteria were resistant against Pen-Strep, the EPF scaffolds were tried to be sterilized using two different methods of heat sterilization: wet heat and dry heat.

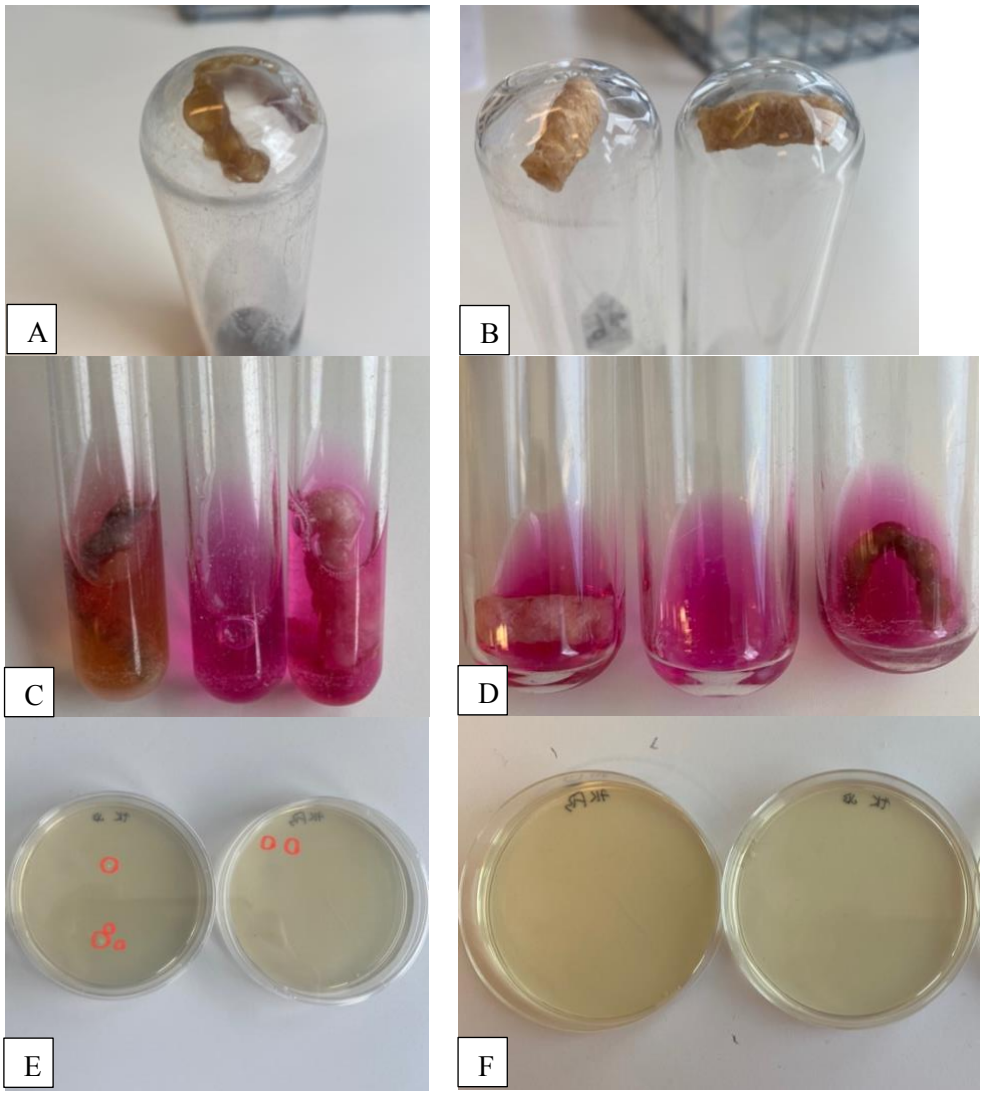

Figure 5.15: *Autoclaved EPF (soy: **A** , faba: **B**). The EPF are reacting with heat and moisture to melt and gelatinize in the bottom of the tube. **C**: Autoclaved EPF after 1 day incubation at 37°C. Negative control in the center, faba on the left, and soy on the right. Samples are vortexed. **D**: Autoclaved EPF after 7 days incubation at 37°C. Negative control in the **center**, soy on the **left** and faba on the **right**. Samples are vortexed. pH indicator is phenol red in DMEM Glutamax. **E**: Autoclaved EPF after 1 day incubation at 37°C. Colonies in both EPF from soy (**left**) and faba (**right**). **F**: Autoclaved EPF after 7 days incubation at 37°C. No colonies in faba (**left**) or soy (**right**).*

During autoclavation (Figure **5.15**) the EPF scaffolds melted due to the heat and moisture resulting in gelatinization in the bottom of the tubes thus altering the structure of the scaffold. In the EPF scaffold (**B**) from faba (**right**), it is possible to see the inside of the scaffold. This effect was bigger on EPF from faba than from soy (**A**). After the EPF were autoclaved

DMEM Glutamax with FBS, PS and FZ was added in the tubes and then placed in the incubator. The vortexed samples (**C**) showed a change in the medium towards acidic state, faba (**left**) more so than soy (**right**). The negative control (**center**) was added to see how the medium with scaffolds would react to incubation. The change in pH could be from bacteria or denatured proteins. We therefore performed bacterial testing to investigate possible bacterial contamination. In the autoclaved EPF (**D**) incubated for 7 days there were no visual difference between the samples containing EPF scaffolds and the negative control (**center**). There were colonies in both samples after 1 day incubation, however, after 7 days there were none.

Simultaneously as the wet heat sterilizing, dry heat sterilizing was carried out to see if there were any difference between the two techniques.

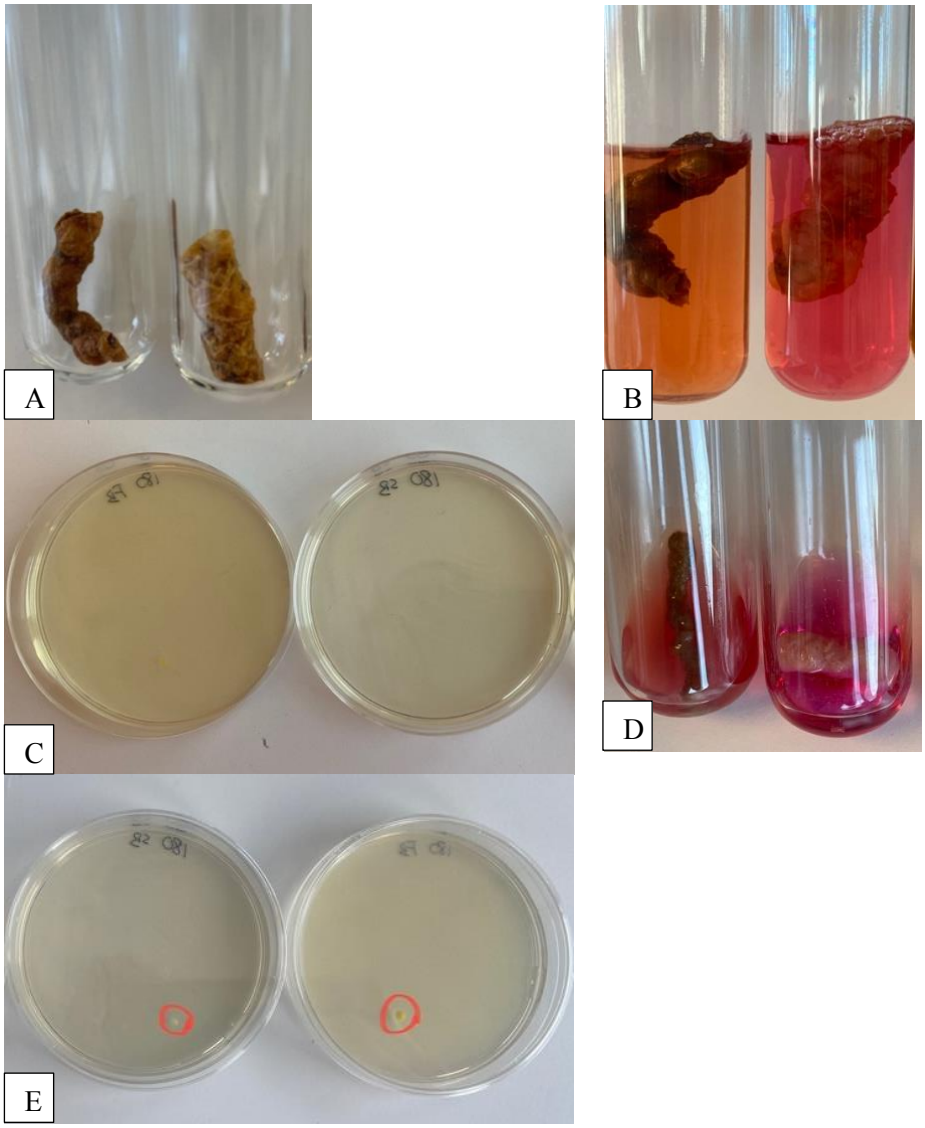

Figure 5.16: ***A****: EPF from faba* ***(left)*** *and soy* ***(right)*** *after dry heat sterilization at 180°C.* **B**: *Dry heat sterilized EPF of faba* ***(left)*** *and soy* ***(right)****after 1 day incubation at 37°C. pH indicator is phenol red in DMEM Glutamax.* **C**: *Dry heat sterilized EPF after 1 day incubation at 37°C. No colonies in faba* ***(left)*** *or soy* ***(right)****.* **D**: *Dry heat sterilized EPF after 7 days incubation at 37°C. Faba on the left and soy on the right.* **E**: *Dry heat sterilized EPF after 7 days incubation at 37°C. One colony in faba* ***(right)*** *and two in soy* ***(left)****. Colonies are circled in red.*

During time in the heat cabinet (Figure **5.10**) the EPF scaffolds (**A**) were clearly affected by the dry heat treatment resulting in a browning of the exterior. The tubes containing EPF were filled DMEM Glutamax, FBS, PS and FZ after the dry heat sterilization and put in the incubator at 37°C. After 1 day incubation (**B**) the pH indicator showed that liquid in the faba sample (**left**) was more acidic than before incubation by becoming orange, while the soy

sample (**right**) only had a slight decrease in pH. In both plates from 1 day incubation (**C**) after dry heat sterilization there were found no colonies.
As with the autoclaved EPF, the dry heat sterilized EPF were also incubated for 7 days to see whether the bacteria count would increase or not. In the dry heat sterilized EPF (**D**) the pH indicator is showing a more acidic liquid in faba than soy. The phenol red in the soy sample (**right**) indicates a slightly basic change in pH. The dry heat sterilized EPF (**E**) showed one colony in faba (**right**) and two colonies in soy (**left**) growing on top of each other after 7 days incubation.

Although heat sterilization was successful in removing bacteria, it was not suitable for this experiment as the physical altercation of the EPF scaffold was too big. A combination of trimethoprim and sulfamethoxazole (Co-trimoxazole) was tested as a non-invasive method.

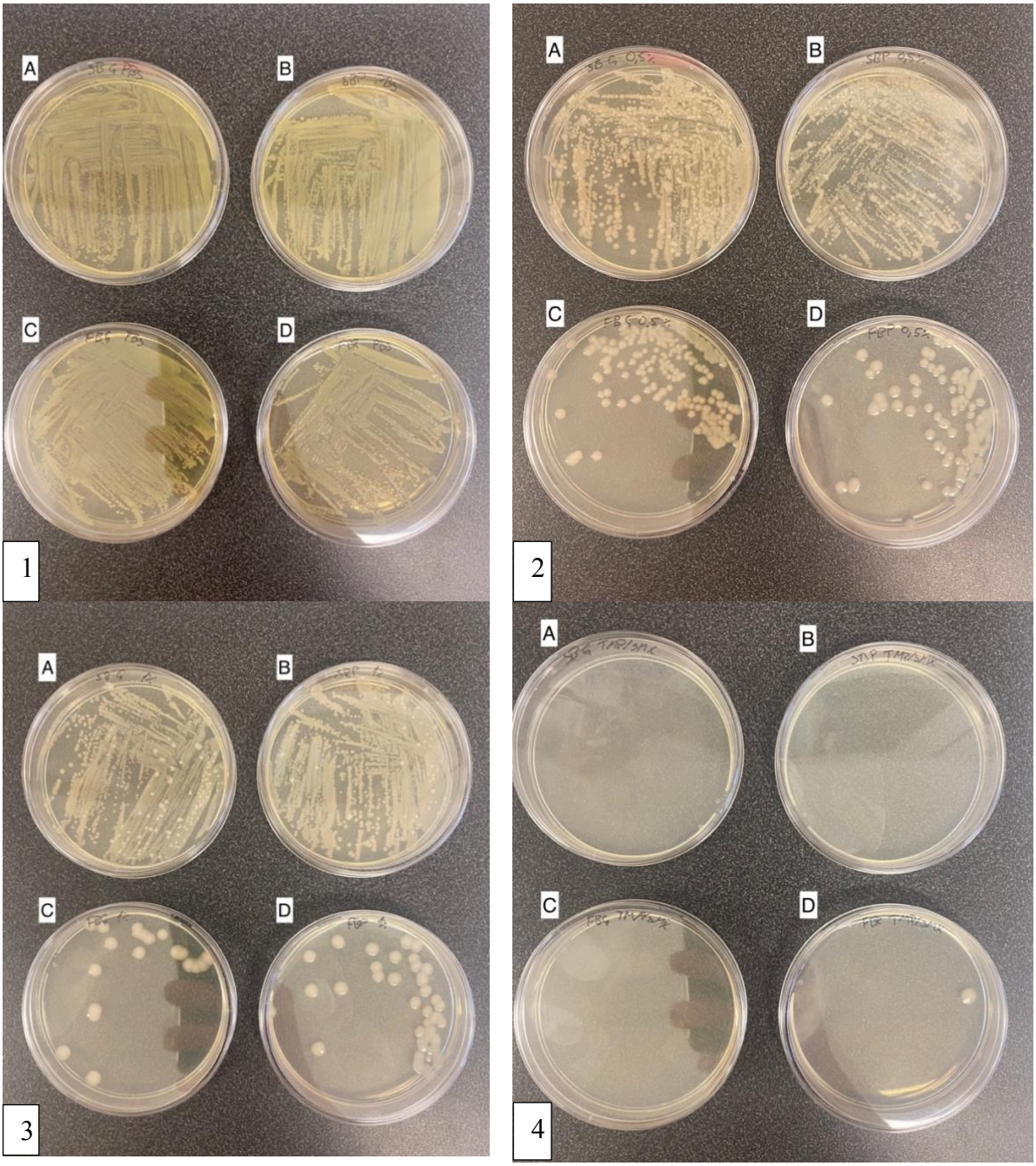

Figure 5.17: *Plates from EPF captured in different solutions. Incubated in* ***1:*** *PBS,* ***2:*** *PBS + 0.5% PS + 0.5% FZ,* ***3:*** *PBS + 1% PS + 1% FZ, and* ***4:*** *PBS + 1% PS + 1% FZ + 2.5% Co-trimoxazole for 2 days at 37°C.* ***A****: Soy captured in glass,* ***B****: Soy captured in plastic bag,* ***C****: Faba captured in glass,* ***D****: Faba captured in plastic bag.*

In the antibiotic sterilization attempt (Figure **5.17**), the starting point of the bacteria count is the EPF scaffolds incubated in PBS (**1**). The effects of PS and FZ sterilization on EPF from faba (**2, 3**) is clear but not effective enough, while the EPF from soy (**2, 3**) is nearly unaffected by PS and FZ. Co-trimoxazole (**4**) was deemed very efficient with only one colony (**4-D**) after incubation.

After the successful sterilization with Co-trimoxazole (Figure **5.17**) different dilutions were tested to see what the least amount of Co-trimoxazole needed to get rid of the bacteria.

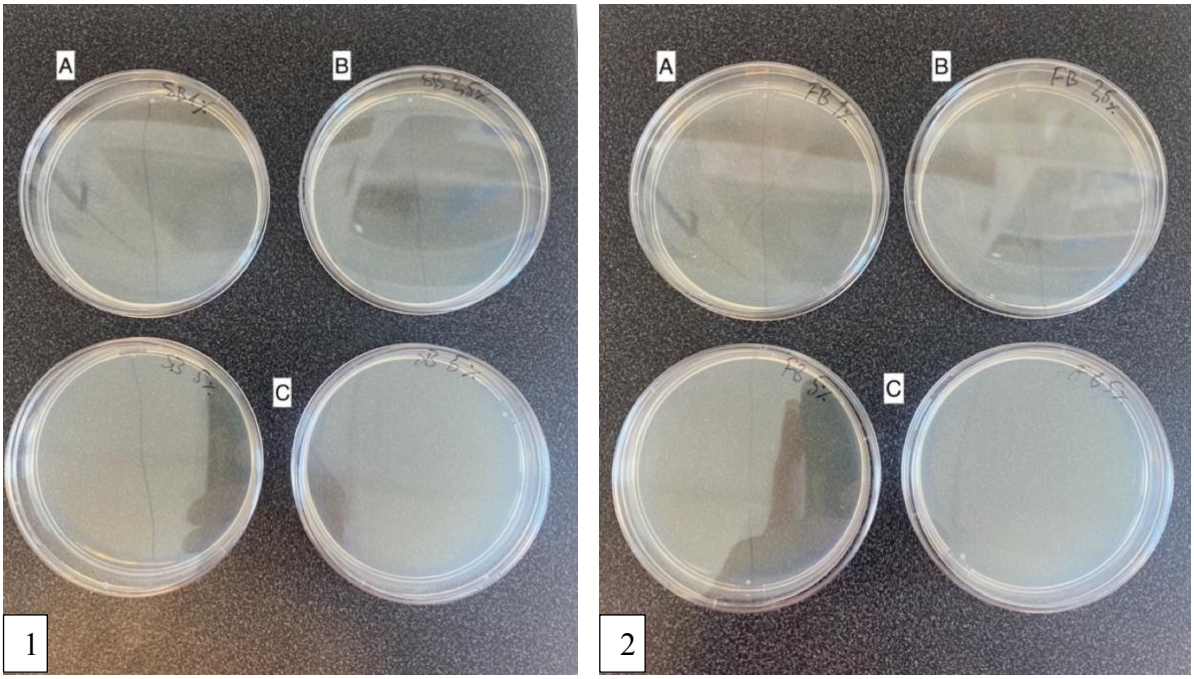

Figure 5.18: *Plates of EPF from **1:** soy and **2:** faba incubated at 37°C for 7 days. **A**: PBS + 1% PS + 1% FZ + 1% Co-trimoxazole, **B**: PBS + 1% PS + 1% FZ + 2.5% Co-trimoxazole, **C**: PBS + 1% PS + 1% FZ + 5% Co-trimoxazole.*

There were found no colonies on any of the plates after 7 days incubation with Co-trimoxazole, suggesting that as low as 1% co-trimoxazole is sufficient for sterilization. After all plates of faba and soy (Figure **5.18**) contained no colonies, an experiment of mass sterilization was conducted to see if they could be sterilized in batches to save time and materials.

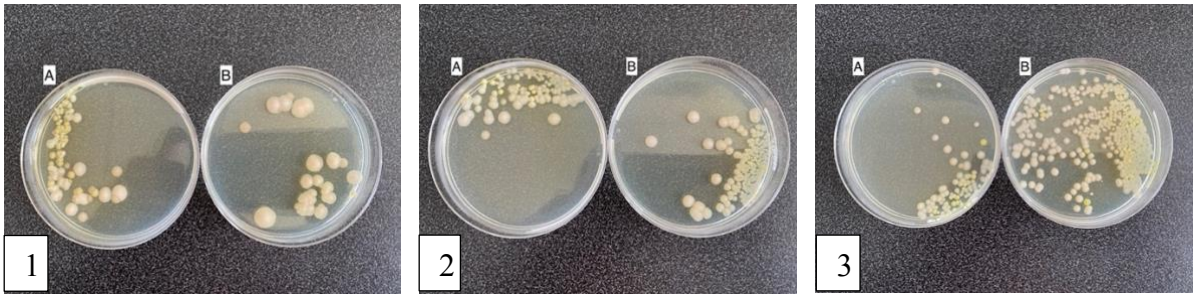

Figure 5.19: *Plates from EPF from soy (**A**) and faba (**B**) mass sterilized for 24 (**1**), 48 (**2**), and 72 (**3**) hours at RT.*

There were colonies in all the plates (Figure **5.19**) showing mass sterilization was not successful. In faba (**B**) it seems like the number of bacterial colonies are growing exponentially, and in soy (**A**) it seems like the number of colonies were the same throughout the incubation period.

To figure out where the source of the bacterial infection came from, the water, soy powder, and an unopened bag of the same faba powder used in the extrusion were tested.

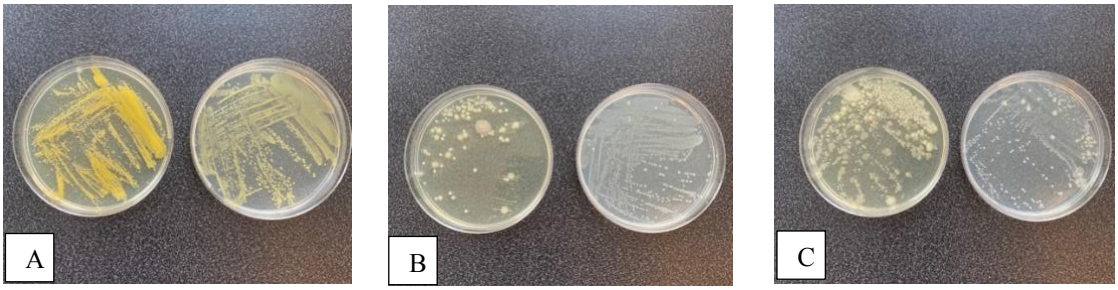

Figure 5.20: *A: Water used in the extrusion process.* ***B****: Powder from soy used in the extrusion process.* ***C****: Powder from an unopened bag of faba used in the extrusion process. Incubated with DMEM Glutamax at 37°C for 7 days. Spread out on TSA (left) and PCA (right).*

In the attempt of finding the origin of the bacteria (Figure **5.20**), the water showed colonies on both agars (**A**) after 7 days incubation, but they were not the same colonies as the previous plates with EPF from soy and faba had shown. There was growth on both plates of EPF from soy (**B**) with similar morphology as previously found in soy samples. There was growth on both plates of EPF from faba (**C**) with similar morphology as previously found in faba samples.

After an initial successful experiment with growing cells on EPF from faba and soy, we wanted to repeat the experiment.

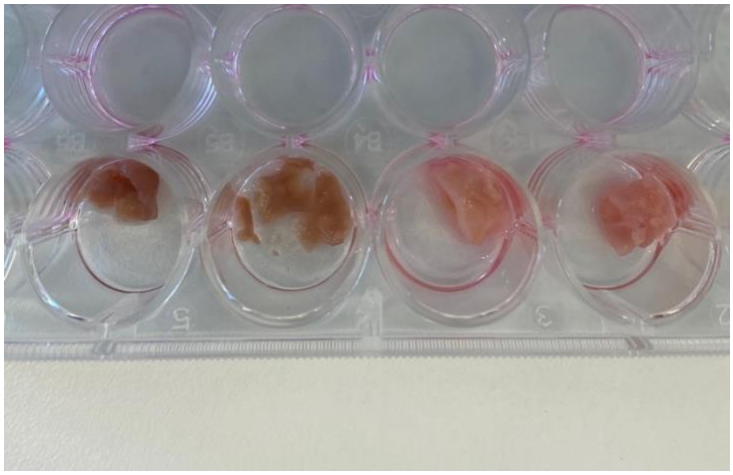

Figure 5.21: *EPF from faba (two left wells) and soy (two right wells) disintegrated during incubation in PM.*

The EPF from faba and soy (Figure **5.21**) disintegrated during incubation and were therefore no longer suitable as a scaffold for cell growth and expansion. Since the last experiment was

unsuccessful due to the disintegration, the experiment was repeated with newly produced EPF from faba and soy.

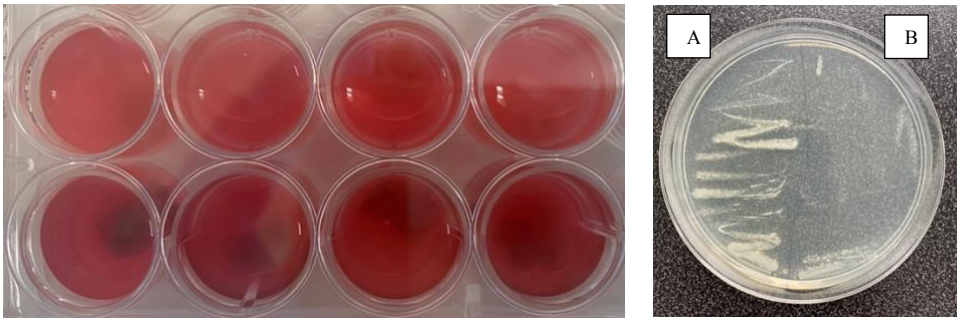

Figure 5.22: *Cloudy samples (**left**) of cells on EPF from soy (top row) and faba (bottom row) after 3 days incubation. Plating confirmed bacterial growth (**right**). **A**: Soy. **B**: Faba.*

The wells containing EPF scaffolds with cells turned cloudy after 3 days incubation. To see if the cloudiness in the samples (Figure 5.22 - **left**) were due to bacterial growth, although incubated with antibiotic solution that was successful before, samples was taken from one soy well and one faba well and spread out on PCA agar. Both samples tested positive for bacterial growth (**right**) and the experiment was therefore discontinued. No further experiment of cell growth on EPF were conducted.

5.3 Cell adhesion properties and biocompability of EPF and BNC scaffolds

After deeming the EPF scaffolds to having the characteristics needed for a CBM scaffold and successful sterilization, 750k cells were seeded on EPF scaffolds and incubated for 7 days. The EPF scaffolds were cryosectioned and immunostained with Hoechst to stain the nucleus of the cells.

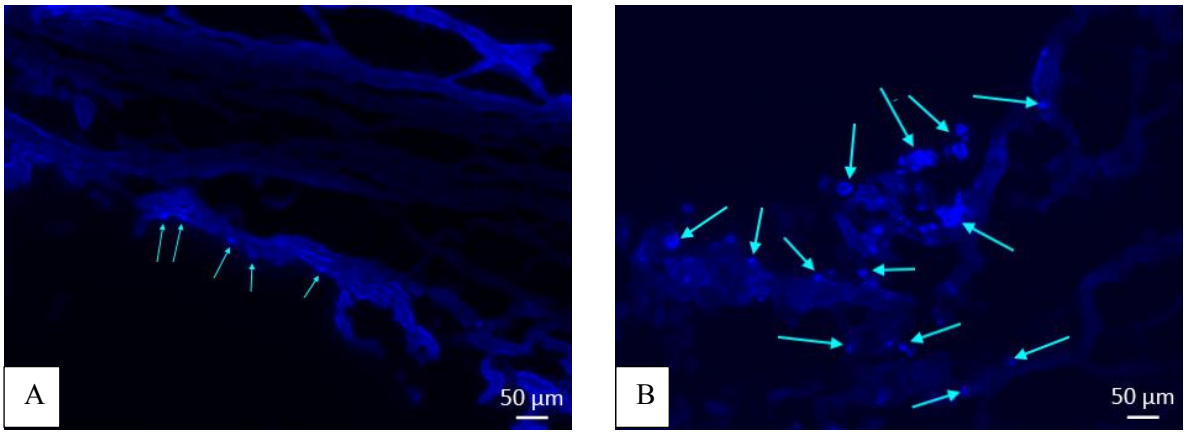

Figure 5.23: *Fluorescent microscopy of 750k cells on EPF of faba after 7 days.* ***A****: Non-coated scaffold.* ***B****: ECL-coated scaffold. Immunostained with Hoechst. Arrows indicating cells. The images are representative for 2 replicates. Scale bar 50 µm.*

The cells that attached to the EPF scaffolds from faba (Figure 5.23 **A** & **B**) were only in the layers available from the outside where the cells were applicated. The cells did not migrate towards to inner layers, data not shown. The cells applicated to EPF from faba with ECL seemed, by visual inspection, to attach more frequently than without ECL coating.

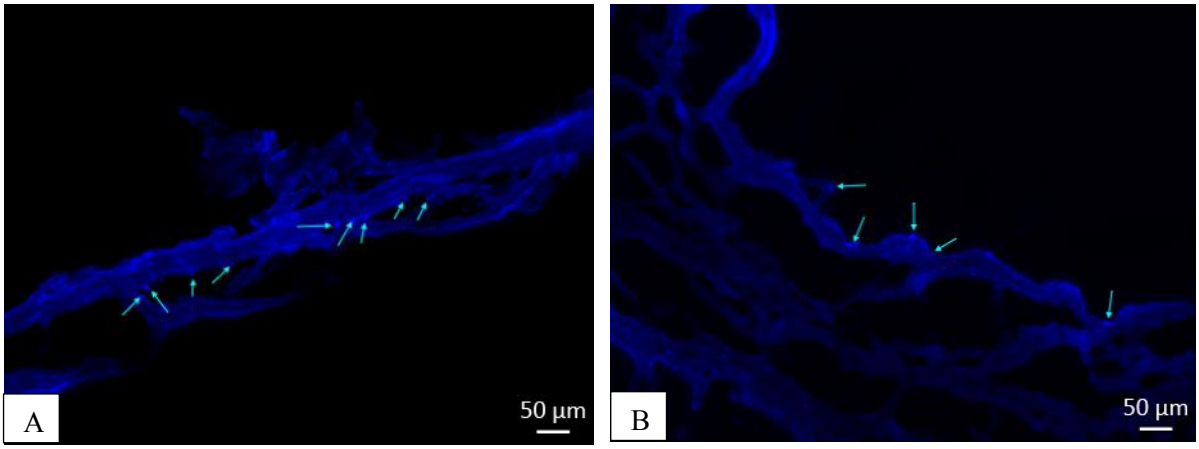

Figure 5.24: *Fluorescent microscopy of 750k cells on EPF of soy after 7 days.* ***A****: Non-coated scaffold.* ***B****: ECL-coated scaffold. Immunostained with Hoechst. Arrows indicating cells. The images are representative for 2 replicates. Scale bar 50 µm.*

The cells that attached to the EPF scaffold from soy (Figure 5.24 **A** & **B**) were only in the layers available from the outside when the cells were applied. The cells did not migrate towards to inner layers here either, data not shown. No difference in cell attachment was obtained between non-coated and ECL-coated EPF scaffolds from soy.

30k cells were seeded on the BNC scaffolds and cultured for 15 days. The development was followed using a light microscope.

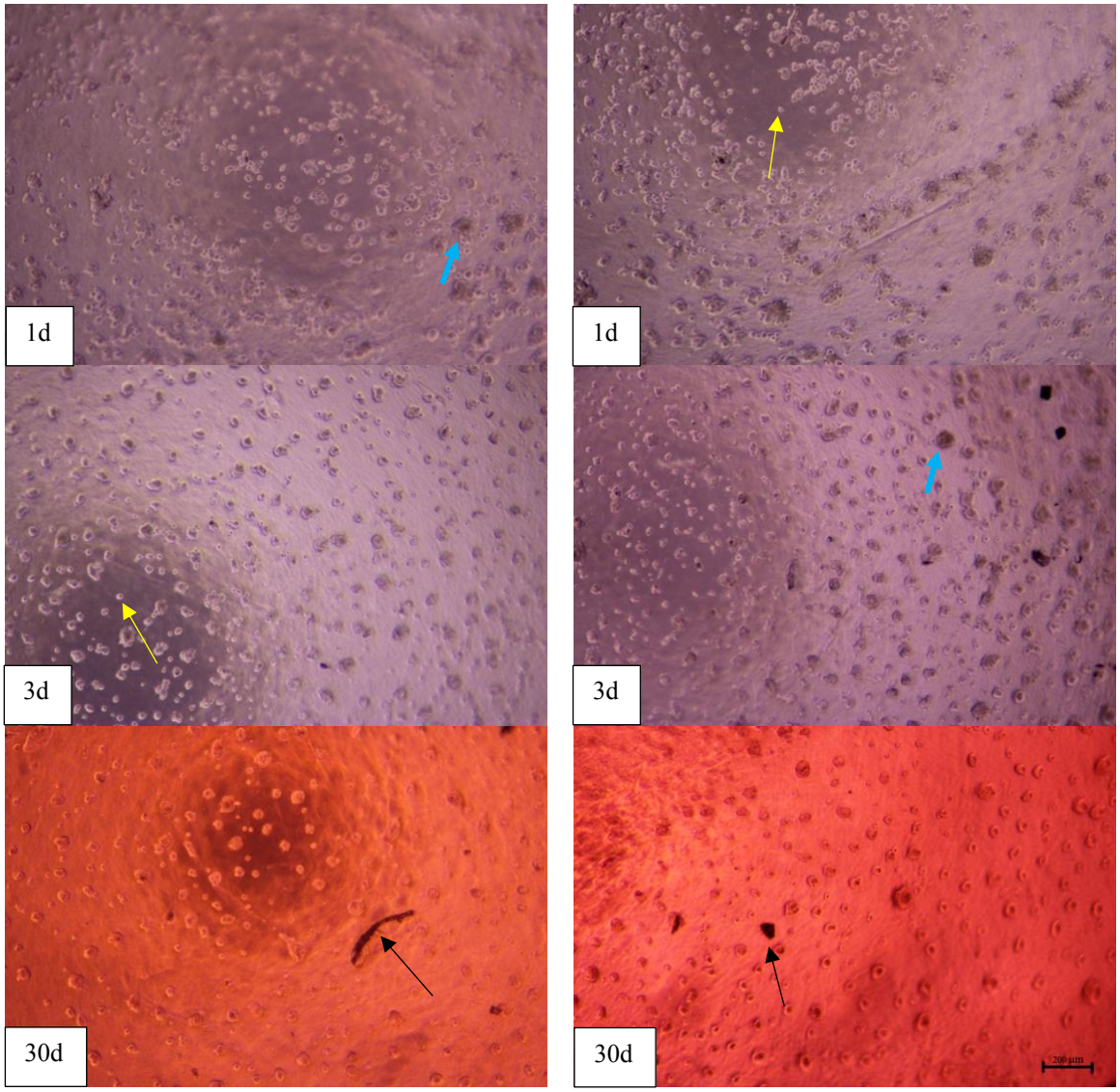

Figure 5.25: *Light microscopy pictures of 30k cells on BNC. On the left: without ECL, on the right: with ECL. Top: 1 day, middle: 3 days, bottom: 30 days.* ***Yellow arrows*** *indicate singular cells,* ***blue arrows*** *indicate clusters of cells, and* ***black arrows*** *indicate debris. The pH in the media is shown by a pH indicator (phenol red). Older media turns slightly more basic giving it a purple hue, while fresh media is at pH 7.4 (red). Cell medium was changed every 3-4 days. This experiment was only carried out once. The images are representative for 30 replicates. Microscopy images taken at 4x magnification. Scale bar seen in 30d with ECL-coating is 200 µm.*

There were no signs of the cells proliferating or differentiating from day 3 to day 30 (Figure **5.25**), therefore the cell count was increased to determine if a higher cell density resulted in better proliferation.

After the reevaluation, 300k cells were seeded on the BNC scaffolds for 15 days. Cell expansion was monitored using a light microscope on day 1, 3 and 15.

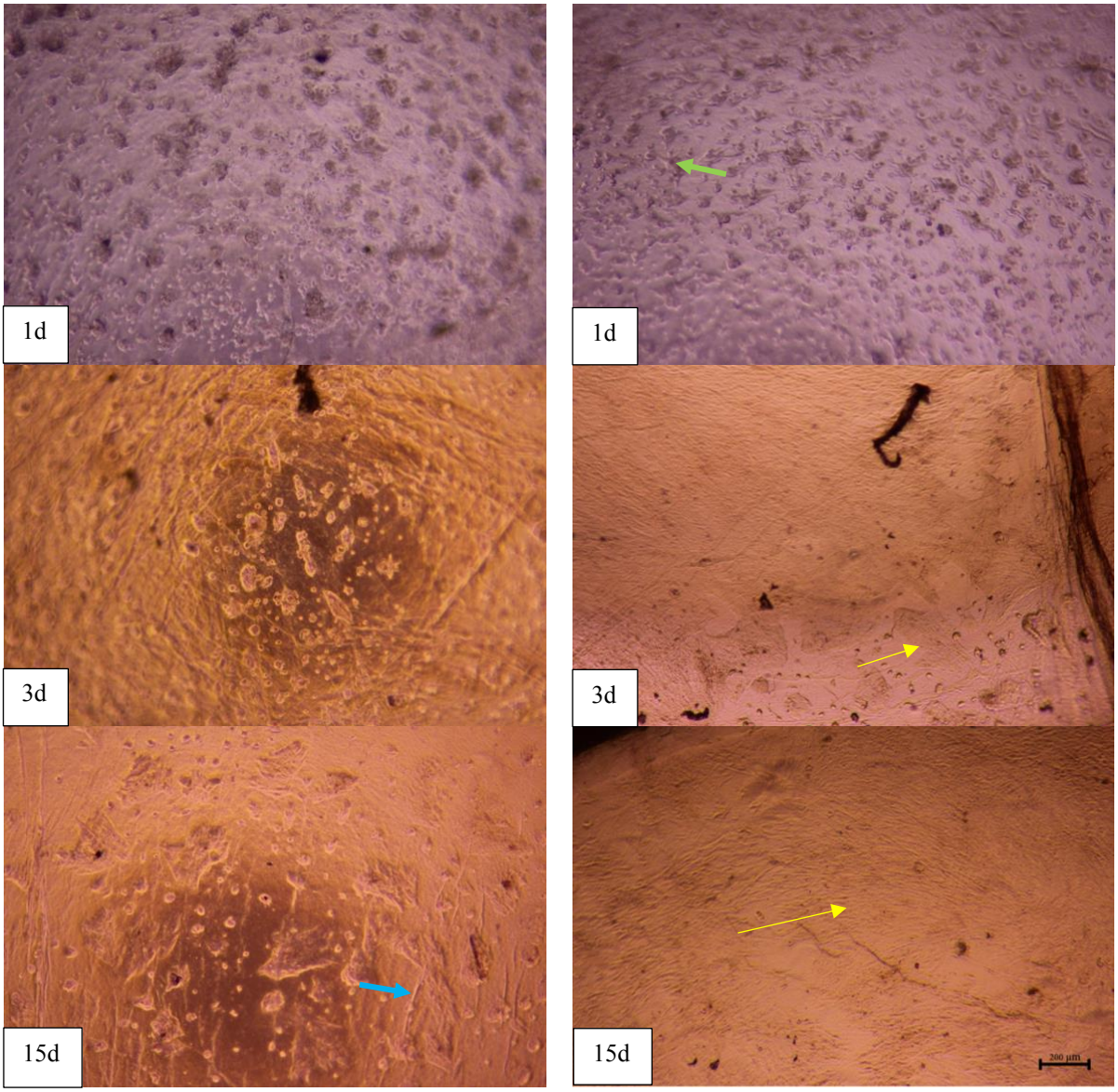

Figure 5.26: *Light microscopy pictures of 300k cells on BNC. Cell medium was changed every 3-4 days. This experiment was carried out in two repetitions. On the* ***left****: without ECL, on the* ***right****: with ECL.* ***Top****: 1 day,* ***middle****: 3 days,* ***bottom****: 15 days.* ***Green arrow*** *indicates the morphology of a proliferating myoblast,* ***blue arrow*** *indicates a singular myotube, and* ***yellow arrows*** *indicate alignment of myotubes. Color change from day 1 to day 3 and 15 is due to how new the media used was, with red color being fresh. The images are representative for 16 replicates. Microscopy images taken at 4x magnification. Scale bar seen in 15d with ECL-coating is 200 µm.*

The light microscopy images (Figure **5.26**) show a comparison of cell proliferation and differentiation on scaffolds with (**right**) and without (**left**) ECL coating of the BNC. The BNC scaffolds coated with ECL showed a much higher confluency on the surface of the scaffold, were the cells on the BNC without ECL tended to cluster together.

The BNC scaffolds were immunostained with NucBlue, Phalloidin 488, rabbit anti-Desmin followed by Alexa 546-conjugated goat anti-rabbit and after 2 and 15 days to determine the cell growth in regards of proliferation and differentiation. The experiment was carried out in two repetitions. Immunofluorescent images are present first, mRNA expression thereafter.

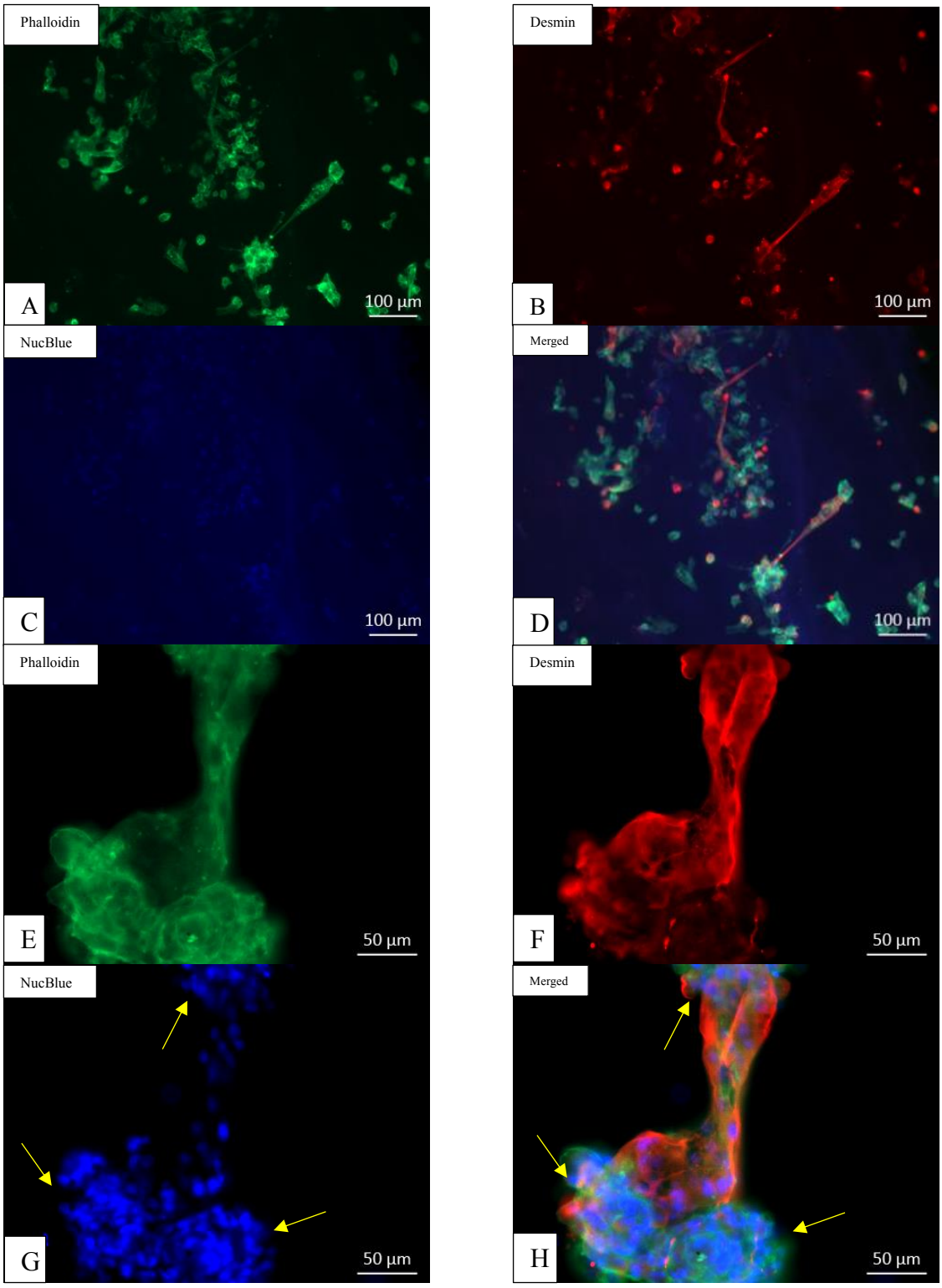

Figure 5.27: *Fluorescent microscopy of 300k cells on BNC without ECL after 2 days incubation. Immunostained with* ***A, E****: Phalloidin 488 (green),* ***B, F****: rabbit anti-Desmin, followed by Alexa 546-conjugated goat anti-rabbit (red),* ***C, G****: NucBlue Live Cell Stain (blue),* ***D, H****: Merged images.* ***Yellow arrows*** *indicating cell clusters. The images are representative for 16 replicates. Scale bar* ***A-D****: 100 µm*, **E-H**: 50 *µm.*

After 2 days on BNC without ECL-coating (Figure **5.27**) myotubes can be seen formed during differentiation (**A, B**), with desmin filaments forming in the myotubes (**B, F**). The myotubes

contain more than one nucleus clustered together (**C, G**). The cell clusters are forming an intercellular bridge through cytoplasmic connections (**E, F, H**).

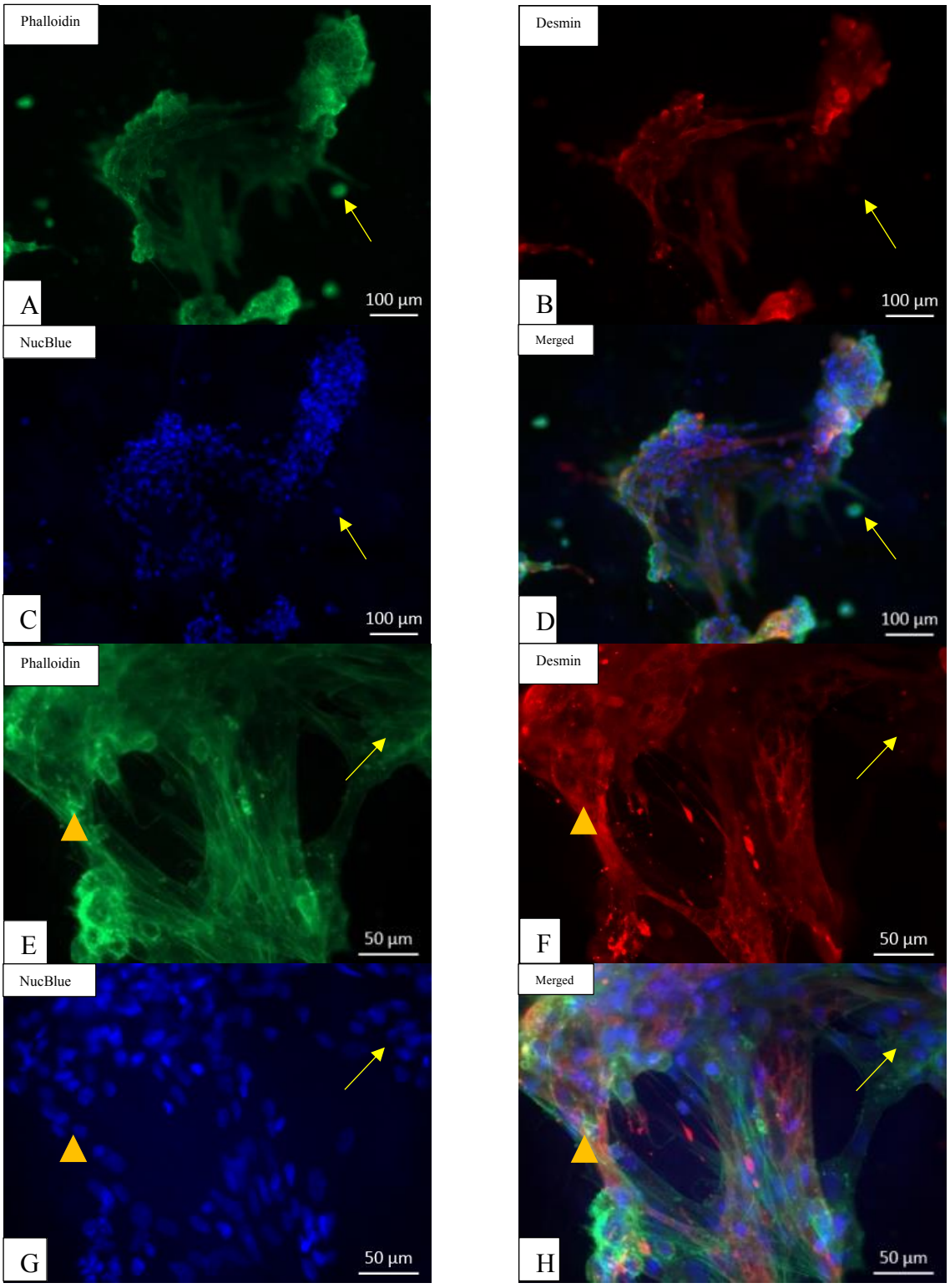

Figure 5.28: *Fluorescent microscopy of 300k cells on BNC coated with ECL after 2 days incubation. Immunostained with* ***A, E****: Phalloidin 488 (green),* ***B, F****: rabbit anti-Desmin, followed by Alexa 546-conjugated goat anti-rabbit (red),* ***C, G****: NucBlue Live Cell Stain (blue), and* ***D, H****: Merged images.* ***Yellow arrows*** *indicate proliferating cells. The top of the* ***yellow triangle*** *indicates a cell that has initiated differentiation. The images are representative for 16 replicates. Scale bar* ***A-D*** *100 µm,* ***E-H****: 50 µm.*

After 2 days incubation on ECL-coated scaffolds (Figure **5.28**) some cells outside this complex cell structure are cells still in the proliferating stage shown with yellow arrows (**A–D**). The lack of desmin is an indication for proliferating cells (**B, F**). In immunofluorescent microscopy images of cells grown on BNC with ECL coating (Figure **5.28**) the myotube configuration seem more complex than without ECL (Figure **5.27**) after incubation for 2 days.

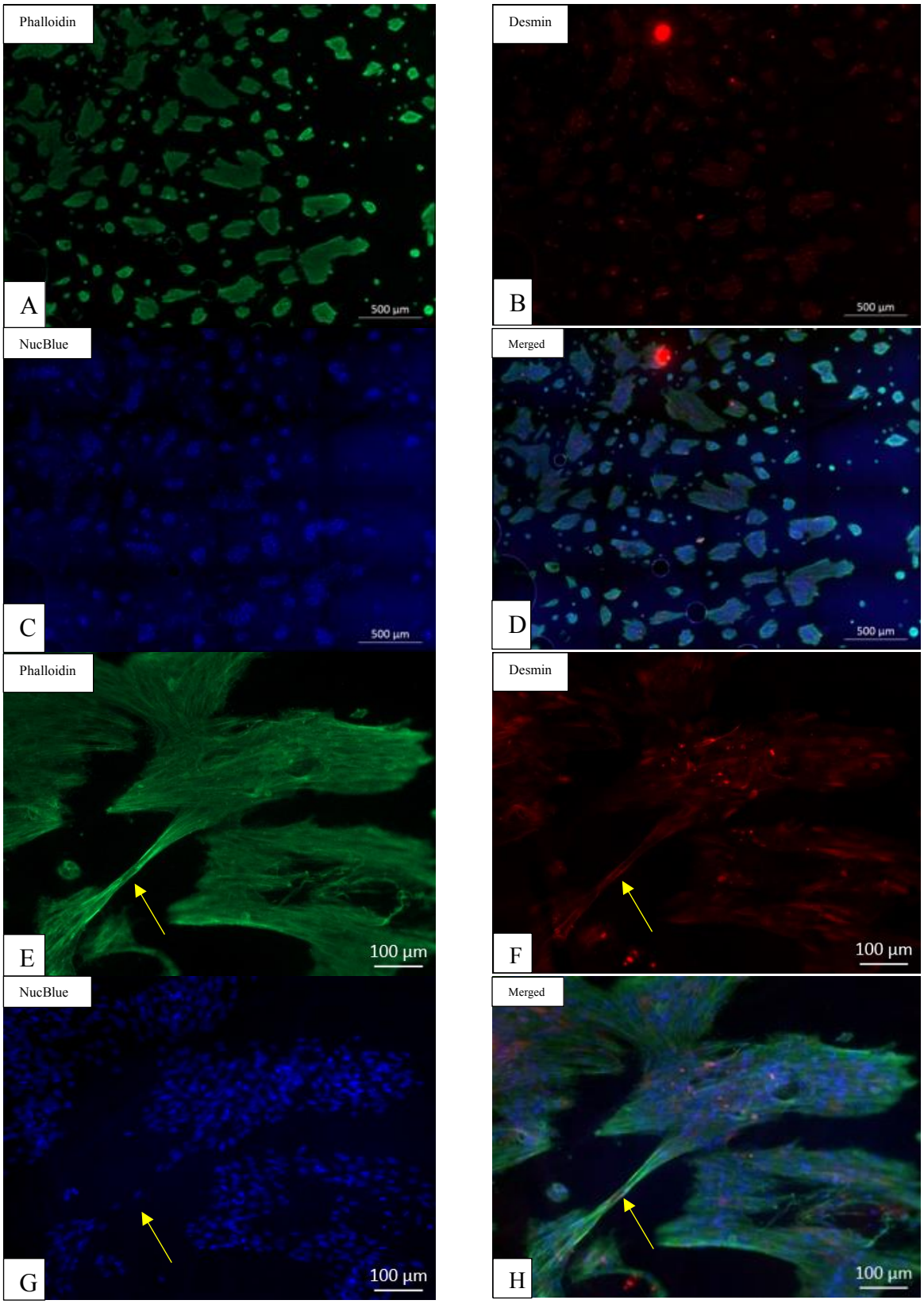

Figure 5.29: *Fluorescent microscopy of 300k cells on BNC without ECL after 15 days incubation. Immunostained with* ***A, E****: Phalloidin 488 (green),* ***B, F****: rabbit anti-Desmin, followed by Alexa 546-conjugated goat anti-rabbit (red),* ***C, G****: NucBlue Live Cell Stain (blue),* ***D, H****: Merged images.* ***Yellow arrow*** *indicates intercellular bridging. The images are representative for 16 replicates. Scale bar* ***A-D****: 500 µm,* ***E-H****: 100 µm.*

After 15 days incubation the immunofluorescent microscopy images (Figure **5.29**) show an overview over the cell clusters on the non-coated BNC scaffold. Within the cell clusters F-actin filaments seem to be aligned (**A, E**), and desmin filaments were forming (**B, F**). The nucleuses gathered in clusters (**C, G**). In the intercellular bridge seen marked by a yellow arrow (**E-H**), very few nucleuses are present. The bright red dot was a droplet from the mounting medium causing disturbance, making the red staining appear weaker (**B, D**).

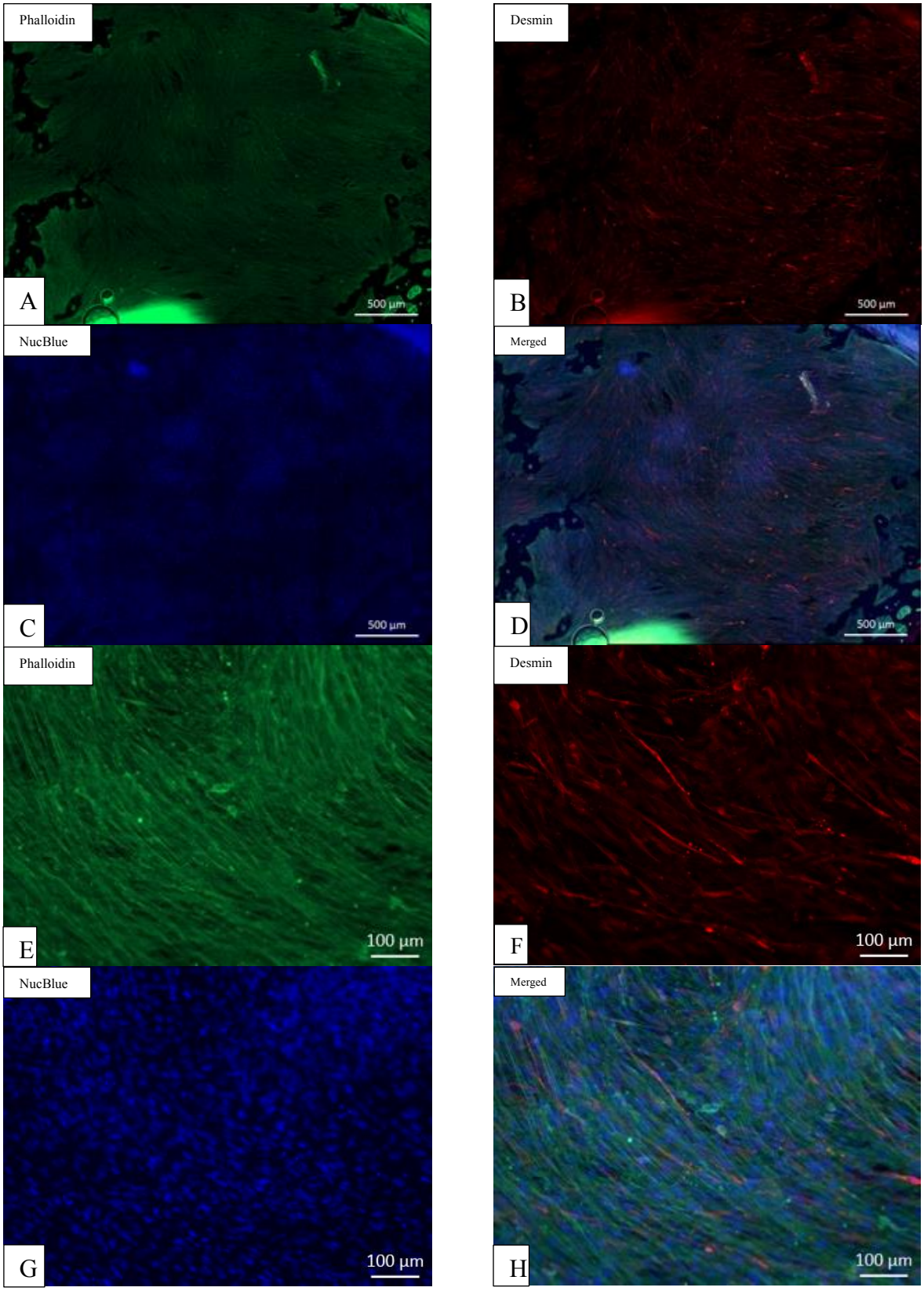

Figure 5.30: *Fluorescent microscopy of 300k cells on BNC with ECL coating after 15 days. Immunostained with* ***A, E****: Phalloidin 488 (green),* ***B, F****: rabbit anti-Desmin, followed by Alexa 546-conjugated goat anti-rabbit (red),* ***C, G****: NucBlue Live Cell Stain (blue), and* ***D, H****: Merged images. The images are representative for 16 replicates. Scale bar* ***A-D****:500 µm,* ***E-H****: 100 µm.*

After 15 days (Figure **5.30**) the immunofluorescent microscopy images show an overview over the BNC scaffold with ECL coating. Myotube formation is seen throughout the scaffold. In the myotubes F-actin arrangement can be seen (**A, E**) together with desmin filament formation (**B, F**). The BNC scaffold is filled with a big cluster of nucleuses (**C, G**). The merged images of cells grown on BNC with ECL coating gives an appreciation of how F-actin and desmin is forming together and aligning when nucleuses are spread over the whole BNC scaffold (**D, H**).

The cells were analyzed for their mRNA expression of myogenic and adhesion markers on the initial cell batches used in the experiment, and 2- and 15-days growth on BNC scaffolds.

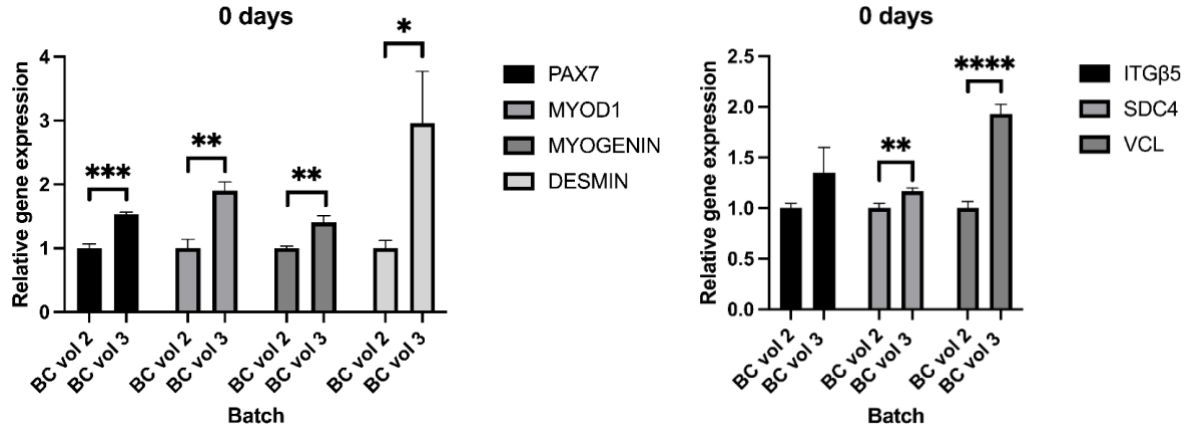

Figure 5.31: *Relative gene expression of muscle specific markers (PAX7, MYOD1, MYOGENIN), differentiation marker (DESMIN), and adhesion markers (ITGβ5, SDC4, VCL) from cell batch used in BNC experiments before seeding on BNC scaffolds.* ***BC vol 2****: first repetition,* ***BC vol 3****: second repetition. BC vol 2 set as benchmark. The data is presented as the average of technical triplicates and representative for 16 replicates. Error bars illustrate SD. * = $p < 0.05$, ** = $p < 0.01$, *** = $p < 0.001$, **** = $p < 0.0001$.*

In the cell batch used in the second repetition (BC vol 3) Pax7, MyoD1, myogenin, and desmin, as well as cell receptor SDC4 and cytoskeleton/focal adhesion molecule VCL was higher expressed compared to the cell batch used in the first repetition (BC vol 2) (Figure **5.31**). No difference in mRNA expression of cell receptor ITGβ5 was obtained.

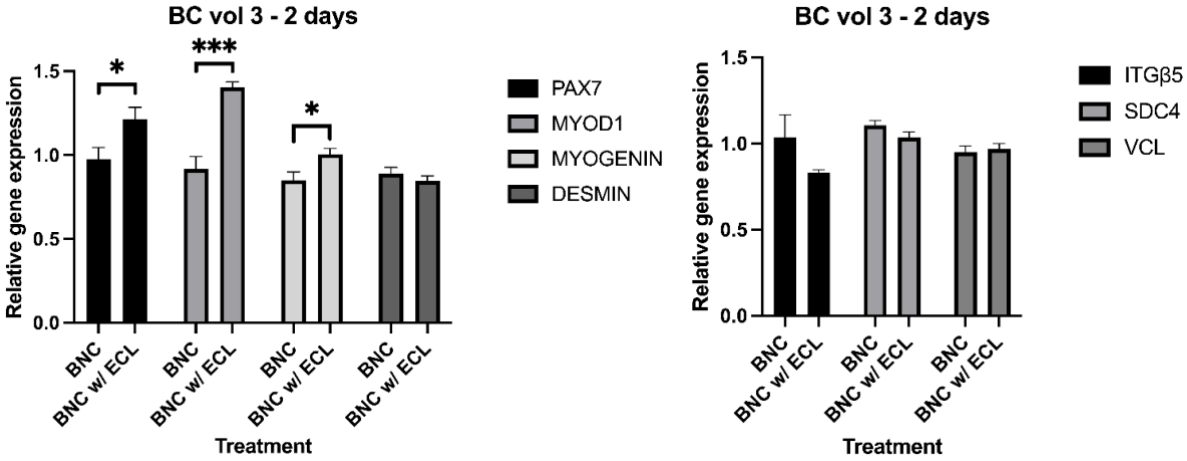

Figure 5.32: *Relative gene expression of muscle specific markers (PAX7, MYOD1, MYOGENIN), differentiation marker (DESMIN, and cell adhesion markers (ITGβ5, SDC4, VCL) from cells grown on BNC for 2 days, experiment 2. BNC without ECL-coating was set as benchmark to see how ECL-coating impact gene expression. The data is presented as the average of technical triplicates and representative for 16 replicates. Error bars illustrate SD. * = p < 0.05, *** = p < 0.001.*

After 2 days culturing (Figure **5.32**) Pax7, MyoD1, and myogenin was higher expressed in ECL-coated scaffolds compared to non-coated scaffolds. No difference in desmin mRNA expression was obtained. Likewise, for cell receptors ITGβ5 and SDC4 and cytoskeleton/focal adhesion molecule VCL no difference in expression was obtained.

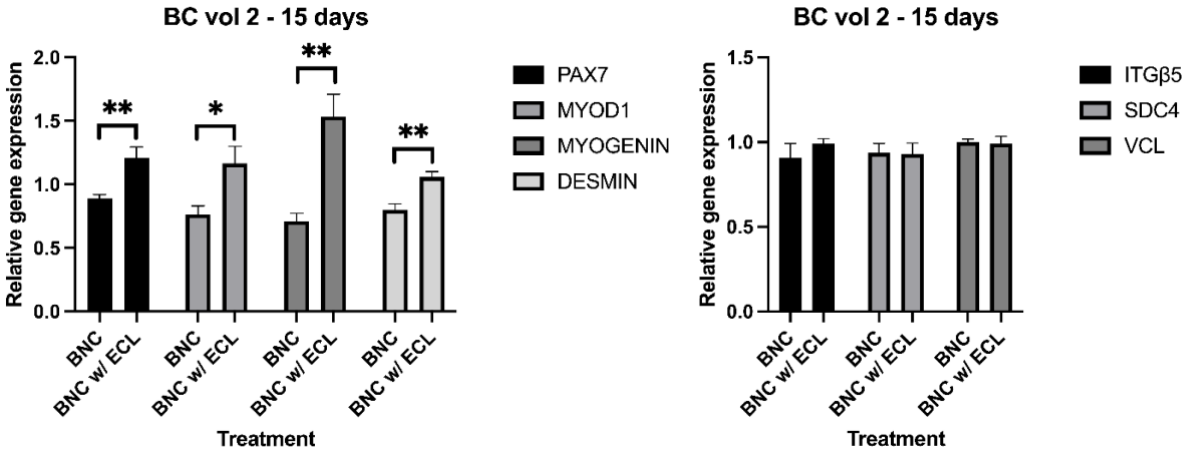

Figure 5.33: BNC vol 2. *Relative gene expression of muscle specific markers (PAX7, MYOD1, MYOGENIN), differentiation marker (DESMIN, and cell adhesion markers (ITGβ5, SDC4, VCL) from cells grown on BNC for 15 days, experiment 1. BNC without ECL-coating was set as benchmark to see how ECL-coating impact gene expression. The data is presented as the average of technical triplicates and representative for 16 replicates. Error bars illustrate SD. * = p < 0.05, ** = p < 0.01.*

After 15 days culturing in the first repetition (Figure **5.33**), Pax7, MyoD1, myogenin, and desmin was higher expressed in ECL-coated scaffolds compared to non-coated scaffolds. For

cell receptors ITGβ5 and SDC4 and cytoskeleton/focal adhesion molecule VCL no difference in mRNA expression was obtained.

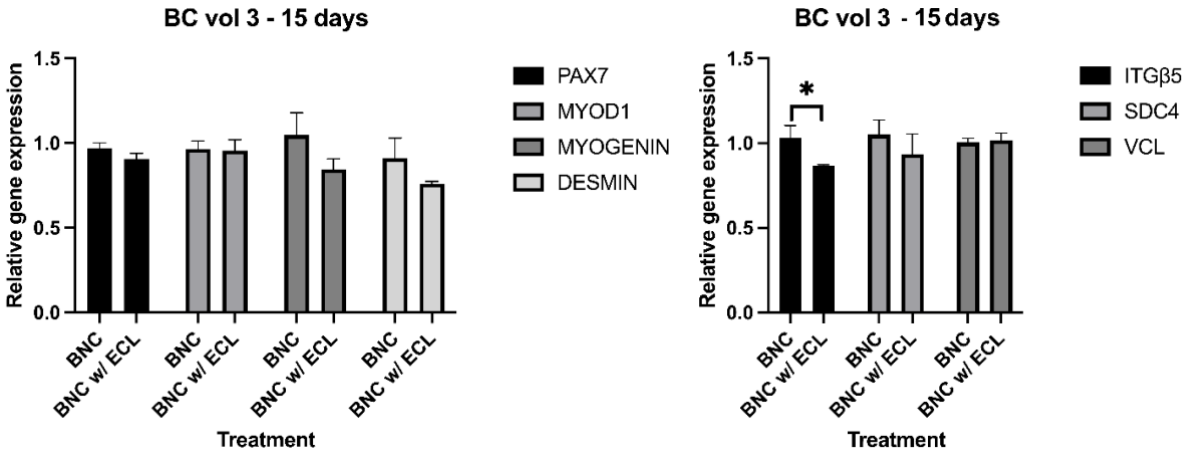

Figure 5.34: BNC vol 3. *Relative gene expression of muscle specific markers (PAX7, MYOD1, MYOGENIN), differentiation marker (DESMIN), and cell adhesion markers (ITGβ5, SDC4, VCL) from cells grown on BNC for 15 days, experiment 2. BNC without ECL-coating was set as benchmark to see how ECL-coating impact gene expression. The data is presented as the average of technical triplicates and representative for 16 replicates. Error bars illustrate SD. * = $p < 0.05$.*

After 15 days culturing in the second repetition (Figure **5.34**), cell receptor ITGβ5 was higher expressed in non-coated scaffolds compared to ECL-coated scaffolds. Pax7 MyoD1, myogenin, and desmin, as well as cell receptor SDC4 and cytoskeleton/focal adhesion molecule VCL no difference in expression was obtained.

The cells that had expanded on the BNC scaffolds for 30 days were trypzinated off the scaffolds and redistributed to wells coated with ECL to see if they were still viable, able to proliferate and differentiate. The cells seeded in the wells were not counted.

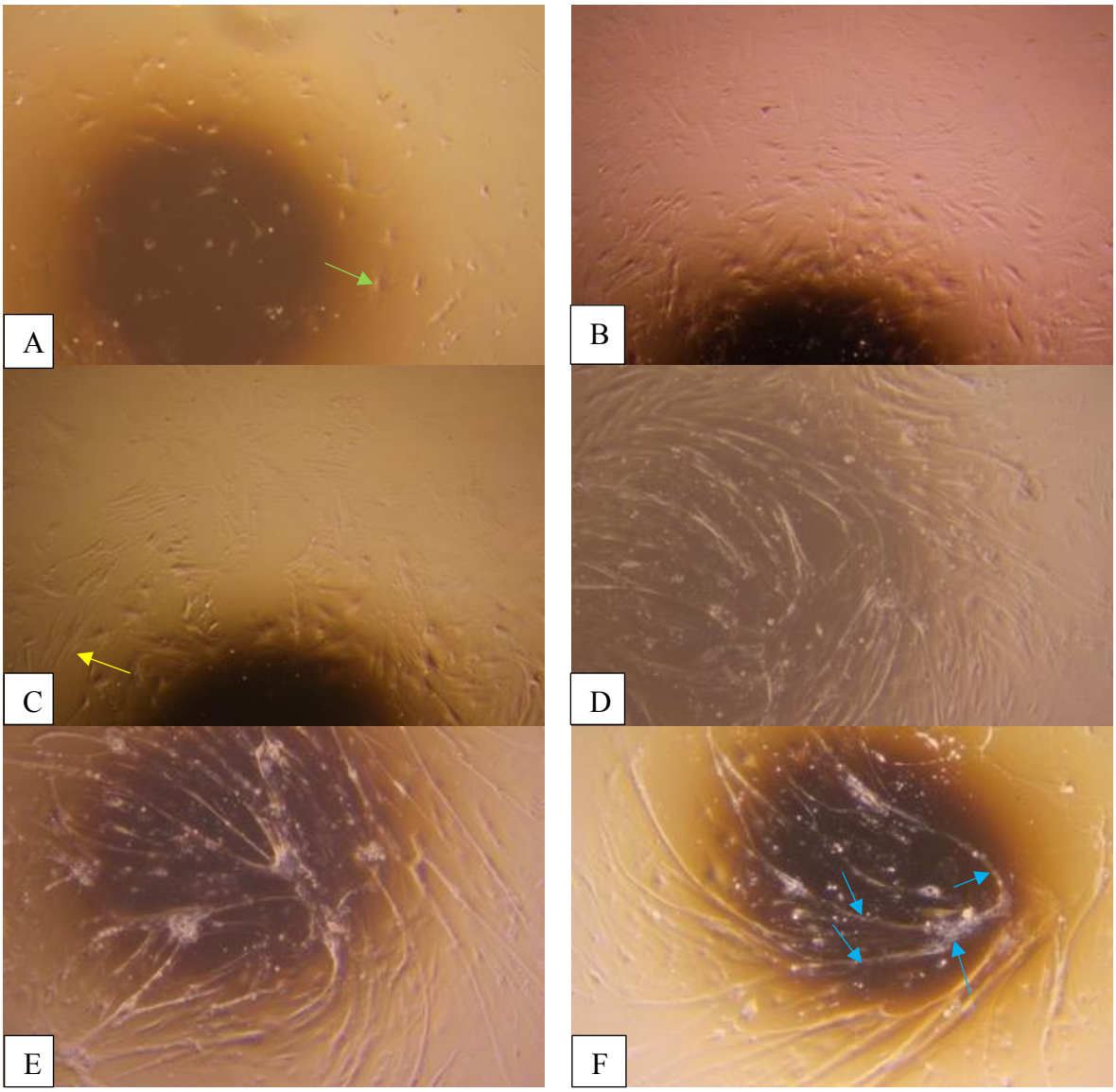

Figure 5.35: *Cells grown on BNC grown for 30 days, trypzinated off and redistributed in wells with PM. Cell medium was changed every 3-4 days.* ***A****: 3 days,* ***B****: 7 days,* ***C****: 10 days, and* ***D****: 14 days. PM was exchanged for DM (****E-F****).* ***E****: 3 days after induced differentiation, and* ***F****: 7 days after induced differentiation.* ***Green arrow*** *indicates the morphology of a proliferating myoblast,* ***yellow arrow*** *indicates aligning myoblasts, and* ***blue arrows*** *indicate connected myotubes. The images are representative for 2 replicates. Images are taken with x4 magnification.*

The cells were still viable after being redistributed to ECL-coated wells (Figure 5.35 **A-C**) and had initiated spontaneous differentiation to form myotubes on day 14 (**D**). PM was substituted with DM after 14 days to induce differentiation. The myotubes started to fuse together after DM induced differentiation (**E, F**).

This experiment was also conducted on cells grown on BNC coated with ECL for 30 days.

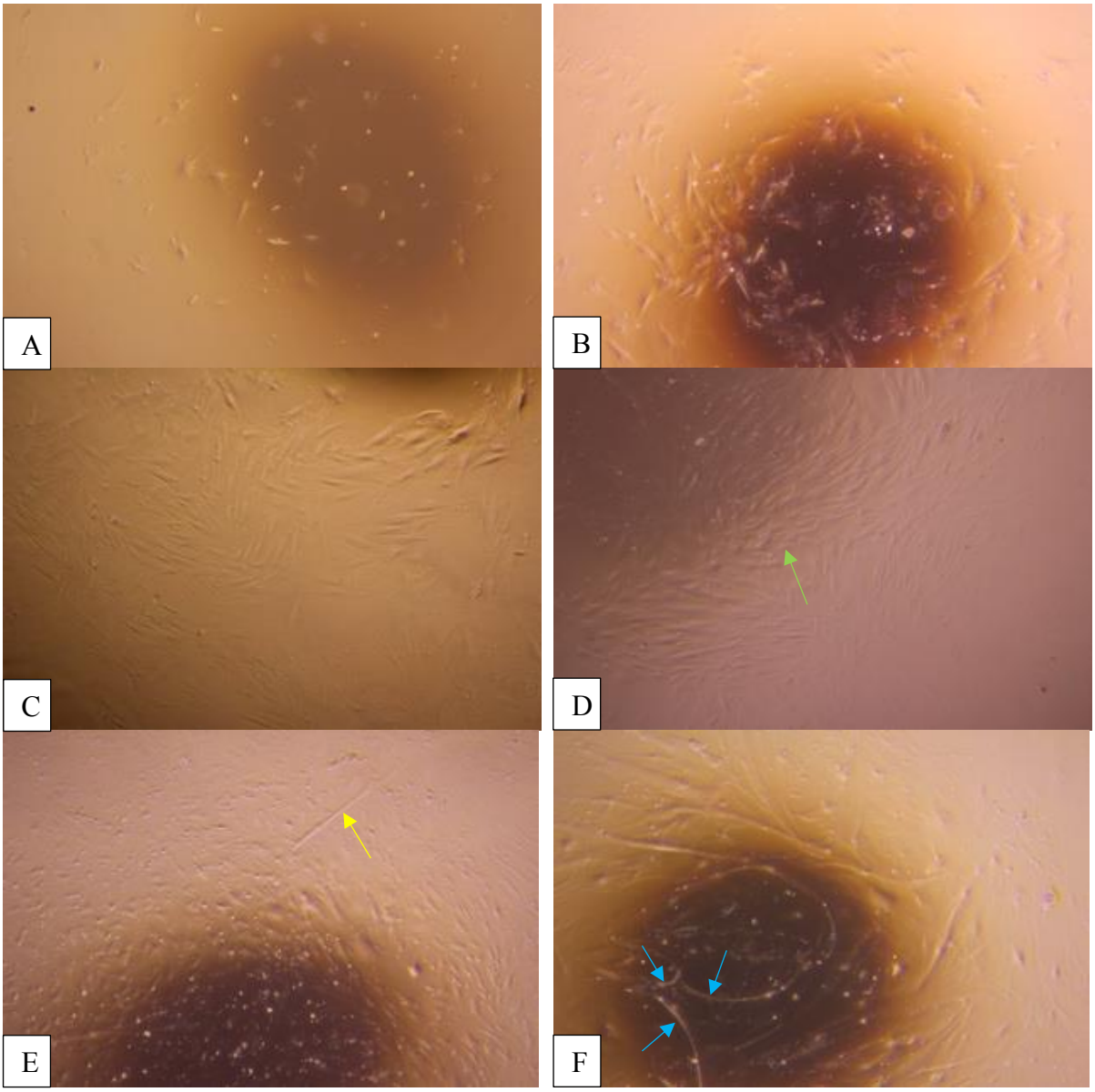

Figure 5.36: *Cells grown on BNC coated with ECL grown for 30 days, trypzinated off and redistributed in wells with PM. Cell medium was changed every 3-4 days.* ***A****: 3 days,* ***B****: 7 days,* ***C****: 10 days, and* ***D****: 14 days. PM was exchanged for DM (****E-F****).* ***E****: 3 days after induced differentiation, and* ***F****: 7 days after induced differentiation.* ***Green arrow*** *indicates aligning myoblasts,* ***yellow arrow*** *indicates a singular myotube, and* ***blue arrows*** *indicate connected myotubes. The images are representative for 2 replicates. Images are taken with x4 magnification.*

The cells were still viable after being redistributed to ECL-coated wells (Figure 5.36 **A-C**). There was some formation of myotubes (**D**). PM was substituted with DM after 14 days to induce differentiation. There were a few myotubes forming after day 3 (**E**), but the differentiation and myotube formation were much more visible after 7 days (**F**).

6. Discussion

6.1 Production of EPF and BNC scaffolds

Initially it was thought that the EPF scaffolds would be sterile exiting the extruder, but the incubation in DMEM Glutamax and dH_2O showed otherwise. 70% ethanol was the first sterilizing technique used because it is less invasive towards the EPF scaffolds as other sterilizing techniques and not an antibiotic that could potentially harm the mitochondria in the muscle cells (Suárez-Rivero, et al., 2021) if not washed away properly after sterilization. In such small quantities as used in the sterilization, it is deemed non-toxic for oral ingestion (Matteucci, 2012), which means it could safely be used in CBM production. The ethanol sterilization was successful in inhibiting further bacterial growth but did not manage to neutralize them and thus other methods was needed.

The idea of sterilizing with Pen-Strep and Fungizone came from these reagents already being utilized in the cell medium. The combination of penicillin and streptomycin eliminate bacteria by inhibiting the peptidoglycan synthesis for bacterial cell wall maintenance (penicillin) (Mucsi, et al., 2013) and by inhibiting protein synthesis in bacterial ribosome (streptomycin) (Sharma, Cukras, Rogers, Southworth, & Green, 2007). The Fungizone binds to ergosterol in the cell membrane of most fungi and causes formation of ion channels which leads to loss of protons and monovalent cations. In turn this leads to concentration-depending cell killing and depolarization (Noor & Preuss, 2022). Fungizone also causes oxidative damage to the cells, increasing membrane permeability and the production of free radicals, as well as having a stimulatory effect on phagocytic cells, which aids in the removal of fungal infections (Noor & Preuss, 2022). There were no fungi on the plates, but the bacteria showed resistance against Pen-Strep concentration used in cell media. These findings made it necessary to pre-sterilize the EPF scaffolds before cell seeding.

After the bacteria were identified as *Burkholderia cepacia* and *Ralstonia* insidiosa using MALDI-TOF, literature showed that *B. cepacia* (Ryan & Adley, 2013) and *R.* insidiosa (de Souza, et al., 2018) are susceptible to Co-trimoxazole treatment. Trimethoprim is a synthetic antibacterial drug that inhibits the di-hydrofolate reductase enzyme (DHFR), found in *Ralstonia spp., t*o target folate biosynthesis. Sulfonamides, another chemotherapeutic drug that targets the di-hydropteroate synthase (DHPS) enzyme, found in *Burkholderia spp.* in the same pathway, is frequently administered alongside trimethoprim in a synergistic manner

(Sánchez-Osuna, Cortés, Llagostera, Barbé, & Erill, 2020). PS and FZ were added in case of presence of other bacteria and fungi in all sterilization attempts with Co-trimoxazole. Due to the successful sterilization with sulfamethoxazole and trimethoprim concentration (23.75/1.25 µg/ml) according to literature (Ryan & Adley, 2013), we wanted to find out the least amount of Co-trimoxazole needed to get rid of the bacteria. The lowest concentration tested of sulfamethoxazole and trimethoprim (9.5/0.5 µg/ml) was also successful. This concentration was not continued into the pre-sterilization treatment of the EPF scaffolds due to the uncertainty of the bacteria amount in each scaffold, and it would therefore put other ongoing experiments in the incubator at risk. The mass sterilization attempt was not successful even after 72 hours in an antibiotic mixture. A hypothesis of why it was not successful is that the bacteria either developed mutational resistance or by acquiring resistance through horizontal gene transfer (Munita & Arias, 2016). The agar plates of EPF from faba showed that there was an exponential increase in colonies over the incubation period, which are results that substantiates the hypothesis.

Ryu et al. (2017) problematizes the usage of antibiotics in cell medium as it potentially can alter the transcription factors and gene expression and pathways from their basal state, with Activating Transcription Factor 3 (ATF3) being one of the most notable. Another problematic aspect of antibiotic use in cell medium is the emergence of antibiotic resistance and how it may cause illness humans through ingestion of resistant bacteria (Chang, Wang, Regev-Yochay, Lipstich, & Hanage, 2014). Due to the interest in keeping the pre-sterilization of scaffolds antibiotic-free, heat sterilizing techniques were attempted. In the dry heat sterilization, the EPF scaffolds were subject for Maillard reaction (Rufían-Henares & Pastoriza, 2016) giving them a coarse and burnt exterior. The oxidation of reducing sugars to the corresponding lactones, which in aqueous media hydrolyze to acids, is catalyzed by oxidoreductases. In the end, the redox process produces hydrogen peroxide, which may then cause additional undesirable protein modification and lipid peroxidation (Lund & Ray, 2017). In turn, hydrogen peroxide produces reactive oxygen species which may lead to DNA damage, cell damage and in worst case cell death (Kang, et al., 2014). In the samples that were wet heat sterilized, the EPF scaffolds denatured, and the starch gelatinized (Black, Tziboula-Clarke, White, Iannetta, & Walker, 2020) in the bottom of the tubes thus leaving the interior of the EPF scaffold from faba exposed. The gelatinization, or lack thereof, of starch is a probable reason for why the gelatinization of EPF scaffolds from soy was not as prominent as in the EPF scaffolds from faba as the soy contains, as previously mentioned, very little

starch. Both heat sterilizing methods in combination with Pen-Strep and Fungizone incubation were deemed successful, but the methods are not suitable for the EPF material. The newly extruded batches of EPF scaffolds did not withstand being in a liquid over time as they disintegrated during the experiment making it unfeasible to check for cell adherence and growth by cryosectioning. The following EPF scaffold experiment was discontinued due to bacterial growth. As there was not enough time left to conduct further experiments on EPF scaffolds, it is still uncertain if these scaffolds are eligible as scaffolds for CBM production.

To track the origin of bacterial infection, the water and legume protein fractions used in the experiment was incubated with DMEM Glutamax for 7 days and spread out on agar plates. The results came back positive for bacterial growth on all plates, but the bacteria in the water sample had different morphology and color from the soy and faba samples who were similar to the colonies found in the plates that were identified. This result indicates that the bacteria come from the soy and faba powder, and thus the source of bacteria is originating from the manufacturer of these commercial protein concentrates. DMEM Glutamax was used as the liquid source in order to eliminate the water sample as a possible contaminator. It was also used to increase the bacterial count in case of a low initial amount but in hindsight, with the long incubation period, it was probably not necessary as the agar plates showed great numbers of colonies in all samples.

Bacterial contamination is common in food and foodstuff grown in fields, but a lot of the bacteria is either sterilizable, not as persistent as *Burkholderia cepacia* and *Ralstonia insidiosa,* or the materials are pre-sterilized to avoid invasive sterilizing techniques. Different sterilization methods such as UV irradiation and gamma irradiation was considered. UV irradiation does not penetrate deep enough to fully sterilize the extruded scaffolds (Wollweber, Krebs, Anders, Heinrich, & Tronnier, 2008), however, it could possibly be used to sterilize the legume powder. Gamma irradiation has been proven successful in sterilized EPF of soy (Ben-Arye, et al., 2020), but due to lack of equipment in Norway, and the regulation of gamma irradiation being only allowed in spices sold in Norway (Lovdata, 2001), the idea was discarded as there would need to be found another successful way of sterilizing the EPF scaffolds if they were to be utilized in Norwegian CBM production. As the bacteria producing the BNC are easily removed through the method explained in 4.1.2, in addition to being a more stable structure, BNC is more eligible as a scaffold compared to EPF.

6.2 Biomaterial properties of EPF and BNC scaffolds

From the exterior of the scaffolds, they look suitable as a 3D scaffold for CBM. The shape of the structure looks by visual inspection beneficiary for formation and alignment of myofibrils due to the elongated structure of both myofibrils and scaffolds. The internal structure of the EPF were analyzed trough cryosectioning the EPF pieces for visualization of the pore structure with a light microscope. This was done to determine whether the pores in the structure were big enough for myoblast migration as well as distribution of nutrients and oxygen to the cells, and waste products transportation (Bomkamp, et al., 2022). A requirement for the scaffold is that its pore structure allows for cell adhesion, proliferation, differentiation, and myofiber maturation. Muscle fibers in terrestrial animals are approximately 10-100 μm in diameter (Lebret, et al., 2016), and therefore the pore size is required to be larger than 100 μm to allow myotubes to mature into myofibers. The pore size diameter is highly dependent on cell type as fibroblast showed optimal growth on a poly(ethyleneglycol terephthalate)-poly(butylene terephthalate) (PEGT-PBT) copolymer scaffold with 200 μm pores (Wang, Pieper, Péters, van Blitterswijk, & Lamme, 2005), and mesenchymal stem cells preferred 300 μm pores in their collagen-hyaluronic acid scaffolds (Matsiko, Gleeson, & O'Brien). Hutmacher (2000) explains that pore sizes of 300-500 μm would be beneficiary for increased diffusion rates of nutrients and by-products to and from the center of the scaffold, though pore sizes alone would not be sufficient in large scaffold volumes. He further explains that a bioreactor would be needed to mimic the fluid-dynamic of interstitial fluid conditions. As some of the main pores in both structures measured >300 μm, they were deemed suitable for usage as a 3D structured scaffold for migration of cells, and transport and exchange of cell media, oxygen, and waste products. The mean pore size also influences the cell morphology and phenotypic expression (Nehrer, et al., 1997). The mechanical strength is compromised when pore size increases (Loh & Choong, 2013), which may have been a reason behind the scaffolds disintegrating during incubation. The cryosection images also revealed a majority of smaller pores (<100 μm) which would be accounted for as vascularization of the scaffold and plays an important part in transport and exchange of media, oxygen, and waste products (Visconti, et al., 2010). It also shows that the scaffold architecture is highly interconnected, which promotes tissue ingrowth and regeneration (Whang, Thomas, Healy, & Nuber, 1995).

Microcarriers (MC) has frequently been successfully used to expand isolated cells (Verbruggen, Luining, van Essen, & Post, 2018); (Andreassen, et al., 2022). Porous MCs are

small, solid, and frequently spherical beads that has a high surface area to volume ratio compared to monolayered cultures. They possess physical properties such as porosity, density, rigidity, and surface chemistry (Cahn, 1990). Commercially available MCs are often made of non-edible materials that require surface treatment such as texturizing, ECM protein coating or ionic charge to promote cell adherence, due to not having the desired topography, epitopes or pore size for cell adherence (Tavassoli, et al., 2018); (Chen, Chen, Choo, Reuveny, & Oh, 2011). When growing cells on a non-edible MC, a chemical or mechanical dissociation step after cell expansion is required, often resulting in a significant cell or tissue yield loss in addition to cost increase (Bodiou, Moutsatsou, & Post, 2020), followed by differentiation in a different system. A solution to this problem could be to carefully degrade the MCs by biochemical and thermal degradation (Bodiou, Moutsatsou, & Post, 2020). Food-grade MCs often lack structural stability required in bioreactor experiments (Andreassen, et al., 2022), however, the dissociation/ degradation step is not required as the MCs would be a part of the end product. With that being said, a food-grade 3D-structured scaffold that would be a part of, have nutritious value, and aid in organoleptic properties in the end product, seem like a more desirable way of growing CBM.

The iodine staining of EPF cryosections from faba beans showed positive results for amylose and amylopectin, the two constituents of starch. This corresponded with literature (Punia, Dhull, Sandhu, & Kaur, 2019) saying starch is the main component of faba beans. Starch-based scaffolds has been shown to support cell adhesion (Mirab, Eslamian, & Bagheri, 2018), proliferation (Santos, et al., 2009) and differentiation (Rodrigues, Gomes, Leonor, & Reis, 2012). The reddish color in the iodine staining comes from a slight affinity between amylopectin and iodine (Jackson, 2003), and the intensity of the color can be seen as amylopectin is the main constituent in the faba bean starch (Punia, Dhull, Sandhu, & Kaur, 2019). Amylose-rich starches are mechanically stronger than amylopectin-rich starches (Koski & Bose, 2019), which might be a reason for the disintegration of EPF scaffolds from faba. The lack of interaction between iodine and starch in the cryosections of EPF from soy comes from very low concentration (0.8-1%) of starch present in soy (Wilson, Birmingham, Moon, & Snyder, 1978); (Choct, 1997).

The amino acids stained for with Aniline Blue – Orange G solution was lysine, histidine, and arginine. Lysine has been shown to function as a building block for protein synthesis, but also more importantly a signal to activate regulation of muscle growth in satellite cells through

mammalian target of rapamycin complex 1 (mTORC1) signaling pathway (Jin, et al., 2019). Histidine is a crucial amino acid in modulated global protein synthesis and eIF2B activity (Kimball, Horetsky, & Jefferson, 1998). If eIF2B is inhibited, the cellular ternary complex concentration decreases, which may trigger integrated stress response (ISR) in the cells. The ISR's task is to protect the cells from stress, or it may induce apoptosis. Many neurodegenerative disorders are cause by ISR dysregulation (Marintchev & Ito, 2020). Arginine increases cytoplasmic Ca^{2+} from extracellular and sarcoplasmic Ca^{2+} thus promoting myogenic differentiation and myotube formation (Gong, Zhang, Qiu, Wang, & Yin, 2021). Arginine also promotes myoblast fusion when it is combined with enhanced nitric oxide synthesis (Long, et al., 2006).

Swelling and water holding capacity of the EPF scaffolds may have led to loss of mechanical strength and structural integrity resulting in the scaffolds disintegrating during incubation, due to soluble non-starch polysaccharides (Felfel, Gideon-Adeniyi, Hossain, Roberts, & Grant, 2019) present in fiber of faba beans (Dhull, Kidwai, Noor, Chawla, & Rose, 2021) and soy (Choct, 1997). TPA was performed in a distinctive two-pressure action mechanism to mimic the human oral cavity's bite pattern (Peleg, 2019). The results showed big variations within the different attributes that were tested, except from the springiness in soy, but showed no statistical significance. This is an indicator for the EPF scaffolds not being homogenous all the way through, which may affect the myofibril formation in the sense of not having pores throughout the scaffold.

BNC were chosen as a scaffold due to its promising nanostructure for cell adhesion (Hickey & Pelling, 2019), mechanical strength, low toxicity, biocompability, hydrophilicity (Ugrin, et al., 2021) and as it has been previously proven as a scaffold for cell proliferation (Vielreicher, et al., 2018). The nanostructure of the BNC makes it impossible for the cells to enter the material, leaving the cells to proliferate and differentiate across the surface of the scaffold (Rybchyn, Biazik, Charlesworth, & le Coutre, 2021). Due to this, an application of this scaffold type in CBM could be to stack sheets of BNC and cells to form a final product. Since BNC has been proven as a fat replacer (Lin & Lin, 2006), in addition to being made of biodegradable polymers, it would suit this purpose. The material is ultra-thin (<1.0 mm) but is still a very strong material due to its dense fiber structure (Felgueiras, Azoia, Goncalves, Gama, & Duorado, 2021), which is a result of its high crystallinity (Kralisch, Hessler, Klemm, Erdmann, & Schmidt, 2009). Cellulose is made up of linear glucan chains that are

packed into microfibrils and held together by intramolecular hydrogen bonds as well as intermolecular van der Waals forces. These linear glucan chains are joined together by β-1,4-glycosidic bonds, with cellobiose residues serving as the repeating unit at various degrees of polymerization (Bai, Yang, & Ho, 2019). A higher degree of polymerization gives the cellulose higher mechanical strength (Tahara, et al., 1997), but lower polymerization gives higher digestibility (Hallac & Ragauskas, 2011). In order to find the most suitable balance, different degrees of polymerization should be tested with cell seeding and complimentary analysis. The monosaccharide gas chromatography analysis showed, as expected according to McNamara, Morgan & Zimmer (2016), that dried BNC consisted of mainly glucose. The incubation of cells on BNC showed stability of the material for 30 days. Due to the cells being detached at this point, it is unsure how long the material is stable for, but it looks promising.

6.3 Cell adhesion properties and biocompability of EPF and BNC scaffolds

Cell seeding on EPF scaffolds of soy had previously been accomplished on EPF from textured soy protein (Ben-Arye, et al., 2020), so we decided to replicate that experiment to a certain extent in addition to test it out on the Norwegian grown faba bean. The cell count of 750k cells per scaffold were copied, but the sterilization method of gamma irradiation could not be copied due to lack of equipment. In addition, the coating of fibrinogen was substituted for ECL due to it being available on hand and good results in cell proliferation in 2D (Rønning, Pedersen, Andersen, & Hollung, 2013).

The immunofluorescent images of the EPF scaffolds incubated for 7 days showed that cells had attached on scaffolds of both legumes. As light microscopy images of this material were difficult to do due to the compact structure, it is not possible to say whether the cells attached to the scaffolds were able to proliferate further. There was not conducted a cell count on the cells attached to the scaffolds, which is a weakness throughout this study in both EPF and BNC scaffolds. For cell adhesion, wettability of the surface is important with cells preferring to adhere to surfaces with a lower contact angle (hydrophilic surface) (Webb, Hlady, & Tresco, 1998); (Ruardy, Schakenraad, van der Mei, & Busscher, 1995). Normally hydrophobic regions in proteins of faba bean would be buried in the internal folded regions of the protein, but the heat treatment in the extruder have possibly led to denaturation and exposure of these hydrophobic regions (Vogelsang-O'Dwyer, et al., 2020) making the scaffolds less suitable for cell adhesion. In the ECL-coated faba bean scaffold there was a noticeable increase in attached cells which were expected due to myoblasts adhering through β1 integrins affinity to collagens and laminins (Yue, 2014) which are two of the components in the ECL matrix. In the extruded soy scaffolds, there were no visual difference between the coated and uncoated scaffolds. This was not expected as Ben-Arye et al. (2020) previously proved cell adherence, proliferation, and differentiation on their textured soy scaffolds coated with fibrinogen, a globular protein promoting cell adherence (Herrick, Blanc-Brude, Gray, & Laurent, 1999). A possible reason for the lack of cells in the immunofluorescent imaging could be that the cells fell off during medium changes or when the scaffolds were removed to new wells. This suggest that the cells struggle to adhere and attach to the scaffolds without coating due to the lack of integrin ligands such as collagen, laminin, fibronectin, and vitronectin in ECM (Marano & Vilaró, 1994). As the scaffolds could not be monitored in the

period between cell seeding and cryosectioning, it is not possible to determine whether the cells on the scaffolds are cells that are a product of proliferation or from the initial seeding. Initially we started with seeding 30k cells on the BNC scaffolds. The cells adhered to the BNC surface indicating that BNC contains epitopes and has a topography required for cell adherence. However, the results where the cells, by visual inspection, did not proliferate or differentiate made it seem like they went into stress-induced senescence (Sapieha & Mallette, 2018). The reasoning behind cells going into senescence, or cell cycle arrest, is activation of the p53 protein, located in the nucleus (Aubrey, Kelly, Janic, Herold, & Strasser, 2017). Functions of the p53 protein include DNA repair, metabolism, antioxidant response, and apoptosis (Chen J. , 2016). This stress-induced senescence may have been caused by transferring the BNC with attached cells to new wells, which was observable the next day after the move. This form of senescence may be categorized as acute senescence and will not turn into an irreversible late senescent cell. Acute senescent cells self-organize their elimination through Senescence-Associated Secretory Phenotype (SASP) components that attract various types of immune cells, making them reversible to proliferating cells again (van Deursen, 2014). From day 3 to day 30, by visual inspection there seems to be no difference in cell count on the BNC scaffolds, which further supports the hypothesis about the cells going into senescence (Rodier & Campisi, 2011). Another hypothesis for the occurrence of senescence is the lack of cell-cell interaction due to the low cell density. The lack of cell-cell interaction may reduce the cell-mediated matrix degradation, leading to reduced cell functions (Bitar, et al., 2008). Cell counting was not conducted after cell seeding in any of the experiments, which is a weakness in this study.

Due to the seemingly induction of senescence on the 30k cells seeded on BNC, we decided to increase the initial cell seeding count by a tenfold to 300k cells allowing the cells to proliferate greatly before exposing them to the potential stress of moving the scaffolds to new wells. The increased seeded cell count allows for more cell to cell interaction, positively impacting proliferation (Nelson & Chen, 2002). The BNC scaffolds containing cells were moved to new wells after 2 days to prevent further cellular communication between the cells on the scaffold and the cells at the bottom of the well. After 3 days incubation on BNC with ECL coating there were clear signs that the cells had proliferated and started spontaneous differentiating to multinucleated myotubes. Within these clusters of differentiating cells there is a clear alignment of fibers, but the alignment differs between the clusters indicating that the direction of expansion may be orientated by the fibrous nanostructure orientation of the

different areas on the scaffold (Cha, Lee, & Koh, 2017); (Wang, Yu, & Tsai, 2010). Cha, Lee & Koh (2017) also showed that the orientation of the nanofibers on the scaffold affects the orientation all the way down on a nuclei level. The cells on BNC without coating may not have had the same amount of proliferation and therefore lack of differentiation (Bitar, et al., 2008) which may have been caused by fewer cells adhering to the scaffold. This substantiates the results from ECL coated EPF of faba showing an increase in cell attachment and thus a better fundament for cell proliferation (Nelson & Chen, 2002). However, after 15 days the cells on BNC without ECL coating started to show clusters of differentiated cells. At this stage, the cells on the ECL coated BNC showed fusion of these differentiated clusters. When the clusters of myotubes fuses, it seems like the myotubes align more frequently. This could be due to the uniaxial orientation of BNC fibril bundles (Swingler, et al., 2021).

The immunofluorescent images showed a surprising high amount of desmin after 2 days incubation for the cells on non-treated BNC. In the light microscopy images, on the other hand, it seems like the cells did not connect with each other in a substantial matter to form multinucleated myotubes. This emphasizes the importance of using additional methods to light microscopy imaging to assess the myogenetic potential. The desmin filaments are the first muscle-specific protein to appear during myogenesis (Carlsson & Thornell, 2001), and is a part of the intermediate filament proteins (Quax, van den Broek, Egberts, Ramaekers, & Bloemendal, 1985). Calrsson & Thornell (2001) additionally explains that the structures of the cell wall are strengthened by desmin filaments, and it works as a binding material for the contractile apparatus (Goldblum, Folpe, & Weiss, 2019). The fluorescent images after 2 days incubation substantiates the hypothesis about the cells preferring ECL coating. Satellite cells bind to the collagen and laminin in ECL through integrins. Laminin is essential for myoblast proliferation, migration, and alignment preceding myotube fusion through, amongst other processes, binding to and suppressing the activity of myostatin, which negatively regulates proliferation and differentiation. In the absence of laminin, myotube formation is noticeably impaired (Grzelkowska-Kowalczyk, 2016). Matrix metalloproteinases (MMPs) degrade collagens and laminin, amongst other ECM components, freeing growth factors and signaling molecules essential for cell activation, migration, and differentiation (Grzelkowska-Kowalczyk, 2016). The cells incubated on BNC with ECL coating are further in the myogenesis with more proliferated cells and cells that has spontaneously differentiated. After 15 days incubation it is clearly visible that the cells incubated on ECL-coated BNC has proliferated profoundly and are more evenly distributed across the BNC scaffold. The clusters

had also connected to each other, creating a cohesive sheet of multinucleated myotubes. This is the trend seen in both repetitions of the experiments and in the samples therein. Further supporting the findings about coating of the scaffold plays a major role in cell proliferation and differentiation. The potential of growing cells without coating is definitely there as the cells will secrete cell-derived ECM (Horton, et al., 2020), though it seems like cells grown this way needs a longer incubation period to achieve the same confluency as with ECL coating.

The senescent cells that had been cultivated on BNC for 30 days was trypzinated off the BNC and seeded in wells coated with ECL to see if they were still viable and able to proliferate and differentiate. Both treatment methods of the BNC scaffold (with and without ECL) resulted in the cells proliferating again. After 7 days there are signs of myotube formation in both treatment methods and after 14 days there are clear signs of spontaneous differentiation in the cells from non-treated BNC. At this point PM was exchanged for DM to induce all cells to differentiate which resulted in clear myotube formation also in the cells from ECL-treated BNC. This experiment was retried with the same cell batches (15 days incubation) that were used for the fluorescent imaging and mRNA expression analysis. These cells did not proliferate after being trypzinated off the BNC scaffolds. A hypothesis for these results is that when the cells are senescent, they still have the ability to be reactivated to proliferation stage through increased telomerase activity and thus override senescence-associated growth arrest (Soto-Gamez & Demaria, 2017) due to upregulation of telomerase found in the collagen in the ECL-coating of the wells (Lee, West, Parker, & Vollmer, 2020). A hypothesis for why the repeated experiments did not work is that the BNC scaffolds contained mostly differentiated cells, leaving the remaining proliferating cells in a too small quantity to continue proliferation (Zhou, Weir, & Xu, 2011).

The results from the RT-qPCR analysis conducted on 300k cells seeded on BNC were inconclusive. Based on myotube formation seen in the immunofluorescent images, it was expected to see an increase in myogenin and desmin, status quo in MyoD1 and a decrease in Pax7 due to downregulation during differentiation after 15 days incubation. This is because myogenin is a late marker of myoblast fusion (Smith, Passey, Greensmith, Mudera, & Lewis, 2011), desmin is a marker for myogenic differentiation (Rangdaeng & Truong, 1991), MyoD1 is coexpressed with Pax7 when quiescent satellite cells are activated and binds to the DNA upstream to keep active up until myotube formation (Gilbert, 2000), and absence of Pax7 will

initiate myogenic differentiation (Florkowska, et al., 2020). In the first repetition of the 300k cells seeded on BNC, there is a statistical significance at day 15 in all muscle specific markers in favor of the ECL-coated BNC which substantiates the hypothesis made from the light microscopy and immunofluorescent images about ECL coating being beneficial. A reason why the second repetition of this experiment show completely different mRNA expression may be that the samples contained a lot of cells still in the proliferating stage due to seemingly, by visual inspection, fewer cells being committed to differentiation. The second repetition might also contain cells expressing high levels of Pax7 which demonstrate slower proliferation rates, lower metabolism, and resistance toward differentiation (Rocheteau, Gayraud-Morel, Siegl-Cachedenier, Blasco, & Tajbakhsh, 2012). Another reason may be that sampling of mRNA is a very delicate method and the cell lysing of the cells and mRNA isolation might not have been adequately performed. At 2 days incubation the results are also in favor of ECL-coated BNC in regard of higher gene expression in Pax7, MyoD1 and myogenin indicating that there are more proliferating and differentiation cells. The lack of difference in desmin expression is unknown. The gene expression for the adhesion markers were consistent for cells cultivated for 2 and 15 days, with the exception of ITGβ5 in the second repetition after 15 days. This indicates that the cells are able to adhere with the adhesion molecules tested to the BNC scaffolds both with and without ECL coating in a similar manner. The initial cell batches that were used showed statistically significant differences in all markers except from ITGβ5, but it had the same trend as the other markers. As the cells used were in the same passage they should have the same gene expression, but they did not. A reason for this might be that after cell harvesting by biopsy, the cells variated in the time it took reach a confluency high enough for being frozen in liquid nitrogen due to the initial cell count and myoblast:fibroblast ratio (Rao, et al., 2013).

6.6 Summing up

The main objective of the study was to develop a non-animal derived scaffold, and that was accomplished with the BNC scaffold. The BNC scaffolds seem like a very suitable scaffold for cell attachment, proliferation, and differentiation. The BNC scaffolds were easily sterilizable, where EPF scaffolds had difficulties in being sterilized with antibiotic treatment. The EPF scaffolds were sterilizable through heat sterilization, but the structure did not withstand the exposure to heat. The subgoal of sterilizing the scaffolds were not completely achieved due to bacterial growth in the last cell seeding experiment. As of now, the EPF scaffolds are not suitable as scaffolds for in vitro cell culturing due to their lack of technical abilities to withstand being in a liquid over a period of time as well as bacterial infections that are uncertain to be sterilized by previously successful methods. However, based on characterization and cell adherence to the scaffolds, EPF scaffold seem like a suitable porous 3D scaffold for cell expansion, as long as sterilization and technical abilities are improved. The subgoal of characterizing the scaffolds were achieved on the EPF scaffolds, but on BNC scaffolds there could be more studies regarding the topography and nanostructure. ECL coating is very beneficiary, but not a necessity for cell growth as the non-treated BNC scaffolds showed potential and could reach the same confluency as with ECL-coated BNC if given time. The last subgoal was to establish whether the scaffolds were eligible for the intended purpose. The BNC seem eligible as they are now to be used in CBM production, and the EPF scaffolds could potentially be eligible but are not as of now. When comparing the EPF scaffolds and BNC scaffolds, BNC seem like a superior biomaterial for CBM production due to its interactive surface allowing cell adherence, proliferation, and differentiation without the need for coating or antibiotic sterilization.

6.7 Further research

Further research on edible scaffolds used in in vitro meat production would be to optimize the EPF 3D structures to withstand being in cell medium over a long enough period of time for cells to proliferate and differentiate as it has been showed that they are able to attach. A solution for the bacterial infections might be to pre-sterilize the protein concentrate before extrusion by either UV-irradiation which would be able to penetrate the small particles in a powder or by investigate different combinations of antibiotics that would ensure sterile products. Another way of using legume protein concentrate could be to make microcarriers of

them to avoid the issue of them disintegrating in cell medium due to their expansion in the extruder.

A research topic that also is relevant to this thesis is to see whether cells seeded on BNC without ECL coating, or any coating for that matter, could reach the confluency, proliferation and differentiation of cells grown on ECL-coated BNC and how long time it would need. In this regard, optimizing of the BNC nanostructure would be essential and to get a greater appreciation of how the cells benefit from its surface. Another point of research could be to find a food grade replacement for ECL attachment matrix, preferably from by-products in the food industry.

Literature

Abmayr, S. M., & Pavlath, G. K. (2012, February 15). Myoblast fusion: lessons from flies and mice. *Development, 139*(4), pp. 641-656.

Adams, G. (2020, June 15). A beginner's guide to RT-PCR, qPCR and RT-qPCR. *Biochemist, 42*(3), pp. 48-53.

Ahmad, K., Lim, J., Lee, E., Chun, H., Ali, S., Ahmad, S. S., . . . Choi, I. (2021, December 15). Extracellular Matrix and the Production of Cultured Meat. *Foods, 10*(12), p. e:3116.

Ahmad, K., Shaikh, S., Ahmad, S., Lee, E. J., & Choi, I. (2020, February 28). Cross-Talk Between Extracellular Matrix and Skeletal Muscle: Implications for Myopathies. *Frontiers in Pharmacology, 11*(142).

Al-Hagar, O. E., & Abol-Fotouh, D. (2022, April 29). A turning point in the bacterial nanocellulose production employing low doses of gamma radiation. *Scientific Reports, 12*, p. e:7012.

Aamodt, J. M., & Grainger, D. W. (2016). Extracellular matrix-based biomaterial scaffolds and the host response. *Biomaterials, 86*, 68-82.

Andreassen, R. C., Rønning, S. B., Solberg, N. T., Grønlien, K. G., Kristoffersen, K. A., Høst, V., . . . Pedersen, M. E. (2022). Production of food-grade microcarriers based on by-products from the food industry to facilitate the expansion of bovine skeletal muscle satellite cells for cultured meat production. *Biomaterials, 286*, p. e:121602.

Aschi, A., Aubert, M., Riah-Anglet, W., Nélieu, S., Dubois, C., Akpa-Vinceslas, M., & Trinsoutrot-Gattin, I. (2017). Introduction of Faba bean in crop rotation: Impacts on soil chemical and biological characteristics. *Applied Soil Ecology, 120*, pp. 219-228.

Aubrey, B. J., Kelly, G. L., Janic, A., Herold, M. J., & Strasser, A. (2017, November 17). How does p53 induce apoptosis and how does this relate to p53-mediated tumour suppression? *Cell Death & Differentiation, 25*, pp. 104-113.

Bach, A. D., Beier, J. P., Stern-Staeter, J., & Horch, R. E. (2004). Skeletal muscle tissue engineering. *Journal of Cellular and Molecular Medicine, 8*(4), pp. 413-422.

Bai, F., Yang, S., & Ho, N. W. (2019). Fuel Ethanol Production From Lignocellulosic Biomass. In M. Moo-Young, *Comprehensive Biotechnology (Third Edition)* (Vol. 3). Waterloo, Ontario, Canada: Elseviewer Science.

Barczyk, M., Carracedo, S., & Gullberg, D. (2010). Integrins. *Cell and Tissue Research, 339*(1), pp. 269-280.

Bateman, J. M., & McNeill, H. (2004, October 1). Temporal control of differentiation by the insulin receptor/tor pathway in Drosophila. *Cell, 119*(1), pp. 87-96.

Ben-Arye, T., Shandalov, Y., Ben-Shaul, S., Landau, S., Zagury, Y., Ianovici, I., . . . Levenberg, S. (2020, March 30). Textured soy protein scaffolds enable the generation of three-dimensional bovine skeletal muscle tissue for cell-based meat. *Nature Food, 1*, pp. 210-220.

Berkes, C. A., & Tapscott, S. J. (2005). MyoD and the transcriptional control of myogenesis. *Seminars in cell & developmental biology, 16*(4-5), pp. 585-595.

Bhat, Z. F., Bhat, H., & Kumar, S. (2020). Cultured meat — a humane meat production system,. In R. Lanza, R. Langer, J. P. Vacanti, & A. Atala, *Principles of Tissue Engineering (Fifth Edition)* (pp. 1369-1388). Academic Press.

Biressi, S., Tagliafico, E., Lamorte, G., Monteverde, S., Tenedini, E., Roncaglia, E., . . . Cossu, G. (2007, April 15). Intrinsic phenotypic diversity of embryonic and fetal myoblasts is revealed by genome-wide gene expression analysis on purified cells. *Developmental Biology, 302*(2), pp. 633-651.

Bitar, M., Brown, R. A., Salih, V., Kidane, A. G., Knowles, J. C., & Nazhat, S. N. (2008). Effect of Cell Density on Osteoblastic Differentiation and Matrix Degradation of Biomimetic Dense Collagen Scaffolds. *Biomacromolecules, 9*(1), pp. 129-135.

Black, K., Tziboula-Clarke, A., White, P. J., Iannetta, P. P., & Walker, G. (2020, December 28). Optimised processing of faba bean (Vicia faba L.) kernels as a brewing adjunct. *Journal of the Institute of Brewing, 127*(1), pp. 13-20.

Bodiou, V., Moutsatsou, P., & Post, M. J. (2020, February 20). Microcarriers for Upscaling Cultured Meat Production. *Frontiers in nutrition, 7*(10).

Bomkamp, C., Skaalure, S. C., Fernando, G. F., Ben-Arye, T., Swartz, E. W., & Specht, E. A. (2022, January). Scaffolding Biomaterials for 3D Cultivated Meat: Prospects and Challenges. *Advanced Science, 9*(3), p. e:2102908.

Borman, A. M., Fraser, M., Palmer, M. D., Szekely, A., Houldsworth, M., Patterson, Z., & Johnson, E. M. (2017, May 31). MIC Distributions and Evaluation of Fungicidal Activity for Amphotericin B, Itraconazole, Voriconazole, Posaconazole and Caspofungin and 20 Species of Pathogenic Filamentous Fungi Determined Using the CLSI Broth Microdilution Method. *Journal of Fungi, 3*(27), p. 2.

Brack, D., Glover, A., & Wellesley, L. (2016). *Agricultural Commodity Supply Chains Trade, Consumption and Deforestation.* London: Chatham House.

Cahn, F. (1990). Biomaterials aspects of porous microcarriers for animal cell culture. *Trends in Biotechnology, 8*, pp. 131-136.

Carlsson, L., & Thornell, L. E. (2001, March). Desmin-related myopathies in mice and man. *Acta physiologica Scandinavia, 171*(3), pp. 341-348.

Cha, S. H., Lee, H. J., & Koh, W. G. (2017, January 11). Study of myoblast differentiation using multi-dimensional scaffolds consisting of nano and micropatterns. *Biomaterials Research, 21*, p. e:1.

Chang, Q., Wang, W., Regev-Yochay, G., Lipstich, M., & Hanage, W. P. (2014). Antibiotics in agriculture and the risk to human health: how worried should we be? *Evolutionary Applications, 8*(3), pp. 240-247.

Chelladurai, K. S., Christyraj, J. D., Rajagopalan, K., Yesudhason, B. V., Venkatachalam, S., Mohan, M., . . . Christyraj, J. R. (2021). Alternative to FBS in animal cell culture - An overview and future perspective. *Heliyon, 7*(8), p. e:07686.

Chen, A. K., Chen, X., Choo, A. B., Reuveny, S., & Oh, S. K. (2011). Critical microcarrier properties affecting the expansion of undifferentiated human embryonic stem cells. *Stem Cell Research, 7*(2), pp. 97-111.

Chen, J. (2016, March). The Cell-Cycle Arrest and Apoptotic Functions of p53 in Tumor Initiation and Progression. *Cold Spring Harbor perspectives in medicine, 6*(3), p. e:026104.

Cheng, R., Zhang, F., Li, M., Wo, X., Su, Y., & Wang, W. (2019, August 23). Influence of Fixation and Permeabilization on the Mass Density of Single Cells: A Surface Plasmon Resonance Imaging Study. *Frontiers in chemistry, 7*, p. e:588.

Cheung, T. H., & Rando, T. A. (2013, May 23). Molecular regulation of stem cell quiescence. *Nature Reviews Molecular Cell Biology, 14*, pp. 329-340.

Choct, M. (1997, June). Feed Non-Starch Polysaccharides: Chemical Structures and Nutritional Significance. *Feed Milling International*(191), pp. 13-26.

Churchill, W. S. (1932). Fifty Years Hence. In *Thoughts and Adventures* (pp. 269-280). London: Thornton Butterworth Limited.

Collins, C. A., Olsen, I., Zammit, P. S., Heslop, L., Petrie, A., Partridge, T. A., & Morgan, J. E. (2005, July 29). Stem Cell Function, Self-Renewal, and Behavioral Heterogeneity of Cells from the Adult Muscle Satellite Cell Niche. *Cell, 122*(2), pp. 289-301.

Dai, Z., Ronholm, J., Tian, Y., Sethi, B., & Cao, X. (2016). Sterilization techniques for biodegradable scaffolds in tissue engineering applications. *Journal of tissue engineering, 7*, p. e:2041731416648810.

Day, L. (2013, July). Proteins from land plants – Potential resources for human nutrition and food security. *Trends in Food Science & Technology, 32*(1), pp. 25-42.

de Souza, D. C., Palmeiro, J. K., Maestri, A. C., Cogo, L. L., Rauen, C. H., Graaf, M. E., . . . Nogueira, K. S. (2018, September-October). Ralstonia mannitolilytica bacteremia in a neonatal intensive care unit. *Sociedade Brasileira Medicina Tropical, 51*(5), pp. 709-711.

Delgado, C. L. (2003, November). Rising consumption of meat and milk in developing countries has created a new food revolution. *The Journal of Nutrition, 133*(11 suppl 2), pp. 3907-3910.

Dhull, S. B., Kidwai, M. K., Noor, R., Chawla, P., & Rose, P. K. (2021, October 28). A review of nutritional profile and processing of faba bean (Vicia faba L.). *Legume Science, 4*(3), p. e:129.

Dodou, E., Xu, S., & Black, B. L. (2003). mef2c is activated directly by myogenic basic helix-loop-helix proteins during skeletal muscle development in vivo. *Mechanisms of Development, 120*(9), pp. 1021-1032.

Dransfield, E. (1977). Intramuscular composition and texture of beef muscles. *Journal of the Science of Food and Agriculture, 28*(9), pp. 833-842.

Evans, N. A., Hoyne, P. A., & Stone, B. A. (1984). Characteristics and Specifity of the Interaction of a Fluorchrome from Aniline Blue (Siroflour) with Polysaccharides. *Carbohydrate Polymers*(4), pp. 215-230.

FAO. (2017a). *The future of food and agriculture - Trends and challenges.* Roma.

FAO. (2017b). *Water pollution from agriculture: a global review.* Roma and Colombo: Food and Agriculture Organization of the United Nations and the International Water Management Institute on behalf of the Water Land and Ecosystems research program. Retrieved from Sustainable Food and Agriculture.

Fasano, J. (2022). *Memorandum.* U.S. Food & Drug Administration.

Felfel, R. M., Gideon-Adeniyi, M. J., Hossain, K. M., Roberts, G. A., & Grant, D. M. (2019, January 15). Structural, Mechanical and Swelling Characteristics of 3D Scaffolds from Chitosan-Agarose blends. *Carbohydrate Polymers*(204), pp. 59-67.

Felgueiras, C., Azoia, N. G., Goncalves, C., Gama, M., & Duorado, F. (2021, March 29). Trends on the Cellulose-Based Textiles: Raw Materials and Technologies. *Frontiers in Bioengineering and Biotechnology, 9*, p. e:608826.

Florkowska, A., Meszka, I., Zawada, M., Legutko, D., Proszynski, T. J., Janzyk-Ilach, K., . . . Grabowska, I. (2020, June 17). Pax7 as molecular switch regulating early and advanced stages of myogenic mouse ESC differentiation in teratomas. *Stem Cell Research & Therapy, 11*, p. e:238.

Frantz, C., Stewart, K. M., & Weaver, V. M. (2010). The extracellular matrix at a glance. *Journal of cell science, 123*(24), pp. 4195-4200.

Fu, X., Wang, H., & Hu, P. (2015, January 9). Stem cell activation in skeletal muscle regeneration. *Cellular and Molecular Life Sciences, 72*(9), pp. 1663-1677.

Gerber, P. J., Steinfeldt, H., Henderson, B., Mottet, A., Opio, C., Falcucci, A., & Tempio, G. (2013). *Tackling climate change through livestock – A global assessment of emissions and mitigation.* Roma: Food and Agriculture Organization of the United Nations (FAO).

Gilbert, S. F. (2000). Myogenesis: The Development of Muscle. In S. F. Gilbert, *Developmental Biology 6th ed.* (pp. 453-454). Sinauer Associates.

Gillies, A. R., & Lieber, R. L. (2011). Structure and function of the skeletal muscle extracellular matrix. *Muscle & Nerve, 44*(3), pp. 318-331.
Gleckman, R., Alvarez, S., & Joubert, D. W. (1979). Drug therapy reviews: trimethoprim-sulfamethoxazole. *American journal of hospital pharmacy, 893-906*, pp. 893-906.
Gleckman, R., Blagg, N., & Joubert, D. W. (1981). Trimethoprim: mechanisms of action, antimicrobial activity, bacterial resistance, pharmacokinetics, adverse reactions, and therapeutic indications. *Pharmacotherapy, 1*(1), pp. 14-20.
Goldblum, J. R., Folpe, A. L., & Weiss, S. W. (2019). Immunohistochemistry for Analysis of Soft Tissue Tumors. In J. R. Goldblum, A. L. Folpe, & S. W. Weiss, *Enzinger and Weiss's Soft Tissue Tumors* (pp. 129-201). Elsevier.
Gong, L., Zhang, X., Qiu, K., Wang, Y., & Yin, J. (2021, December). Arginine promotes myogenic differentiation and myotube formation through the elevation of cytoplasmic calcium concentration. *Animal Nutrition, 7*(4), pp. 1115-1123.
Graybill, J. R., Burgess, D. S., & Hardin, T. C. (1997, Jan 16). Key issues concerning fungistatic versus fungicidal drugs. *European journal of clinical microbiology & infectious diseases : official publication of the European Society of Clinical Microbiology*(1), pp. 42-50.
Grifone, R., Demignon, J., Houbron, C., Souil, E., Niro, C., Seller, M. J., . . . Maire, P. (2005). Six1 and Six4 homeoproteins are required for Pax3 and Mrf expression during myogenesis in the mouse embryo. *Development, 132*(9), pp. 2235-2249.
Grzelkowska-Kowalczyk, K. (2016). The Importance of Extracellular Matrix in Skeletal Muscle Development and Function. In F. Travascio, *Composition and Function of the Extracellular Matrix in the Human Body* (pp. 3-24). InTechOpen.
Hallac, B. B., & Ragauskas, A. J. (2011). Analyzing cellulose degree of polymerization and its relevancy to cellulosic ethanol. *Biofuels, Bioproducts and Biorefining, 5*(2), pp. 215-225.
Halpern, J. (2022, July 4). *Starch and Iodine.* Retrieved from LibreTexts Chemistry: https://chem.libretexts.org/Bookshelves/Biological_Chemistry/Supplemental_Modules_(Biological_Chemistry)/Carbohydrates/Case_Studies/Starch_and_Iodine
Herrick, S., Blanc-Brude, O., Gray, A., & Laurent, G. (1999). Fibrinogen. *The International Journal of Biochemistry & Cell Biology, 31*(7), pp. 741-746.
Hickey, R. J., & Pelling, A. E. (2019, March 22). Cellulose Biomaterials for Tissue Engineering. *Frontiers in Bioengeneering and Biotechonlogy, 7*(45).
Horton, E. R., Vallmajo-Martin, Q., Martin, I., Snedeker, J. G., Ehrbar, M., & Blache, U. (2020, March 3). Extracellular Matrix Production by Mesenchymal Stromal Cells in Hydrogels Facilitates Cell Spreading and Is Inhibited by FGF-2. *Advanced Healthcare Materials, 9*(7), p. e:1901669.
Huang, S., & Ingber, D. E. (1999). The structural and mechanical complexity of cell-growth control. *Nature Cell Biology, 1*(5), pp. 131-138.
Hutmacher, D. W. (2000). Scaffolds in tissue engineering bone and cartilage. *Biomaterials, 21*(24), pp. 2529-2543.
Im, K., Mareninov, S., Diaz, M. F., & Yong, W. H. (2019). An introduction to Performing Immunofluorescence Staining. *Methods in molecular biology, 1897*, pp. 299-311.
Islam, M. S., Aryasomayajula, A., & Selvaganapathy, P. R. (2017, March 1). A Review on Macroscale and Microscale Cell Lysis Methods. *Micromachines, 8*(3), p. e:83.
Jackson, D. S. (2003). STARCH | Structure, Properties, and Determination. In B. Caballero, *Encyclopedia of Food Sciences and Nutrition (Second Edition)* (pp. 5561-5567). Academic Press.

Jin, C., Ye, J., Yang, J., Gao, C., Yan, H., Li, H., & Wang, X. (2019, November 30). mTORC1 Mediates Lysine-Induced Satellite Cell Activation to Promote Skeletal Muscle Growth. *Cells, 8*(12), p. e:1549.

Jin, X., Kim, J., Oh, M., Oh, H., Sohn, Y., Pian, X., . . . Whang, K. Y. (2007, December 21). Opposite roles of MRF4 and MyoD in cell proliferation and myogenic differentiation. *Biochemical and Biophysical Research Communications, 364*(3), pp. 476-482.

Kang, K. A., Piao, M. J., Kim, K. C., Cha, J. W., Zheng, J., Yao, C. W., . . . Hyun, J. W. (2014, Januar). Fisetin attenuates hydrogen peroxide-induced cell damage by scavenging reactive oxygen species and activating protective functions of cellular glutathione system. *In vitro cellular & developmental biology - Animal, 50*(1), pp. 66-74.

Kanisicak, O., Mendez, J. J., Yamamoto, S., Yamamoto, M., & Goldhamer, D. J. (2009, August 1). Progenitors of skeletal muscle satellite cells express the muscle determination gene, MyoD. *Developmental Biology, 332*(1), pp. 131-141.

Kassar-Duchossoy, L., Gayraud-Morel, B., Gomés, D., Rocancourt, D., Buckingham, M., Shinin, V., & Tajbakhsh, S. (2004, September 23). Mrf4 determines skeletal muscle identity in Myf5:Myod double-mutant mice. *431*, pp. 466-471.

Kearns, J. P., Rokey, G. J., & Huber, G. R. (1988). Extrusion of Texturized Proteins. In T. H. Applewhite, *Proceedings of the World Congress: Vegetable Protein Utilization in Human Foods and Animal Feddstuffs* (pp. 353-362). Kraft, Inc.

Kim, S., Kim, J., Okajima, T., & Cho, N. (2017, March 20). Mechanical properties of paraformaldehyde-treated individual cells investigated by atomic force microscopy and scanning ion conductance microscopy. *Nano convergence, 4*(1), p. e:5.

Kimball, S. R., Horetsky, R. L., & Jefferson, L. S. (1998, November 20). Implication of eIF2B Rather Than eIF4E in the Regulation of Global Protein Synthesis by Amino Acids in L6 Myoblasts. *The Journal of biological chemistry, 273*(47), pp. 30945-30953.

King, T. (2019). Meat re-imagined: The global emergence of alternative proteins - what does it mean for Australia? *Food Frontiers, 71*(3).

Klippenstein, S. R., Khazaei, H., & Schoenau, J. (2021, November 5). Nitrogen and phosphorus uptake and nitrogen fixation estimation of faba bean in western Canada. *Agronomy Journal, 114*(1), pp. 811-824.

Koski, C., & Bose, S. (2019, December). Effects of Amylose Content on the Mechanical Properties of Starch-Hydroxyapatite 3D Printed Bone Scaffolds. *Additive Manufacturing, 30*, p. e:100817.

Kralisch, D., Hessler, N., Klemm, D., Erdmann, R., & Schmidt, W. (2009, Januar). White biotechnology for cellulose manufacturing—The HoLiR concept. *Biotechnology and Bioengineering, 105*(4), pp. 740-747.

Lai, T., Cao, J., Yang, P., Tsai, C., Lin, C., Chen, C., . . . Lee, C. (2022, April 5). Different methods of detaching adherent cells and their effects on the cell surface expression of Fas receptor and Fas ligand. *Scientific Reports, 12*, p. e:5713.

Lebret, B., Louveau, I., Astruc, T., Bonnet, M., Lefaucheur, L., Picard, B., & Bugeo, J. (2016). How Muscle Structure and Composition Influence Meat and Flesh Quality . *The Scientific World Journal*, p. e:3182746.

Lee, G., West, V., Parker, T., & Vollmer, D. (2020). A Multi-Type Collagen-Based Drink Supplement Significantly Improved Markers of Aging, both in vitro and in a Human Clinical Study. *Journal of Clinical & Experimental Dermatology Research, 11*(5), pp. 1-9.

Lin, K. W., & Lin, H. Y. (2006). Quality Characteristics of Chinese-style Meatball Containing Bacterial Cellulose (Nata). *Journal of Food Science, 69*(3), pp. 107-111.

Listrat, A., Lebret, B., Louveau, I., Astruc, T., Bonnet, M., Lefaucheur, L., . . . Bugeon, J. (2016, February 28). How Muscle Structure and Composition Influence Meat and Flesh Quality. *The Scientific World Journal, 2016*, p. e:3182746.

Loh, Q. L., & Choong, C. (2013). Three-Dimensional Scaffolds for Tissue Engineering Applications: Role of Porosity and Pore Size. *Tissue engineering. Part B, Reviews, 19*(6), pp. 485-502.

Long, J. H., Lira, V. A., Soltow, Q. A., Betters, J. L., Sellman, J. E., & Criswell, D. S. (2006, October 19). Arginine supplementation induces myoblast fusion via augmentation of nitric oxide production. *Journal of muscle research and cell motility, 27*(8), pp. 577-584.

Lovdata. (2001, May 1). Forskrift om behandling av næringsmidler med ioniserende stråling. Norway.

Lund, M. N., & Ray, C. A. (2017, May 23). Control of Maillard Reactions in Foods: Strategies and Chemical Mechanisms. *Journal of Agricultural and Food Chemistry, 65*(23), pp. 4537-4552.

Ma, P. X. (2004). Scaffolds for tissue fabrication. *Materials Today, 7*(5), pp. 30-40.

Marano, R. P., & Vilaró, S. (1994). The role of fibronectin, laminin, vitronectin and their receptors on cellular adhesion in proliferative vitreoretinopathy. *Investigative ophthalmology & visual science, 35*(6), pp. 2791-2803.

Marintchev, A., & Ito, T. (2020, April 7). eIF2B and the Integrated Stress Response: a structural and mechanistic view. *Biochemistry, 59*(13), pp. 1299-1308.

Matsiko, A., Gleeson, J. P., & O'Brien, F. J. (n.d.). Scaffold mean pore size influences mesenchymal stem cell chondrogenic differentiation and matrix deposition. *Tissue engineering. Part A, 21*(3-4), pp. 486-497.

Matteucci, M. J. (2012). Isopropyl Alcohol. In K. R. Oslon, *Poisining & Drug Overdeose* (p. Ch.89). McGraw-Hill.

Mauro, A. (1961). Satellite cell of skeletal muscle fibers. *The Journal of biophysical and biochemical cytology, 9*(2), pp. 493-495.

Mayran, A., Pelletier, A., & Drouin, J. (2015, July 24). Pax factors in transcription and epigenetic remodelling. *Seminars in Cell & Developmental Biology, 44*, pp. 135-144.

McNamara, J. T., Morgan, J. L., & Zimmer, J. (2016, Januar 12). A Molecular Description of Cellulose Biosynthesis. *Annual Review of Biochemistry, 84*(895-921).

Meadows, E., Cho, J., Flynn, J. M., & Klein, W. H. (2008, October 15). Myogenin regulates a distinct genetic program in adult muscle stem cells. *Developmental Biology, 322*(2), pp. 406-414.

Meftahi, A., Khajavi, R., Rashidi, A., Sattari, M., Yazdanshenas, M. E., & Torabi, M. (2010). The effects of cotton gauze coating with microbial cellulose. *Cellulose, 17*, pp. 199-204.

Meiliana, A., Dewi, N. M., & Wijaya, A. (2015). Molecular Regulation and Rejuvenation of Muscle Stem (Satellite) Cell Aging. *The Indonesian Biomedical Journal, 7*(2), pp. 73-86.

Michelfelder, A. J. (2009). Soy: a complete source of protein. *American family physician, 79*(1), pp. 43-47.

Mirab, F., Eslamian, M., & Bagheri, R. (2018, August). Fabrication and Characterization of a Starch-Based Nanocomposite Scaffold with Highly Porous and Gradient Structure for Bone Tissue Engineering. *Biomedical Physics & Engineering Express, 4*(5).

Moellering Jr, R. C., Medoff, G., Leech, I., Wennersten, C., & Kunz, L. J. (1972, Jan 1). Antibiotic Synergism Against Listeria monocytogenes. *Antimicrobial Agents and Chemotherapy*(1), pp. 30-34.

Moore, J. C., DeVries, J. W., Griffiths, J. C., & Abernethy, D. R. (2010). Total Protein Methods and Their Potential Utility to Reduce the Risk of Food Protein Adulteration. *Comprehensive Reviews in Food Science and Food Safety, 9*, pp. 330-357.

Morgan, M. R., Humphries, M. J., & Bass, M. D. (2007). Synergistic control of cell adhesion by integrins and syndecans. *Nature Reviews Molecular Cell Biology, 8*, pp. 957-969.

Mucsi, Z., Chass, G. A., Ábrányi-Balogh, P., Jójárt, B., Fang, D., Ramirez-Cuesta, A. J., . . . Csizmadia, I. G. (2013). Penicillin's catalytic mechanism revealed by inelastic neutrons and quantum chemical theory. *Physical chemistry chemical physics, 15*(47), pp. 20447-20455.

Mukund, K., & Subramaniam, S. (2020). Skeletal muscle: A review of molecular structure and function, in health and disease. *Systems biology and medicine, 12*(1), p. e:1462.

Munita, J. M., & Arias, C. A. (2016). Mechanisms of Antibiotic Resistance. *Microbiology spectrum, 4*(2).

Nehrer, S., Breinan, H. A., Ramappa, A., Young, G., Shortkroff, S., Louie, L. K., . . . Spector, M. (1997). Matrix collagen type and pore size influence behaviour of seeded canine chondrocytes. *Biomaterials, 18*(11), pp. 769-776.

Nelson, C. M., & Chen, C. S. (2002, March 13). Cell-cell signaling by direct contact increases cell proliferation via a PI3K-dependent signal. *FEBS Letters, 514*(2-3), pp. 238-242.

Nikiforova, M. N., & Nikiforov, Y. E. (2011). Molecular Anatomic Pathology: Principles, Techniques, and Application to Immunohistologic Diagnosis. In D. J. Dabbs. Theranostic and Genomic Applications.

Niro, C., Demignon, J., Vincent, S., Liu, Y., Giordani, J., Sgarioto, N., . . . Maire, P. (2010). Six1 and Six4 gene expression is necessary to activate the fast-type muscle gene program in the mouse primary myotome. *Developmental Biology, 338*(2), pp. 168-182.

Noor, A., & Preuss, C. V. (2022). Amphotericin B. In StatPearls, *Treasure Island [Internet]*. Florida: StatPearls. Retrieved from National Center for Biotechnology Informaiton: https://www.ncbi.nlm.nih.gov/books/NBK482327/

OECD/FAO. (2021). *OECD-FAO Agricultural Outlook 2021–2030.* Paris: OECD Publishing.

O'Riordan, K., Fotopoulou, A., & Stephens, N. (2017). The first bite: Imaginaries, promotional publics and the laboratory grown burger. *Public understanding of science, 26*(2), pp. 148-163.

Peleg, M. (2019, February). The Instrumental Texture Profile Analysis (TPA) Revisited. *Journal of Texture Studies, 50*(5), pp. 1-7.

Pin, C. L., & Merrifield, P. A. (1998, December 7). Regionalized expression of myosin isoforms in heterotypic myotubes formed from embryonic and fetal rat myoblasts in vitro. *Developmental Dynamics, 208*(3), pp. 420-431.

Post, M. J. (2012). Cultured meat from stem cells: Challenges and prospects. *Meat Science, 92*, pp. 297-301.

Prescott, L. M., Harley, J. P., & Klein, A. K. (2005). The use of chemical agents in control. In L. M. Prescott, J. P. Harley, & A. K. Klein, *Microbiology 6th edition* (pp. 134-146). McGraw-Hill.

Punia, S., Dhull, S. B., Sandhu, K. S., & Kaur, M. (2019, November 21). Faba bean (Vicia faba) starch: Structure, properties, and in vitro digestibility—A review. *Legume Science, 1*(1), p. e18.

QIAGEN. (2022). *www.qiagen.com*. Retrieved December 2022, from A Review on Macroscale and Microscale Cell Lysis Methods

Quax, W., van den Broek, L., Egberts, W. V., Ramaekers, F., & Bloemendal, H. (1985, November 1). Characterization of the hamster desmin gene: Expression and formation of desmin filaments in nonmuscle cells after gene transfer. *Cell, 43*(1), pp. 327-338.

Randolph, M. E., & Pavlath, G. K. (2015, October 7). A muscle stem cell for every muscle: variability of satellite cell biology among different muscle groups. *Frontiers in Aging Neuroscience, 7*, p. e:190.

Rangdaeng, S., & Truong, L. D. (1991). Comparative Immunohistochemical Staining for Desmin and Muscle-Specific Actin: A Study of 576 Cases. *American Journal of Clinical Pathology, 96*(1), pp. 32-45.

Rao, N., Evans, S., Stewart, D., Spencer, K. H., Sheikh, F., Hui, E. E., & Christman, K. L. (2013). Fibroblasts influence muscle progenitor differentiation and alignment in contact independent and dependent manners in organized co-culture devices. *Biomed Microdevice, 15*(1), pp. 161-169.

Rashed, A. M., Hetta, A. M., Hashem, Z. S., & El-Katatny, M. H. (2020, May 4). Validation of moist and dry heat processes used for sterilization and depyrogenation during ampoules manufacturing. *Journal of Advanced Biomedical and Pharmaceutical Sciences*(3), pp. 177-183.

Rønning, S. B., Pedersen, M. E., Andersen, P. V., & Hollung, K. (2013). The combination of glycosaminoglycans and fibrous proteins improves cell proliferation and early differentiation of bovine primary skeletal muscle cells. *Differentiation; research in biological diversity, 86*(1-2), pp. 13-22.

Rodgers, J. T., King, K. Y., Brett, J. O., Cromie, M. J., Charville, G. W., Maguire, K. K., . . . Rando, T. A. (2014, May 25). mTORC1 controls the adaptive transition of quiescent stem cells from G0 to GAlert. *Nature, 510*, pp. 393-396.

Rodier, F., & Campisi, J. (2011, February 14). Four faces of cellular senescence. *Journal of Cell Biology, 192*(4), pp. 547-556.

Rodrigues, A. I., Gomes, M. E., Leonor, I. B., & Reis, R. L. (2012, October). Bioactive starch-based scaffolds and human adipose stem cells are a good combination for bone tissue engineering. *Acta biomaterialia, 8*(10), pp. 3765-3776.

Ruardy, T. G., Schakenraad, J. M., van der Mei, H. C., & Busscher, H. J. (1995). Adhesion and spreading of human skin fibroblasts on physicochemically characterized gradient surfaces. *Journal of biomedical materials research, 29*(11), pp. 1415-1423.

Rubin, E., & Rottenberg, H. (1982). Ethanol-induced injury and adaptation in biological membranes. *Federation proceedings, 41*(8), pp. 2465-2471.

Rudnicki, M. A., Schnegelsberg, P. N., Stead, R. H., Braun, T., Arnold, H. H., & Jaenisch, R. (1993). MyoD or Myf-5 is required for the formation of skeletal muscle. *Cell, 75*(7), pp. 1351-1359.

Rufían-Henares, J. A., & Pastoriza, S. (2016). Maillard Reaction. In B. Caballero, P. M. Finglas, & F. Toldrá, *Encyclopedia of Food and Health* (pp. 593-600). Academic Press.

Ryan, M. P., & Adley, C. C. (2013, July 1). The antibiotic susceptibility of water-based bacteria Ralstonia pickettii and Ralstonia insidiosa. *Journal of Medical Microbiology, 62*(7), pp. 1025-1031.

Rybchyn, M. S., Biazik, J. M., Charlesworth, J., & le Coutre, J. (2021, December 1). Nanocellulose from Nata de Coco as a Bioscaffold for Cell-Based Meat. *ACS Omega, 6*(49), pp. 33923-33931.

Ryu, A. H., Eckalbar, W. L., Kreimer, A., Yosef, N., & Ahituv, N. (2017, August 8). Use antibiotics in cell culture with caution: genome-wide identification of antibiotic-induced changes in gene expression and regulation. *Scientific Reports*(7), p. e7533.

Santos, M. I., Pashkuleva, I., Alves, C. M., Gomes, M. E., Fuchs, S., Unger, R. E., . . . Kirkpatrick, C. J. (2009, June). Surface-modified 3D starch-based scaffold for improved endothelialization for bone tissue engineering. *Journal of Materials Chemistry, 19*(24), pp. 4091-4101.

Sapieha, P., & Mallette, F. A. (2018, August). Cellular Senescence in Postmitotic Cells: Beyond Growth Arrest. *Trends in Cell Biology, 28*(8), pp. 595-607.

Sastri, V. R. (2022). Material Requirements for Plastics Used in Medical Devices. In V. R. Sastri, *Plastics in Medical Devices: Properties, Requirements, and Applications (3rd ed.)* (pp. 65-112). William Andrew.

Sánchez-Osuna, M., Cortés, P., Llagostera, M., Barbé, J., & Erill, I. (2020, September 24). Exploration into the origins and mobilization of di-hydrofolate reductase genes and the emergence of clinical resistance to trimethoprim. *Microbial Genomics, 6*(11).

Seah, J. S., Singh, S., Tan, L. P., & Choudhury, D. (2021, June 20). Scaffolds for the manufacture of cultured meat. *Critical Reviews in Biotechnology, 42*(2), pp. 311-323.

Sharma, D., Cukras, A. R., Rogers, E. J., Southworth, D. R., & Green, R. (2007). Mutational analysis of S12 protein and implications for the accuracy of decoding by the ribosome. *Journal of molecular biology, 374*(4), pp. 1065-1076.

Smith, A. S., Passey, S., Greensmith, L., Mudera, V., & Lewis, M. P. (2011, November 7). Characterization and optimization of a simple, repeatable system for the long term in vitro culture of aligned myotubes in 3D. *Journal of Cellular Biochemistry, 113*(3), pp. 1044-1053.

Soto-Gamez, A., & Demaria, M. (2017, May). Therapeutic interventions for aging: the case of cellular senescence. *Drug Discovery Today, 22*(5), pp. 786-795.

Suárez-Rivero, J. M., Pastor-Maldonado, C. J., Povea-Cabello, S., Álvarez-Córdoba, M., Villalón-García, I., Talaverón-Rey, M., . . . Sánchez-Alcázar, J. A. (2021, July 17). Mitochondria and Antibiotics: For Good or for Evil? *Biomolecules, 11*(7), p. 1050.

Svanes, E., Waalen, W., & Uhlen, A. K. (2022). Environmental impacts of field peas and faba beans grown in Norway and derived products, compared to other food protein sources. *Sustainable Production and Consumption, 33*, pp. 756-766.

Swingler, S., Gupta, A., Gibson, H., Kowalczuk, M., Heaselgrave, W., & Radecka, I. (2021). Recent Advances and Applications of Bacterial Cellulose in Biomedicine. *Polymers, 13*(3), p. e:412.

Tahara, N., Tabuchi, M., Watanabe, K., Yano, H., Morinaga, Y., & Yoshinaga, F. (1997). Degree of Polymerization of Cellulose from Acetobacter xylinum BPR2001 Decreased by Cellulase Produced by the Strain. *Bioscience, biotechnology, and biochemistry, 61*(11), pp. 1862-1865.

Tavassoli, H., Alhosseini, S. N., Tay, A., Chan, P. P., Oh, S. K., & Warkiani, M. E. (2018). Large-scale production of stem cells utilizing microcarriers: A biomaterials engineering perspective from academic research to commercialized products. *Biomaterials, 181*, pp. 333-346.

Teti, A. (1992, April 1). Regulation of Cellular Functions by Extracellular Matrix. *Journal of the American Society of Nephrology, 2*(10), pp. 83-87.

Tuomisto, H. L. (2019). The eco-friendly burger. *EMBO Report, 20*(1).

Ugrin, M. R., Dinic, J., Jeremic, S., Dragicevic, S., Deri, B. B., & Nikolic, A. (2021). Bacterial Nanocellulose as a Scaffold for In Vitro Cell Migration Assay. *Nanomaterials, 11*(9), p. e:2322.

Valdoz, J. C., Johnson, B. C., Jacobs, D. J., Franks, N. A., Dodson, E. L., Sanders, C., . . . van Ry, P. M. (2021, November 24). The ECM: To Scaffold, or Not to Scaffold, That Is the Question. *International Journal of Molecular Sciences, 22*(23), p. e: 12690.

van Deursen, J. M. (2014, May 22). The role of senescent cells in ageing. *Nature, 509*(7501), pp. 439-446.

van Dijk, M., Morley, T., Rau, M. L., & Yashar, S. (2021, July 21). A meta-analysis of projected global food demand and population at risk of hunger for the period 2010-2050. *Nature Food, 2*, pp. 494-501.

Verbruggen, S., Luining, D., van Essen, A., & Post, M. J. (2018). Bovine myoblast cell production in a microcarriers-based system. *Cytotechnology, 70*, pp. 503-512.

Vielreicher, M., Kralisch, D., Völkl, S., Sternal, F., Arkudas, A., & Friedrich, O. (2018, June 20). Bacterial nanocellulose stimulates mesenchymal stem cell expansion and formation of stable collagen-I networks as a novel biomaterial in tissue engineering. *Scientific Reports, 8*, p. e:9401.

Visconti, R. P., Kasyanov, V., Gentile, C., Zhang, J., Markwald, R. R., & Mironov, V. (2010). Towards organ printing: engineering an intra-organ branched vascular tree. *Expert opinion on biological therapy, 10*(3), pp. 409-420.

Vogelsang-O'Dwyer, M., Petersen, I. L., Joehnke, M. S., Sørensen, J. C., Bez, J., Detzel, A., . . . Zannini, E. (2020). Comparison of Faba Bean Protein Ingredients Produced Using Dry Fractionation and Isoelectric Precipitation: Techno-Functional, Nutritional and Environmental Performance. *Foods, 9*(3), p. e:322.

Waltz, E. (2021). Club-goers take first bites of lab-made chicken. *Nature Biotechnology, 39*, pp. 257-258.

Wang, H., Pieper, J., Péters, F., van Blitterswijk, C. A., & Lamme, E. N. (2005). Synthetic scaffold morphology controls human dermal connective tissue formation. *Journal of biomedical materials research. Part A, 74*(4), pp. 523-532.

Wang, J., Wang, Q., Wang, C., Reinholdt, B., Grant, A. L., Gerrard, D. E., & Kuang, S. (2015, June 1). Heterogeneous activation of a slow myosin gene in proliferating myoblasts and differentiated single myofibers. *Developmental Biology, 402*(1), pp. 72-80.

Wang, P. Y., Yu, H. T., & Tsai, W. B. (2010, June 1). Modulation of alignment and differentiation of skeletal myoblasts by submicron ridges/grooves surface structure. *Biotechnology and Bioengineering, 106*(2), pp. 285-294.

Webb, K., Hlady, V., & Tresco, P. A. (1998). Relative importance of surface wettability and charged functional groups on NIH 3T3 fibroblast attachment, spreading, and cytoskeletal organization. *Journal of biomedical materials research, 41*(3), pp. 422-430.

Whang, K., Thomas, C. H., Healy, K. E., & Nuber, G. (1995). A novel method to fabricate bioarbsorbable scaffolds. *Polymers, 36*, pp. 837-842.

Wilson, L. A., Birmingham, V. A., Moon, D. P., & Snyder, H. E. (1978, September-October). Isolation and characterization of starch from mature soybeans. *The American Association of Cereal Chemists, 55*(5), pp. 661-670.

Wollweber, M., Krebs, R., Anders, A., Heinrich, U., & Tronnier, H. (2008). Wavelength-dependent penetration depths of ultraviolet radiation in human skin. *Journal of Biomedical Optics, 13*(4), p. e:044030.

WWF. (2014). *The Growth of Soy: Impacts and Solutions.* Gland, Switzerland: WWF International.

Yue, B. (2014). Biology of the Extracellular Matrix - An Overview. *Journal of Glaucoma, 23*(8), 20-23.

Zaman, M. H., Ferdouse, S., & Hossain, M. M. (2013, Oct 14). Sterilization Pattern of Dental Clinics in Rangpur City. *Bangladesh Journal of Dental Research & Education, 3*(2), pp. 1-4.

Zammit, P. (2017). Function of the myogenic regulatory factors Myf5, MyoD, Myogenin and MRF4 in skeletal muscle, satellite cells and regenerative myogenesis. *Seminars in Cell & Developmental Biology, 72*, pp. 19-32.

Zeltinger, J., Sherwood, J. K., Graham, D. A., Müeller, R., & Griffith, L. G. (2001, October). Effect of pore size and void fraction on cellular adhesion, proliferation, and matrix deposition. *Tissue Engineering, 7*(5), pp. 557-572.

Zhou, H., Weir, M. D., & Xu, H. H. (2011). Effect of Cell Seeding Density on Proliferation and Osteodifferentiation of Umbilical Cord Stem Cells on Calcium Phosphate Cement-Fiber Scaffold. *Tissue Engineering. Part A, 17*(21-22), pp. 2603-2613.

Zhu, C., Gong, H., Luo, P., Dong, L., Zhang, G., Shi, X., & Rong, W. (2020, Dec 23). Oral Administration of Penicillin or Streptomycin May Alter Serum Serotonin Level and Intestinal Motility via Different Mechanisms. *Frontiers in Physiology, 11*(605982).

Zinge, C., & Kandasubramanian, B. (2020, June 15). Nanocellulose based biodegradable polymers. *European Polymer Journal, 133*, p. e:109758.

Norges miljø- og biovitenskapelige universitet
Noregs miljø- og biovitskapelege universitet
Norwegian University of Life Sciences

Postboks 5003
NO-1432 Ås
Norway